Spring 7-17-2014

Numerical Modeling of Consolidation Processes in Hydraulically Deposited Soils

Nicholas Robert Brink
University of Colorado at Boulder, nicholas.brink@colorado.edu

NUMERICAL MODELING OF CONSOLIDATION PROCESSES IN HYDRAULICALLY DEPOSITED SOILS

by

NICHOLAS ROBERT BRINK

B.S., Colorado State University, 2012

A thesis submitted to the

Faculty of the Graduate School of the

University of Colorado in partial fulfillment

of the requirements for the degree of

Master of Science

Department of Civil, Environmental, and Architectural Engineering

2014

This thesis entitled:

Numerical Modeling of Consolidation Processes in Hydraulically Deposited Soils

Written by Nicholas Robert Brink

has been approved for the Department of Civil, Environmental and Architectural Engineering

_____

Dobroslav Znidarcic

_____

Richard Regueiro

Date: _____

The final copy of this thesis has been examined by the signatories, and we Find that both the content and the form meet acceptable presentation standards Of scholarly work in the above mentioned discipline.

ABSTRACT

Brink, Nicholas Robert (M.S., Civil, Environmental and Architectural Engineering)
Numerical Modeling of Consolidation Processes in Hydraulically Deposited Soils
Thesis directed by Professor Dobroslav Znidarcic

Hydraulically deposited soils are encountered in many common engineering applications, including storage of mine tailing in tailing storage facilities (TSFs), hydraulic dredging operations and geotextile tubes filled with slurries. Consolidation settlement of these slurry materials is often of interest to geotechnical and mining engineers, as these materials may undergo significant volume change under the influence of relatively small stresses. The consolidation process for hydraulically deposited soils is highly nonlinear, as the soil compressibility and hydraulic conductivity may change by several orders of magnitude. Classical consolidation theory, which assumes that the material properties remain constant throughout consolidation, clearly cannot be applied to such highly compressible soils. Instead, numerical techniques are often required.

Several commercially available finite element codes poses the ability to model soil consolidation, and it was the goal of this research to assess the ability of two of these codes to model the large-strain, two-dimensional consolidation processes

which occur in hydraulically deposited soils. For this research, the codes ABAQUS and PLAXIS were chosen due to their market availability and their common use by geotechnical engineers.

First, a series of one-dimensional consolidation models was created with the goal of verifying the ability of these codes to model large-strain consolidation. Results were compared to solutions given by the finite strain theory developed by Gibson et al. (1967). Solutions to the Gibson equation were derived using a custom finite difference code titled CONDES. Several limitations to the ABAQUS and PLAXIS codes were discovered during this process, including the existence of a minimum initial effective stress below which numerical solutions become unstable. Then, with the ABAQUS and PLAXIS codes having been verified, a series of rectangular models were created in which seepage was allowed both vertically and horizontally. These models were created to represent two-dimensional drainage scenarios without including the full complexities of more realistic and irregular geometries. With the successful creation of these two-dimensional numerical models, more realistic scenarios were then modeled including a geotextile tube filled with fine-grained slurry and a tailing storage facility in which tailing is deposited as a slurry.

ACKNOWLEDGEMENTS

The author wishes to thankfully acknowledge Kunsan National University in the Republic of Korea for their support of this research. A close partnership between our two universities has been developed, and the future of this partnership is bright.

Funding for this research was provided through the Ministry of Land, Transport and Maritime Affairs in the Republic of Korea. Your financial support is greatly appreciated.

CONTENTS

TABLES

FIGURES

1. INTRODUCTION

The process of consolidation governs the long-term behavior of many engineered soil structures in which saturated, fine-grained soils are utilized. As a result, substantial effort has been put forth to better understand how soils consolidate and what factors affect the process of consolidation. Karl von Terzaghi was among the first to develop an analytical theory to explain and predict the process in fine-grained soils (Craig, 2004). His theory made use of several assumptions which may be valid for many common applications in geotechnical engineering. Among these is the assumption that the ratio of the soil's compressibility and hydraulic conductivity remains relatively constant throughout the consolidation process. Most soils for which this theory is applied are relatively dense at the beginning of the consolidation process, such that their total consolidation-induced volumetric strain is relatively small. For soils such as these, the soil's compressibility and hydraulic conductivity may only change by a small percentage, resulting in a relatively constant ratio of compressibility to hydraulic conductivity. The net result is that, for initially dense soils, the assumption of constant material properties remains valid.

However, this assumption must be relaxed when considering hydraulically deposited, fine-grained soils. For the purposes of this thesis, only fine-grained soils are considered, and the term "soil" is herein used in reference only to fine-grained

materials unless otherwise stated. Also for the purposes of this thesis, hydraulically deposited soils are defined as soils which are deposited in a slurry state and which experience a state of zero effective stress immediately after deposition. This state of zero effective stress is present after deposition because the excess pore pressures are sufficient to support the entire weight of the soil. As the excess pore pressures begin to dissipate, these soils may undergo significant consolidation-induced volumetric strains which are driven purely by gravity. Herein, this process of gravity-driven consolidation is termed "self-weight consolidation." Self-weight consolidation is commonly encountered in mining operations (in the form of consolidating tailing slurries) and in dredging operations where fine-grained soils are dredged and allowed to settle. Engineers are often required to accurately estimate the time-dependent behavior of these soils as they consolidate, including the soil geometry, the rate of consolidation and the effective stress state within the soil.

From a constitutive standpoint, the volumetric strains observed during self-weight consolidation may occur as the result of relatively small increases in effective stress. This property of hydraulically deposited soils presents several challenges in modeling their time-dependent behavior. Firstly, the soil's constitutive and hydraulic properties can no longer be assumed to remain constant during consolidation. As the soil undergoes volumetric strains during self-weight consolidation, the material's compressibility and hydraulic conductivity may decrease by several orders of magnitude causing the soil to behave more stiffly and

the dissipation of excess pore pressures to occur more slowly as consolidation progresses. Changing material properties then lead to a great deal of nonlinearity in the constitutive and hydraulic behaviors of these soils as they consolidate. Classical, small-strain consolidation theory does not have the ability to model such nonlinearities in the material properties, and so alternative theories must be adopted.

Gibson et al. (1967) developed a finite strain consolidation theory which is purely analytical and makes use of no restrictive assumptions. However, the mathematical representation of this theory takes the form of a nonlinear differential equation for which no analytical solution exists. Thus, numerical methods are required to arrive at an approximate solution. Custom numerical codes have been created which directly solve Gibson's finite strain consolidation equation. One such code, titled CONDES, is a finite difference code developed at the University of Colorado which provides a numerical solution to Gibson's equation for one-dimensional consolidation (i.e. consolidation of a soil column in which displacements and drainage only occur along one direction) (Yao et al. 2002). Implicit forms of Gibson's finite strain consolidation theory are available in many commercially-available numerical codes. These codes often do not directly solve the differential equation proposed by Gibson, but instead they independently account for the stiffening of the soil and the reduction of the soil's hydraulic conductivity as the soil's volume is reduced. An advantage of these commercial codes is that they often have the capability of modeling consolidation in two dimensions, which allows

the engineer to predict the outcome of the consolidation process in soils which naturally take on more complicated geometries as in tailing storage facilities (TSFs), dredged fills, and hydraulically filled geotextile tubes. However, these codes also contain some potentially severe restrictions.

Numerical codes provide powerful tools for geotechnical engineers, but only if they are designed to handle the processes which are being modeled. All numerical codes are limited by the assumptions used in their derivations. Most commercially available numerical codes are primarily designed to model small-strain consolidation processes in soils, while some codes offer implicit finite-strain capabilities as described above. However, few numerical codes exist which are specifically intended to model the consolidation of hydraulically deposited soils. The state of zero effective stress present at the beginning of the consolidation process often presents numerical challenges for these commercial codes, as near-zero effective stress values may lead to singularities in the numerical scheme which prevent the code from correctly modeling the initial state of the soil.

However, several geotechnical situations exist where it becomes important to predict the consolidation of hydraulically deposited soils. In these situations, numerical codes are often the primary tool used to make these predictions. One common example is the need to predict the long-term behavior of hydraulically deposited mine tailing in conventional tailing storage facilities (TSFs). Accurate predictions of the consolidation of mine tailing are required to design and/or predict the capacity of a tailing storage facility, and inaccuracies in these predictions may

lead to substantial monetary losses to the mine owners and operators. Another example deals with the consolidation of hydraulic fills inside geotextile tubes. Although sandy fills are typically used in geotextile tubes, some scenarios exist where the only practically available fill is composed of fine-grained soils. Here, predicting the consolidation time and the consolidated shape of the geotextile tube may become important for the purposes of project planning, budgeting, and scheduling.

Despite their restrictions, commercial codes may still be successfully implemented to model these example situations. However, many restrictions exist which limit the applicability and the usefulness of these codes in predicting the consolidation of hydraulically deposited soils. It is the goal of this thesis to better understand the limits of commercially available numerical codes when used to model the consolidation of hydraulically deposited soils.

Two commercially available, two-dimensional finite element software packages were selected for this undertaking based upon their availability in the geotechnical engineering industry. The first code, PLAXIS (PLAXIS, 2013), is a code written specifically for geotechnical applications, while the second code, ABAQUS (Dassault Systems, 2013), is a more generalized code which has built-in geotechnical modeling capabilities. Both codes were first verified using one-dimensional models to better understand the basic limitations of each code. Results from the one-dimensional models were then compared to the predictions made by CONDES, which has been independently verified and validated using soils similar

to those used in the one-dimensional models (Abu-Hejleh, 1996). Both codes were then used to create simplified two-dimensional consolidation models using rectangular geometries to determine if additional limitations exist in two-dimensional models. Finally, both codes were used to create example TSF models and models of geotextile tubes. Each of these modeling stages is described in detail herein, and the limitations of these commercial numerical codes are discussed.

2. CONSOLIDATION CHARACTERISTICS OF HYDRAULICALLY DEPOSITED SOILS

As described above, the material compressibility and hydraulic conductivity of hydraulically deposited soils may change by several orders of magnitude throughout the consolidation process, even when consolidation is driven purely by the material's self-weight. As a result, unique models must be established to predict how the soil compressibility and hydraulic conductivity change while undergoing relatively large volumetric strains. Somogyi (1979) and Liu and Znidarcic (1991) proposed empirical models which relate these soil properties to the effective stress state present in the soil. These models were derived specifically for hydraulically deposited soils, and have been found to accurately represent the behavior of such soils as they consolidate. For this reason, these models were chosen for use in this research.

The proposed models rely on five parameters which are derived experimentally. Values for each of these parameters are assigned based upon the results of seepage-induced consolidation tests (SICTs). Detailed testing procedures and parameter fitting instructions are available in the paper published by Abu-Hejleh et al. (1996) but are outside of the scope of this thesis.

Models such as these can either be directly implemented in numerical solutions to Gibson's finite strain equation, or they can be used as inputs into more

general numerical codes. Most general purpose codes require the user to input soil compressibility and hydraulic conductivity parameters in the form of pre-defined models. Thus, in order to use the models developed by Somogyi (1979) and Liu and Znidarcic (1991), the parameters used in the pre-defined material models must be calibrated to fit the models described below. Implementation of the Somogyi (1979) and Liu and Znidarcic (1991) models in numerical codes is discussed further at the end of this section.

2.1. Material Characteristics

The compressibility model (also known as the constitutive model) proposed by Liu and Znidarcic (1991) predicts the void ratio of the soil as a function of the vertical effective stress. This model is represented by (1) below.

$$e = A(\sigma' + Z)^B \quad \textbf{(1)}$$

Here, e is the void ratio, σ' is the vertical effective stress, and the parameters A, B and Z are derived from SICT results. Parameters σ' and Z both take on units of stress, while the parameter B is unitless. The parameter A is dependent upon the units σ' and Z, and takes on hypothetical units of stress to the power of –B.

When a soil is first deposited as a slurry its individual soil particles theoretically experience a state of zero effective stress. This state exists immediately after the process of sedimentation is completed. In this state, the soil

particles throughout the soil body are not yet in contact, and the weight of the soil is carried entirely by the excess pore pressures which were generated during deposition. The void ratio of the soil in this state (termed the initial void ratio, e_0) can be approximated using (1) by setting the vertical effective stress equal to zero. This initial void ratio becomes important when calibrating parameters from other constitutive models to match the constitutive model in (1).

Additionally, the hydraulic conductivity model developed by Somogyi (1979) predicts the soil's hydraulic conductivity as a function of the void ratio. As the void spaces in the soil shrink during consolidation, the cross-sectional area available for water to flow through decreases causing the hydraulic conductivity to be reduced. The model represented by (2) predicts that the hydraulic conductivity increases with increasing void ratio as expected.

$$k = Ce^D \quad \textbf{(2)}$$

Here, k is the hydraulic conductivity, e is the void ratio, and C and D are parameters derived from SICT results. Both k and C take on units of velocity, while e and D have no units.

For the purposes of this research, four soils with unique sets of material properties were chosen to be modeled. Soils were selected for this project to provide a wide range of initial void ratios and soil stiffness. These soils are kaolin clay (KAO), east coast dredged material (ECM), Gulf of Mexico dredged material (GOM)

and an example mine tailing from a conference held in Keystone, Colorado (KEX). SICTs were carried out on each of these materials, and the resulting compressibility and hydraulic conductivity parameters are shown in Table 1 below. Included in this table is the specific gravity of solids, G_s, and the initial void ratio, e_0, of each material. Plots of the material compressibility and hydraulic conductivity models for each soil are also shown in Figure 1 and Figure 2 respectively.

Table 1: Material Parameters for Four Materials

Parameter	KAO	KEX	GOM	ECM
A	3.31	3.40	1.52	5.51
Z (kPa)	5.0	0.6	0.1	0.1
B	-0.148	-0.170	-0.193	-0.249
C (m/s)	2.3E-10	1.5E-09	2.5E-09	4.4E-11
D	4.30	4.40	4.24	2.42
G_s	2.66	2.70	2.70	2.59
e_0	2.61	3.71	2.37	9.78

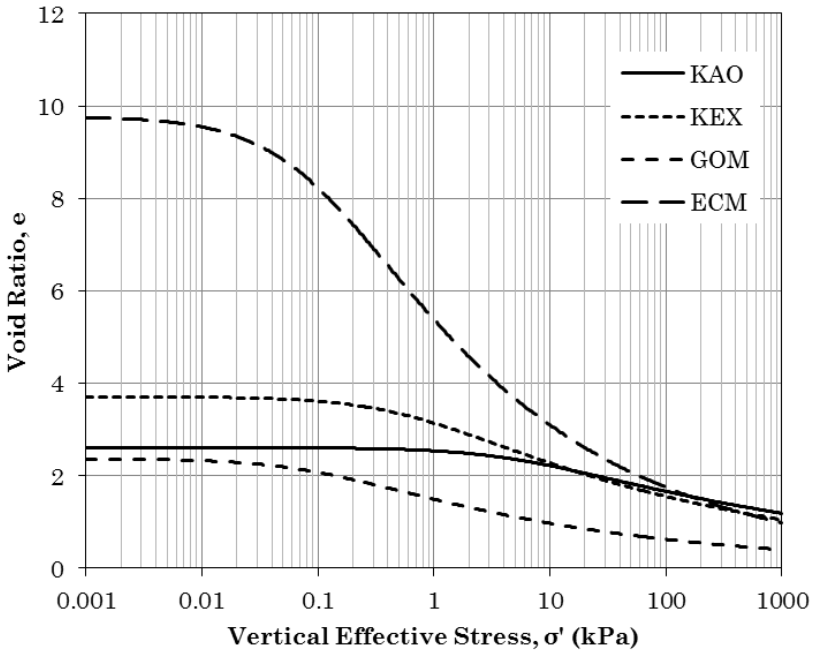

Figure 1: Constitutive Models for Four Soils

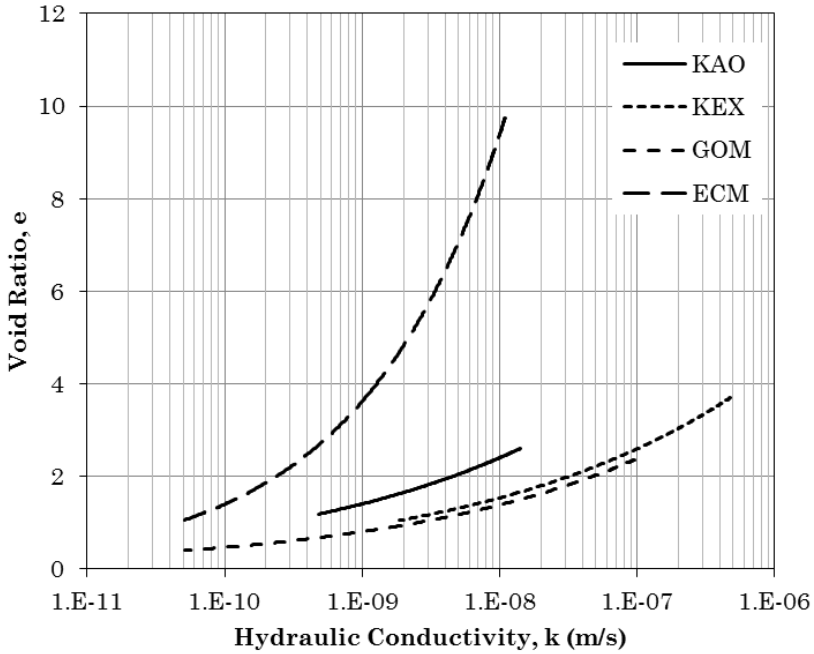

Figure 2: Hydraulic Conductivity Models for Four Soils

2.2. Integration into Numerical Codes

As mentioned previously, implementing the models shown in (1) and (2) into generic, commercially available numerical codes is not straightforward. Although the codes PLAXIS and ABAQUS allow the user to directly input a customized constitutive model, the process of doing so requires the user to have substantial experience using the code and with various programming languages. Additionally, the user would need to develop a new three-dimensional constitutive model which would generalize the one-dimensional relationships into a three-dimensional stress space. Most geotechnical engineers in the industry would likely not have the background required to implement these custom models. The only available alternative is then to calibrate one of the constitutive models which are pre-defined in these codes to match the desired material properties.

2.2.1. Constitutive Models

Of the many constitutive models pre-programmed into these codes, two have the ability to be calibrated to approximate the material models shown in Figure 1: the Modified Cam Clay model and the capped Drucker-Prager model. The Modified Cam Clay model uses an elliptical yield surface and an associated plastic potential surface, and is generally applicable for normally consolidated and lightly overconsolidated clays (Wood, 1990). The capped Drucker-Prager model, on the other hand, uses a linear failure surface which is similar to the Mohr-Coulomb

failure surface, and which is capped by a partial ellipse with a similar form to the Modified Cam Clay model ellipse (Helwany, 2007). Details regarding the formulations of these two models are not the focus of this thesis, and the reader is referred to the above references when additional information is needed.

Both of these constitutive models make use of the input parameters λ and κ, which represent the log-slopes of the normally consolidated line (NCL) and recompression line (RCL) in the compression plane. The compression plane is defined as a plot using mean effective stress, p', on the abscissa and void ratio on the ordinate.

Note that the curves in Figure 1 show a general trend of having a less-steep slope at lower effective stress and a steeper slope at greater effective stresses. These two regions within each curve can be reasonably approximated by log-linear lines with constant slopes. Also recall that the Modified Cam Clay model parameters λ and κ represent the slopes of two log-linear lines in the compression plane. If the value of the at-rest horizontal stress ratio, K_0, is known, the vertical effective stress can be transformed into a mean effective stress as follows. Here, it is assumed that the vertical effective stress is equivalent to the major principal stress and that the two horizontal effective stress components are equivalent to the minor principal stress. The relationship in (3) also assumes that the at-rest condition is present, meaning that displacements in the soil are limited to the vertical direction. Clearly this condition is only truly met in the case of one-

dimensional consolidation where the soil is only allowed to settle and drain vertically.

$$p' = \frac{1}{3}(\sigma'_1 + 2\sigma'_3) = \frac{1}{3}(\sigma'_v + 2\sigma'_h) = \frac{\sigma'_v}{3}(1 + 2K_0) \quad \textbf{(3)}$$

In this relationship, σ'_1 and σ'_3 represent the major and minor principal effective stresses respectively, σ'_v and σ'_h represent the vertical and horizontal effective stresses respectively, and K_0 is the at-rest lateral earth pressure coefficient.

Several methods are available to estimate the value of K_0 for a normally consolidated clay. This value of K_0 is denoted as K_{0nc}. Many commonly used expressions estimate K_{0nc} as a function of the internal friction angle (i.e. Jaky's equation). However, K_{0nc} may also be estimated using the basic Modified Cam Clay constitutive parameters λ and κ. For the one-dimensional consolidation condition, it can be shown that $\delta\varepsilon_p/\delta\varepsilon_q = 3/2$ according to equation 10.5 in Wood's (1990) book. The elastic and plastic components of volumetric and distortional strains may be substituted into this definition to arrive at a relationship which is used to define a value for the principal stress ratio for a normally consolidated clay, η_{nc}, which is defined as the ratio of q to p' for a normally consolidated clay. This relationship, which is equivalent to equation 10.12 in Wood's (1990) publication, is as follows.

$$\frac{\eta_{nc}(1+\nu')(1-\Lambda)}{3(1-2\nu')} + \frac{3\eta_{nc}\Lambda}{M^2-{\eta_{nc}}^2} = 1 \quad \textbf{(4)}$$

Here, v' is the value of Poisson's ratio in terms of effective stresses, M represents the critical state stress ratio (i.e. the value of $\eta = q/p'$ at critical state), and Λ is a variable which incorporates the Modified Cam Clay constitutive parameters such that $\Lambda = (\lambda-\kappa)/\lambda$.

The value of η_{nc} is directly related to the value of K_{0nc} according to the following relationship, which can be derived by assuming one-dimensional consolidation and using the standard definitions of q and p'. The assumption of one-dimensional consolidation again remains, and the assumption that the major and minor principal effective stresses are equivalent to the vertical and horizontal effective stresses remains.

$$K_{0nc} = \frac{3-\eta_{nc}}{3+2\eta_{nc}} \quad \textbf{(5)}$$

A value of M is also required for use in (4). The value of M is directly related to the value of the angle of internal friction, φ', using the following relationship which is derived by assuming that the soil's apparent cohesion is equal to zero (Helwany, 2007).

$$M = \frac{6\sin\varphi'}{3-\sin\varphi'} \quad \textbf{(6)}$$

Thus, the value of K_{0nc} can be determined using (4), (5) and (6), providing that values of λ and κ are known. Because the goal of this curve fitting is to

determine the values of these parameters, the following iterative process is required.

1. First, a value of K_{0nc} must be assumed and used to transform the curves shown in Figure 1 into the compression plane using (3). An initial approximation for K_{0nc} may be found using Jaky's equation, where $K_{0nc} = 1 - \sin \varphi'$.
2. Next, log-linear lines should be fit to the transformed curves such that one line is fit to the portion of the transformed curve at lower effective stresses, and another line should be fit to the portion of the curve at higher effective stresses. Values of λ and κ should then be computed as the slopes of these fitted lines.
3. Using the new values of λ and κ, a new estimate of K_{0nc} should be computed using (4), (5) and (6). The curves in Figure 1 should again be transformed into the compression plane using the new value of K_{0nc}, and new log-linear lines should be fit to the transformed curves. If the newest values of λ and κ are not substantially different from those derived initially, then no additional iterations are required.
4. Otherwise, K_{0nc} should be recomputed and new log-linear lines should be fit until the values of λ and κ do not change substantially.

This process lends itself to being coded in a variety of languages, including Visual Basic for Applications (VBA) inside the framework of Microsoft Excel.

Note that at higher effective stresses, the curves in Figure 1 begin to vary significantly from the assumed linear trend. Because these curves are not perfectly linear, the fitted values of λ and κ depend upon the range of stresses to which they are fit. The range of stresses chosen differed for each soil based upon the expected range of stresses within the geometries of each numerical model. However, as initial estimates, values of λ and κ were fit for stresses ranging from 0.001 kPa to 50 kPa. For all soils except ECM, this stress range represents a region in which the constitutive behavior as defined by (1) is roughly log-linear, and so the fitted parameters should reasonably represent the curves shown in Figure 1.

For the purposes of parameter fitting, it was assumed that the angle of internal friction, φ', is equal to 21 degrees for all four soils. Using (6), this relates to a critical state stress ratio of $M = 0.814$. Although this assumption does not perfectly represent the soils' strength characteristics, it provides sufficient accuracy to assess the ability of PLAXIS and ABAQUS to correctly model the behavior of each soil. The validity of this assumption is confirmed in section 0.

Fitted lines for all four soils are shown in Figure 3 through Figure 6 below. Note that these plots use the specific volume in the place of the void ratio. The values of the fitted parameters λ and κ are then included in the following discussion of the ABAQUS and PLAXIS constitutive model input parameters.

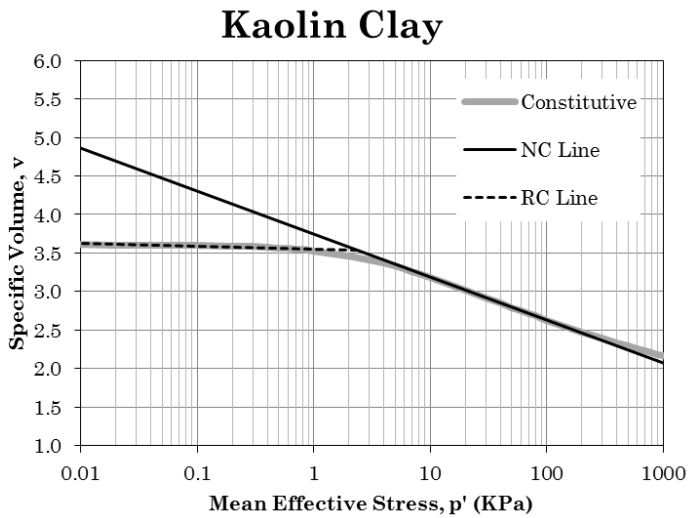

Figure 3: Constitutive Fitting Plot - KAO

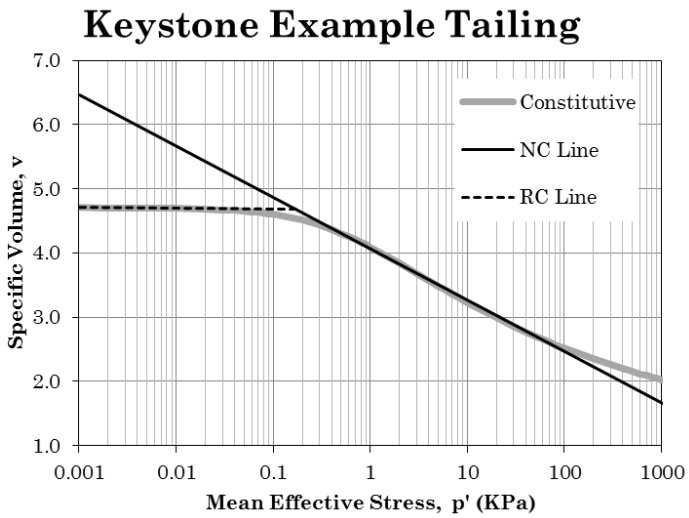

Figure 5: Constitutive Fitting Plot – KEX

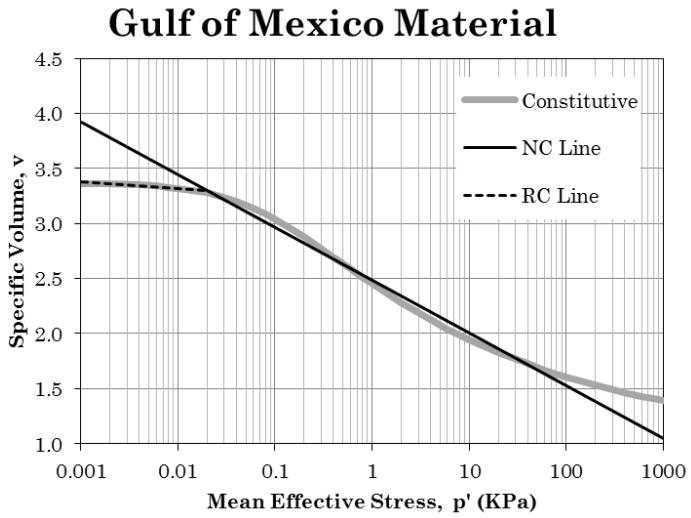

Figure 4: Constitutive Fitting Plot – GOM

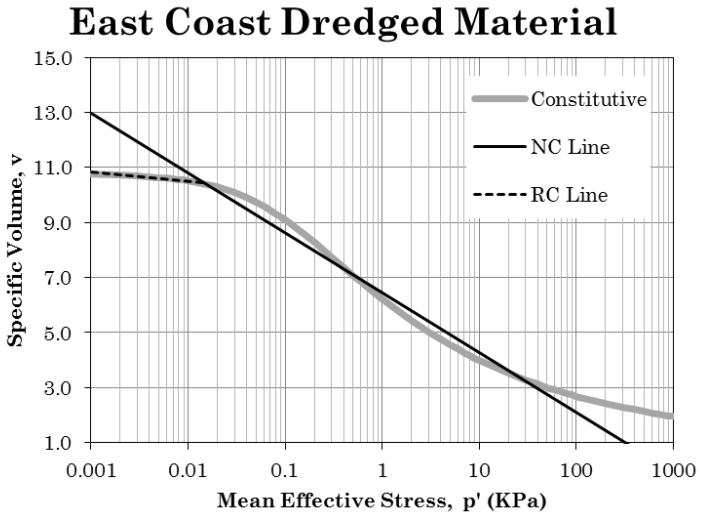

Figure 6: Constitutive Fitting Plot - ECM

Additional input parameters are also required by PLAXIS and ABAQUS. These parameters include the Poisson's ratio, initial preconsolidation stress, (p_{c0}' in ABAQUS and POP in PLAXIS), saturated unit weight, γ_{sat}, and the dry density, ρ_{dry}. The initial preconsolidation stress is equivalent to the mean effective stress at which the NCL and RCL intersect in Figure 3 through Figure 6. In the Modified Cam Clay plasticity model, this value represents the maximum mean effective stress value on the yield ellipse at the soil's initial state immediately after deposition.

Note that PLAXIS requires that the preconsolidation stress (which PLAXIS calls the Pre-Overburden Pressure, POP) be input as a vertical effective stress instead of a mean stress. The POP is then defined as the difference between the initial vertical effective stress and the preconsolidation vertical effective stress. Theoretically the initial vertical effective stress should be zero. However, through modeling experience it was discovered that PLAXIS by default assumes a minimum initial vertical effective stress of 1 kPa. Thus, the POP is computed as the preconsolidation vertical effective stress less 1 kPa. The POP values listed in Table 2 were computed using the given p_{c0}' and K_0 values and solving for the vertical effective stress using (3). However, the POP computes as a negative value for all soils except KAO due to the PLAXIS assumption that the initial vertical effective stress can be no less than 1 kPa. The POP values listed in Table 2 show zeroes for any soil which would otherwise have a negative POP value because PLAXIS does not allow negative POP values to be input. Note that when a POP value of zero is

input, PLAXIS computes the initial vertical effective stress *and the preconsolidation stress of the soil* to be 1 kPa.

ABAQUS also requires the user to input an initial vertical effective stress. Here, the initial stress state is directly input by the user and is a separate input from the preconsolidation stress. This initial vertical effective stress value varies depending upon the model complexity and the soil stiffness parameters. Simpler geometries with stiffer soils might allow for smaller values of the initial vertical effective stress to be input, while more complex models with softer soils may require larger initial stresses to avoid numerical errors. Because these initial stress values were so highly dependent upon the numerical models themselves, they are not given in Table 2. For the one-dimensional numerical models, initial vertical effective stress values of 10 kPa were sufficiently large to allow the numerical scheme to successfully calculate most models with heights of 2.5 m. Experimentation showed that as the model height increased, this initial vertical effective stress value had to increase accordingly. For more complicated two-dimensional models, the values changed drastically from one soil to the next, and with the model dimensions. When creating numerical models, the user must adjust this input value in an iterative fashion to achieve a reasonably low value which is high enough to avoid numerical errors, and so this initial stress is not a static input in ABAQUS.

The standard input parameters for the Modified Cam Clay model and the general parameters required by both numerical codes are listed in Table 2. Note

that the values of λ and κ listed in Table 2 are the values which were fitted for stresses ranging from 0.001 kPa to 50 kPa.

Table 2: Input Parameters for the Modified Cam Clay Model

Parameter	KAO	KEX	GOM	ECM
κ	0.0171	0.0066	0.0270	0.1409
λ	0.2415	0.3474	0.2082	0.9440
e_0	2.608	3.708	2.371	9.776
M	0.814	0.814	0.814	0.814
ν'	0.281	0.281	0.281	0.281
K_{0nc}	0.810	0.816	0.803	0.800
p_{c0}' (kPa) [1]	2.352	0.171	0.020	0.014
POP (kPa) [2]	1.693	-0.805	-0.977	-0.984
γ_{sat} (kN/m^3) [2]	14.32	13.35	14.76	11.26
ρ_{dry} (kN/m^3) [1]	0.737	0.573	0.801	0.240

[1] Parameter only required in ABAQUS

[2] Parameter only required in PLAXIS

The Capped Drucker-Prager model makes use of several additional parameters as well. Firstly, the PLAXIS code uses constitutive parameters λ* and κ* which are equivalent to the λ and κ values from the Modified Cam Clay model normalized by a constant void ratio. The void ratio by which λ and κ were normalized, e_{norm}, is specific to each soil type and to each model geometry. Its value was chosen as the average void ratio across the model at the initial state. The ABAQUS code, on the other hand, directly uses the λ and κ values listed in Table 2 for the Capped Drucker-Prager model.

PLAXIS makes use of a Modified Cam Clay cap as part of its yield surface for the Capped Drucker-Prager model (PLAXIS, 2013). However, the ABAQUS code uses a cap which resembles, but is not equivalent to, the Modified Cam Clay cap used in the PLAXIS code. ABAQUS uses a more generalized cap surface which is a function of the initial preconsolidation stress, p_{c0}', the slope of the failure line, ß, the apparent cohesion, d, and a new variable which represents the eccentricity of the elliptical cap, R. Additionally, the ABAQUS cap is modified so that it does not necessarily have a vertex at the origin in the stress plane (Helwany, 2007). In order to maintain consistency between ABAQUS and PLAXIS, a value of R was chosen so that the ABAQUS yield surface cap would more closely match the Modified Cam Clay cap used by PLAXIS. The yield surface cap function is given by equation 2.82 in Helwany's book. A detailed description of the ABAQUS Capped Drucker-Prager model may also be found there.

Both ABAQUS and PLAXIS require the user to input a measure of the apparent cohesion and a measure of the internal friction angle. PLAXIS directly requires the apparent cohesion, c', and the internal friction angle, φ'. However, ABAQUS makes use of the parameters d and ß, which are equivalent to c' and φ' transformed into the q vs. p' space. These transformed values are computed according to the following relationships (Helwany, 2007).

$$\tan\beta = M = \frac{6\sin\varphi'}{3-\sin\varphi'} \quad \textbf{(7)}$$

$$d = \frac{18c' \cos\varphi\prime}{3-\sin\varphi} \quad \textbf{(8)}$$

The parameters c' and φ', as well as their transformed equivalents d and ß, define the linear failure surface in the Capped Drucker-Prager model. Many of the same input parameters which are used in the Modified Cam Clay model are also used in the Capped Drucker-Prager model to define the elliptical cap yield surface. The input parameters which are specific to the Capped Drucker-Prager model are listed in Table 3. Note that the input parameters which are shared between the Capped Drucker-Prager model and the Modified Cam Clay model are not listed in Table 3, and are only listed in Table 2.

Table 3: Input Parameters for the Capped Drucker-Prager Model

Parameter	KAO	KEX	GOM	ECM
κ* [2]	0.0053	0.0017	0.0105	0.0199
λ* [2]	0.0741	0.0917	0.0812	0.1332
e_{norm} [2]	2.260	2.788	1.564	6.087
R [1]	1.098	1.320	1.279	1.371
c (kPa) [2]	0.01	0.01	0.001	0.001
d (kPa) [1]	63.6	63.6	6.36	6.36
φ' (deg.) [2]	21.0	21.0	21.0	21.0
ß' (deg.) [1]	39.1	39.1	39.1	39.1

[1] Parameter only required in ABAQUS

[2] Parameter only required in PLAXIS

Within the ABAQUS code, the hardening rule for the yield surface cap is not accounted for automatically. Instead, the user is required to directly input a

piecewise function for the hardening rule in the form of a series of yield-stress/volumetric-plastic-strain pairs. PLAXIS, on the other hand, automatically computes the yield surface hardening using the Modified Cam Clay hardening rule. In an effort to maintain consistency between the two codes, the Modified Cam Clay hardening rule was used to generate the piecewise hardening functions for each soil in ABAQUS. This hardening rule is shown in (9), where the variable ε_v^p represents the plastic volumetric strain.

$$\varepsilon_v^p = \frac{\lambda-\kappa}{1+e_0} \ln \frac{p'}{p_{c0}'} \quad \textbf{(9)}$$

2.2.2. Hydraulic Conductivity Models

As a hydraulically deposited soil undergoes significant volumetric strain its void spaces reduce in size, leading to a reduction in the size of the available flow channels through which pore water is allowed to seep. Shrinkage of the flow paths also causes the tortuosity of the available seepage pathways to increase. As a result of the shrinking void spaces, the hydraulic conductivity of the soil will decrease. The net result of the reduced hydraulic conductivity is that the rate of consolidation may be reduced by several orders of magnitude as consolidation progresses through time. Additionally, note that the hydraulic conductivity may not be homogeneous. Regions within the soil which experience greater increases in effective stresses will ultimately undergo greater volumetric strains than regions with smaller effective

stress increases. In combination, (1) and (2) show that the regions undergoing larger volumetric strains (i.e. greater reduction in void ratio) will exhibit lower hydraulic conductivity due to the reduced void space.

Both ABAQUS and PLAXIS have the ability to model changes in hydraulic conductivity as a function of changes in the void ratio. ABAQUS allows the user to directly enter this function in the form of a list of void ratio-hydraulic conductivity pairs. The code then interpolates between pairs to provide a true representation of the function which the user has input. In this way, ABAQUS allows the user to easily input any hydraulic conductivity function which relates the hydraulic conductivity to the void ratio.

PLAXIS, however, uses a pre-defined function to represent the relationship between void ratio and hydraulic conductivity. Using more advanced methods, PLAXIS may be able to make use of user-defined hydraulic conductivity functions, but the procedure for doing this again requires advanced knowledge of programming languages and integration of custom codes into the PLAXIS model library. Because most practicing engineers do not have the ability to do this, only the pre-defined hydraulic conductivity function was used in the PLAXIS code.

The hydraulic conductivity function used by PLAXIS is shown in (10) below.

$$\log \frac{k}{k_0} = \frac{e - e_0}{C_k} \qquad \textbf{(10)}$$

Here, k represents the hydraulic conductivity at the void ratio e, and k_0 and e_0 represent the hydraulic conductivity and void ratio at some reference point. For use in this research, the reference point was chosen to be the initial condition immediately after the soil is deposited. C_k controls the rate at which the hydraulic conductivity changes with changes in the void ratio. Extremely large values of C_k cause the hydraulic conductivity to remain approximately constant with changing void ratio.

The function in (10) is logarithmic in nature, while (2) is an exponential relationship. Thus, these two relationships cannot be exactly matched. The PLAXIS relationship in (10) can be approximately fitted to (2) by properly calibrating the value of C_k. Here again, a simple algorithm implemented in Microsoft Excel may be used to accomplish this fitting.

As inputs for the hydraulic conductivity model, PLAXIS requires three parameters: the initial hydraulic conductivity in the x-direction, hydraulic conductivity in the y-direction, and the rate-of-change constant C_k. It was assumed that most hydraulically deposited soils exhibit isotropic hydraulic conductivity, such that the initial hydraulic conductivity in both the x and y directions can be represented by a single permeability, k_0. The k_0 value for each of the four soils is provided in Table 4, along with the fitted values of C_k.

Table 4: PLAXIS Hydraulic Conductivity Model Parameters

Parameter	KAO	KEX	GOM	ECM
k_0 (m/s)	1.419E-08	4.790E-07	9.720E-08	1.104E-08
C_k	1.212	1.565	0.842	7.360

Figure 7 through Figure 10 then show the fitted PLAXIS hydraulic conductivity models and the ABAQUS models for each soil. Recall that ABAQUS allows the user to directly input data points to create a linear piecewise hydraulic conductivity function. Thus, the ABAQUS curves in these figures also represent the hydraulic conductivity relationships from (2) using the input parameters C and D from Table 1. It is desirable to fit the PLAXIS curves to the approximate range of void ratios which are expected in the numerical model throughout the consolidation process. The initial void ratio, e_0, is calculated as described in section 2.1. The minimum void ratio in the fully-consolidated state can then be estimated by using the buoyant unit weight of the soil and the maximum model height, both in the *initial state,* to estimate the maximum vertical effective stress in the model at the fully consolidated state. This maximum vertical effective stress can then be used in (1) to provide the minimum void ratio which can be expected in the model. The initial and minimum void ratios represent the range across which the PLAXIS hydraulic conductivity models should be fit.

Note that the PLAXIS curves in Figure 7 through Figure 10 extend below the minimum expected void ratios in a 2.5 m tall model. As a result, the left side of each PLAXIS curve is not well matched to the desired ABAQUS curve. This was done intentionally to show how the two hydraulic conductivity models can

potentially deviate substantially from each other when the void ratio lies outside the expected range. This is especially true for lower void ratios, where small changes in the void ratio lead to relatively large changes in the hydraulic conductivity. Thus, it is critically important that the hydraulic conductivity models in PLAXIS be matched across the full range of void ratios which are observed in any given model. After modeling is complete, the range of void ratios computed by PLAXIS should be inspected and compared to the range of void ratios for which the hydraulic conductivity model was calibrated to ensure that a proper fit was achieved.

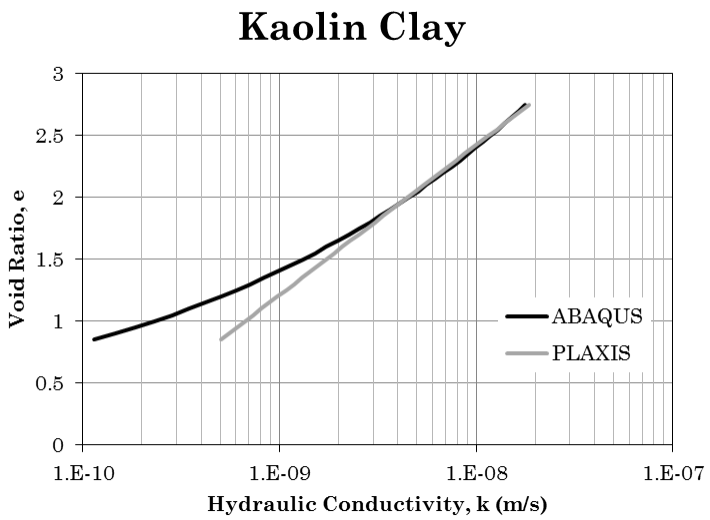

Figure 7: Hydraulic Conductivity Models - KAO

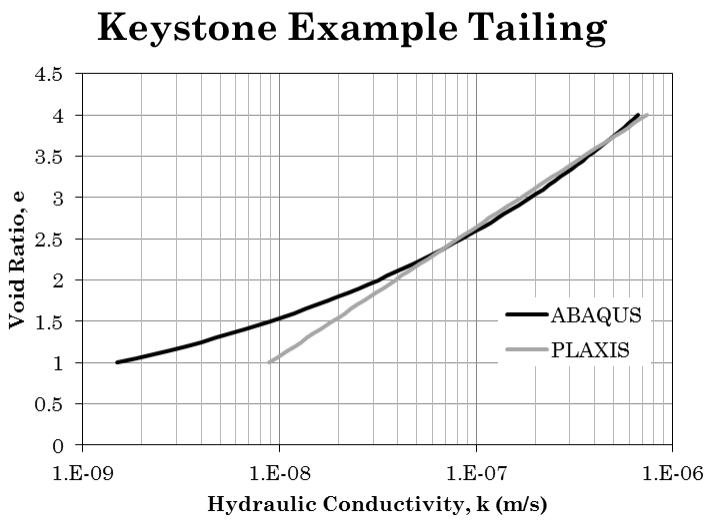

Figure 9: Hydraulic Conductivity Models - KEX

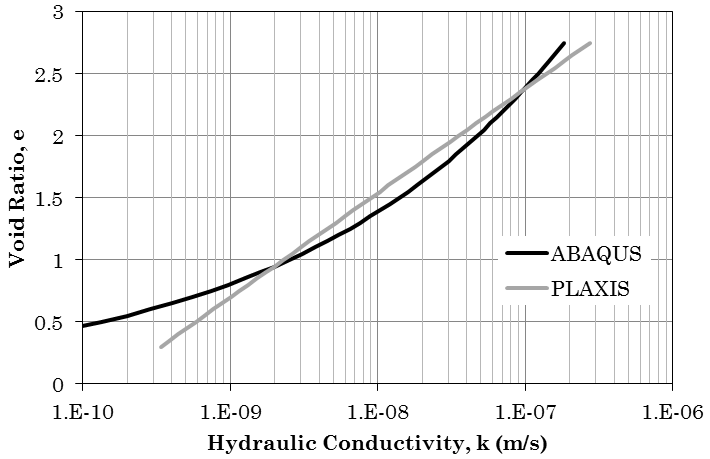

Figure 8: Hydraulic Conductivity Models - GOM

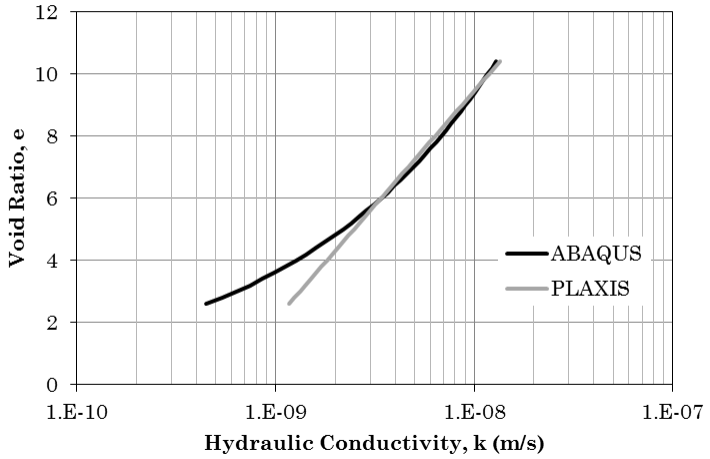

Figure 10: Hydraulic Conductivity Models - ECM

3. ONE-DIMENSIONAL CONSOLIDATION MODELING

Before more complex geometries could be modeled, it was first desired to verify that ABAQUS and PLAXIS have the ability to model highly compressible soils in simpler geometric configurations. For the purpose of this validation, a series of simple, one-dimensional consolidation models were generated in both codes. The results were compared to the results produced by the custom finite difference code, CONDES. CONDES provides a direct numerical solution to the one-dimensional finite strain consolidation equation proposed by Gibson (1967). Additionally, CONDES makes direct use of the constitutive and hydraulic conductivity models in (1) and (2), such that the parameters in Table 1 may be directly input into CONDES with no need for conversion. CONDES is also known to produce accurate results when properly used, and it has been both validated and verified (Yao et al., 2002).

3.1. Model Creation and Execution

Square geometries were used for the purpose of validating the PLAXIS and ABAQUS codes. Each numerical model used side lengths of 2.5 m, which roughly approximates the dimensions of a larger geotextile tube. A total of 16 models were created, eight in ABAQUS and eight in PLAXIS. Two numerical models were

created within each code for each of the four soils discussed previously: one using the Modified Cam Clay plasticity model and one using the Capped Drucker-Prager plasticity model. These numerical models were used to compare the Modified Cam Clay and Capped Drucker-Prager plasticity models and to assess which plasticity model provides a better fit to the constitutive relationship in (1). Here, the goal was to choose one of the two plasticity models for use in the remainder of the research.

3.1.1. Creation of ABAQUS Models

The following is a basic procedure which was followed to create each one-dimensional model in ABAQUS. After the first model was created, the remaining models were created using the first as a template. Note that all models were created in the axisymmetric condition to better approximate the consolidation of a discrete column of soil. Also note that ABAQUS does not specify units for any of its inputs or outputs. Instead, it assumes that the user will remain dimensionally consistent with all inputs. For this reason, all inputs were converted into standard SI units prior to inputting them into ABAQUS, such that all outputs were also in SI units. If needed, the output data was post-processed to convert it into the desired units.

ABAQUS is not a straight-forward code to use. Some experience is required with ABAQUS before the user is able to successfully create a model and correctly interpret its results. Thus, the procedures outlined below assume that the user has a basic understanding of how to create and manage a simple, single-part model in ABAQUS.

1. First, the soil geometry was created from the Part module. A vertical construction line was also created through the origin. This construction line represents the line of axisymmetry used by ABAQUS to perform an axisymmetric analysis.
2. From the Property module, a material model was created using the input parameters described above for either the Modified Cam Clay or Capped Drucker-Prager model. In total, ABAQUS requires the user to input four sets of material properties: soil density information, a plastic behavior model, an elastic behavior model, and a pore fluid flow model. All material properties were entered through the Edit Material dialog box. First, the material density was input using the Density property under the General tab. Note that the mass density required by ABAQUS is not the total density of the soil, but the dry density of the soil skeleton, ρ_{dry}, at the initial void ratio. Next, the plasticity model was created. ABAQUS offers two plasticity models: the Clay Plasticity model which corresponds to the Modified Cam Clay model, and the Cap Plasticity model which corresponds to the Capped Drucker-Prager model. Note that if the Cap Plasticity (Capped Drucker-Prager) plasticity model is chosen, the cap hardening rule must be explicitly defined as a "Cap Hardening" sub-property. Discrete values produced using (9) were input as a list. The elasticity model, titled "Porous Elastic," was then created from the Mechanical tab, under the Elasticity submenu. This

Porous Elastic model works in conjunction with either the Cap Plasticity or Clay Plasticity models. Both of these plasticity models require that the Porous Elastic model be defined as well. Finally, the hydraulic conductivity relationship was input using the Permeability model, found in the Other tab under the Pore Fluid submenu. Here, the piecewise hydraulic conductivity relationship produced from (1) was input as a list of data points. Also note that the unit weight of the wetting fluid (i.e. water) must be input as well. For all models, a unit weight of 9810 N/m^3 was used.

3. Within the Property module, a geometry section was created to represent the soil body. Then, a section assignment was created to assign the material model previously created to the new geometry section.
4. From the Assembly tab, a new instance of the recently created square soil part was created. Here, it is important to ensure that no more than one instance of soil body is created. It is relatively easy for a user to accidentally create a second instance of the same part, and so this must always be double checked before proceeding to the next steps. Any additional instances will not have boundary or initial conditions assigned to them, and so the calculation of the model will fail if any additional instances are not deleted.
5. Calculation steps were then created from the Step module. ABAQUS automatically places a step named "Initial" into the calculation procedure. This step is required and cannot be deleted. A second step was created and named "Consolidation." This step was chosen to be of the Soils type, and set

to be a “Transient Consolidation” analysis so as to capture the transient effects of dissipating pore pressures. The checkbox for the option “Include creep/swelling/viscoelastic behavior” was unchecked. Also, the option “Nlgeom” was enabled for this consolidation step. Nlgeom represents the finite strain approximation available in ABAQUS, which independently accounts for changes in compressibility and hydraulic conductivity with changes in the void ratio. Enabling this option is critical; without this option the consolidation calculations would precede using small-strain assumptions which are not valid for the consolidation of hydraulically deposited soils. The Time Period field should then be set to a duration long enough to allow the soil to fully consolidate. Under the Incrementation tab, automatic time stepping was always chosen with a maximum of 1000 increments allowed. The initial, minimum and maximum increments were specific to each soil, and the user must choose appropriate values. Note that if the maximum increment is set too small, the code may not converge. The exact cause of this failure is unknown, but it is theorized that the failure occurs when the time increment becomes small enough that small numerical oscillations occur in the solutions which would normally be averaged out if the time increment were larger. These small oscillations would then be amplified as the calculation progresses, eventually causing the calculation to diverge completely. All other options in the Step dialog box were left to their default values.

6. Boundary conditions were then established from the Load module. Two mechanical boundary conditions were created during the Consolidation step to constrain the soil's movements. The first condition set zero displacement in the horizontal direction (i.e. U1 in ABAQUS) for both of the vertical edges of the model, and the second condition set zero displacement in the vertical direction (i.e. U2) for the bottom edge of the soil. A pore pressure boundary condition was also created in the Consolidation step, which set the pore pressure at the top edge of the soil equal to zero at the beginning of the step. Thus, the soil was allowed to drain from the top surface only.
7. Initial conditions were also set from the Load module. Three initial conditions are required for ABAQUS to initialize the calculations: an initial stress distribution, an initial pore pressure distribution, and an initial void ratio distribution. The initial void ratio distribution was set to a homogeneous value of e_0 from Table 2 for the material being modeled. Theoretically, the initial effective stress should be zero everywhere in the soil. However, a zero-effective-stress state causes numerical issues in both ABAQUS and PLAXIS, such that some non-zero value must be specified. Ideally the lowest possible value should be specified to better approximate the initial state of zero effective stress. For all of the models using 2.5 m heights, an initial effective stress of 0.01 kPa was found to work well. Note that ABAQUS treats compressive stresses as negative, such that the value of the initial effective stress input into ABAQUS should be negative. ABAQUS

also requests a value for K_0 as part of the initial effective stress input. This value was set to 1.0 to approximate the initial fluidic state of the soil slurry immediately upon deposition. ABAQUS then later made use of updated values of K_0 as the soil consolidated. Next, the initial pore pressure distribution was entered by first creating an analytical field which represented the pore pressure as a function of elevation. As an example for the KAO material with saturated unit weight 14.32 kN/m^3 and initial height of 2.5 m, the analytical field expression took the form "14320(2.5-Y)". This analytical field was then called through a pore pressure initial condition and applied to the entire soil body. Finally, the initial saturation was defined as a homogeneous value of 1.0 throughout the soil. This definition is optional, but it was included to ensure that ABAQUS initializes the soil in a saturated state.

8. Two loads were then defined from within the Load module. A gravity load was first defined, having an acceleration of -9.81 m/s^2. This load was applied instantaneously (i.e. not ramped over time) and was applied to the entire soil body. A second surcharge load was then created and applied to the top surface of the soil in an effort to balance the non-zero stresses created by the effective stress initial condition. The surcharge thus took on the same magnitude as the initial effective stress.
9. A mesh was then created for the soil body. The mesh consisted of a grid of 10 elements by 10 elements for these square models. Structured, quadrilateral

elements were chosen, using the element type CAX8P (i.e. using a standard calculation procedure of quadratic order, with 8-noded elements of family type Pore Fluid/Stress). Note that reduced integration as *not* used in these calculations, as this option was found to cause numerical instability in models using some of the more compressible soils (e.g. ECM).

10. A new calculation job was then created in the Job module using the default calculation and memory allocation settings. Running this job allowed ABAQUS to successfully compute each model.

3.1.2. Creation of PLAXIS Models

PLAXIS provides a much more user-friendly interface than PLAXIS, though some experience with the code is still required before creating a successful and meaningful model. Thus, it is again assumed that the reader has some experience using the PLAXIS code prior to implementing the procedures discussed herein.

1. When a new model is created in PLAXIS, the Project Properties dialog box appears which asks the user to specify several options for the model. From the Project tab of this window, an axisymmetric model type was selected and 15-node elements were chosen. From the Model tab, the user is asked to choose which units to use. For these models, the default units of m, kN, and days were selected. The remaining grid options (such as snap grid spacing, grid size, etc.) were model-specific and can be easily modified to accommodate larger or smaller models.

2. The model geometry was then created by entering a series of coordinate pairs. These coordinates represented the four vertices of a square having side lengths of 2.5 m and with an origin at the bottom left vertex.
3. Material property sets were then input for each model. The PLAXIS code does not allow the user to specify the initial pore pressure conditions, and so the code must be allowed to compute the initial pore pressures itself. However, PLAXIS was not explicitly designed to model self-weight consolidation processes, and it does not recognize that the application of a gravity load leads to the development of excess pore pressures. To compensate, three sets of material properties were created for each PLAXIS model: one set with zero unit-weight, one set with full unit weight but with undrained conditions specified, and one set with full unit weight and with drained conditions specified. Note that PLAXIS allows the user to input both the saturated and unsaturated unit weights of the soil under the General tab. Because the soil was expected to remain saturated throughout the consolidation process, the unsaturated unit weight should never enter into the calculation. The initial void ratio was also entered into the General tab. PLAXIS labels this parameter as e_{init}, and it is equivalent to e_0 in Table 2. Also on this tab, the user is asked to specify a material model. The Modified Cam Clay model is directly available in this drop-down menu, though the Capped Drucker-Prager model is named the "Soft Soil Model" in PLAXIS. Then, under the Parameters tab, the parameters from Table 2 or Table 3

were input depending upon the selected plasticity model. Under the Flow Parameters tab, the hydraulic conductivities k_x and k_y were given the value of k_0 from Table 4. The C_k value from Table 4 was also entered under this tab. Under the Initial tab, the value of the lateral earth pressure coefficient was set to Automatic. The POP values from Table 2 were also entered from this tab. All other inputs to each material model were left to their default values.

4. Mechanical boundary conditions were then applied to the left, right, and bottom of the soil body. Similarly to the ABAQUS models, horizontal displacements were fixed on the left and right vertical faces of the model, and vertical displacements were fixed on the bottom surface of the model.
5. A finite element mesh was then generated for the model. Global coarsness for each model was set to "Fine."
6. Next, the model was transferred into the PLAXIS Calculations program. An initialization calculation phase was created by default. Under the Parameters tab for this phase, the Define button was used to apply the zero-unit-weight material parameter set to the soil for this phase only. Here, the phreatic level was also set at the soil's top surface to specify that the soil was saturated and to provide a baseline from which the pore pressures would be computed. The left, right and bottom soil surfaces were also set to undrained flow boundaries, while the top surface was set to a "Free" (i.e. drained) flow

boundary with the pressure head being specified by the location of the phreatic line.

7. A second phase was then created in the Calculations program, and the calculation type was set to Plastic. PLAXIS uses Plastic phases to compute steady state excess pore pressures prior to a consolidation calculation. For this phase, the material property set using full unit weight and undrained conditions was applied to the soil body. The phreatic and drainage conditions from the initialization step were carried over into the newly created Plastic step. Note that although drainage was allowed through the top pore pressure boundary condition, the material property was explicitly defined as undrained so that no seepage flux was allowed through any boundary. Under the General tab of the Calculations program, the Advanced button was used to enable the Updated Mesh Analysis option. This option activates the finite strain approximation in PLAXIS, and is thus required to account for the changing material properties throughout the consolidation process.
8. A third phase was created with the calculation type set to Consolidation. For this phase, the material property set which used the soil's full unit weight and which was set to drained conditions was applied to the model. Again, the hydraulic boundary conditions and phreatic level from the previous phase were carried over into this phase. PLAXIS allows the consolidation process to be calculated in a single phase. However, graphical outputs are only generated for the end of each calculation phase. Thus, the consolidation

process was broken into several (usually 10 or more) calculation phases with the end of each phase representing a time at which an output was desired. Phases were established such that the initial conditions for each phase were taken from the final conditions of the preceding phase. Time intervals for each calculation phase were computed so as to achieve the desired output times at the end of each phase. All other inputs were left to their default values, with the exception of the phase names.

9. From the Calculations program, several curve points were selected throughout the finite element mesh for use in plotting data after the analysis was complete. However, PLAXIS is somewhat limited in its ability to produce meaningful plots. Thus, instead of relying on the PLAXIS Output program to generate the desired plots, the raw data from the Output program was exported in the form of text files. A custom VBA macro based in Microsoft Excel was used to post-process all the data which was eventually used to generate results plots and summary tables.

3.2. One-Dimensional Modeling Results

Recall that the primary goal of the one-dimensional modeling effort was to validate the ability of both PLAXIS and ABAQUS to model the consolidation of hydraulically deposited soils. Within each code, two models were created for each of the four soils described in section 2.1. One numerical model made use of the

Modified Cam Clay plasticity model, while the other made use of the Capped Drucker-Prager plasticity model.

A secondary goal of this one-dimensional modeling effort was to compare the two available plasticity models and to determine which plasticity model provides a better approximation of the constitutive model represented by (1). The plasticity model which provided the better fit would then be implemented in the remaining research efforts.

Herein, the results of the one-dimensional modeling effort are presented for each of the four soils. Results include plots of the time-dependent settlement of the soil column, void ratio and effective stress distributions across the height of the soil column at various times, stress paths at various locations within the soil column, and plots of the constitutive relationships followed by the numerical codes. The settlement predicted by each numerical model was of primary interest during this stage of modeling, as it represents the total change in volume of the soil. Practicing engineers will likely be more concerned with this behavior of the soil over all other properties. However, settlement alone does not fully describe the consolidation process. Effective stress and void ratio profiles provide insight into the transient behavior predicted by each numerical model, and comparison of these profiles to those which are theoretically expected provides additional criteria by which the accuracy of each model can be judged. One-dimensional consolidation stress paths should theoretically follow a straight line representing the K_0 condition, and this provides another measure of the accuracy of each model. Finally, the constitutive

behavior predicted by each model can be directly compared to the desired constitutive model given by (1). This comparison provides a method for determining the most appropriate plasticity model for use in additional modeling efforts.

Settlement curves and void ratio profiles were directly comparable to the outputs from the code CONDES for the purpose of validating the PLAXIS and ABAQUS predictions. The remaining outputs were compared to the theoretical behaviors which were expected.

Examples of the one-dimensional consolidation model geometries are presented in Figure 11 and Figure 12 for the PLAXIS and ABAQUS codes respectively. Within each figure, the left image represents the model geometry as it was input into the numerical code. The right image then represents the model geometry in its fully consolidated state as computed by the PLAXIS and ABAQUS codes respectively. The examples in these figures both use Kaolin clay properties and the Modified Cam Clay plasticity model.

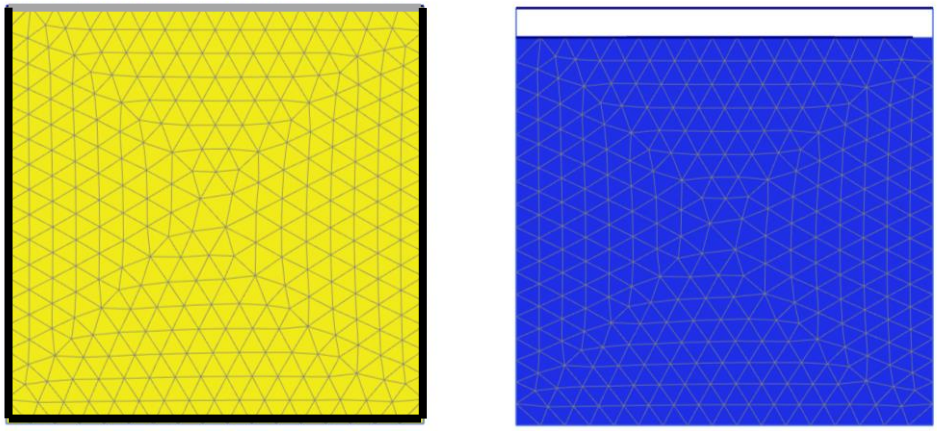

Figure 11: Example PLAXIS 1D Model Before and After Consolidation

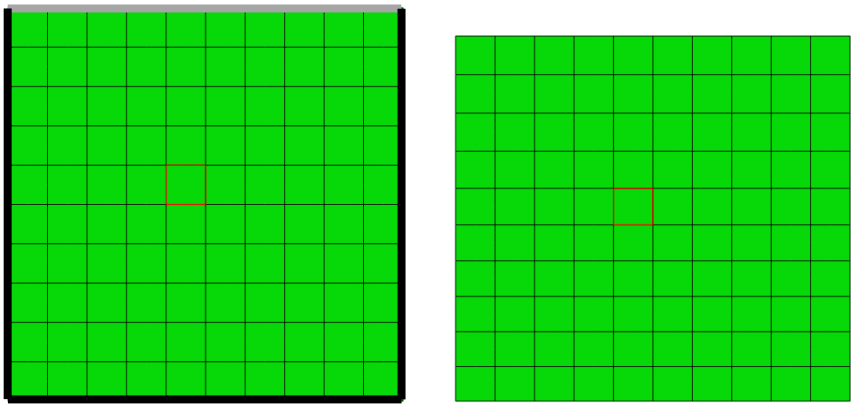

Figure 12: Example ABAQUS Model Before and After Consolidation

The left (initial state) images in these two figures also show the seepage boundary conditions which were used. Grey boundaries represent those where zero pore pressure conditions were specified to allow drainage. Recall that drainage was only allowed from the top surface of the geometry in all one-dimensional consolidation models. Black boundaries then represent no-flow boundaries, where zero seepage flux was specified.

Results from each set of one-dimensional consolidation models are presented and briefly discussed in the following sections. Images showing the initial and final geometries of each model are not shown for each soil, as they all follow the same form as those in Figure 11 and Figure 12.

3.2.1. One-Dimensional Results: Kaolin Clay

Kaolin clay (KAO material) is a widely available, kaolinite-based clay which is commonly mined in the United States (Dana et al., 1977). This clay was chosen because it is readily available, and because it is relatively easy to obtain samples. The kaolin clay used in this research was purchased in a dry form and then

reconstituted into a slurry through the addition of water and by mixing action. Tap water was added to the dry clay in sufficient quantities so as to achieve a water content 2.5 times greater than the clay's liquid limit. SICTs were then performed on the slurry to derive the material properties listed in Table 1.

Kaolin represents a relatively stiff fine-grained slurry. Its initial void ratio is the second lowest of the four soils tested, and its preconsolidation stress is the largest. As a result, it was expected that Kaolin clay would present the fewest difficulties in developing a numerical consolidation model. The settlements predicted by each of the four numerical models using KAO properties are shown in Figure 13 and Figure 14 below. Figure 13 shows the results predicted by the Modified Cam Clay model, and Figure 14 shows those predicted by the Capped Drucker-Prager model. The settlement predicted by CONDES is also shown on each plot as a means of comparing the accuracy of the models. Recall that CONDES directly implements the constitutive and hydraulic conductivity models in (1) and (2), and thus it serves as the baseline for comparing the PLAXIS and ABAQUS predictions.

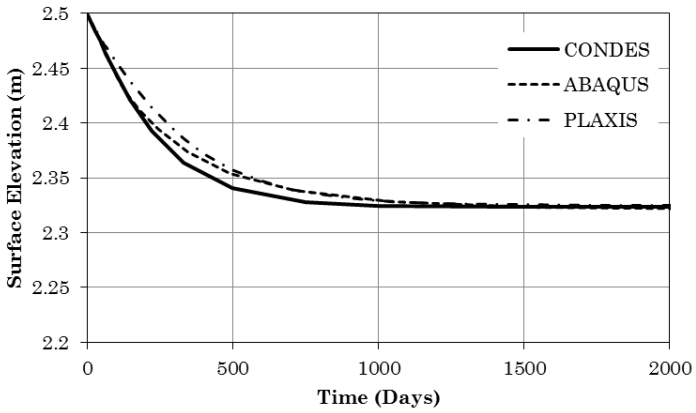

Figure 13: KAO Settlements Predicted by the Modified Cam Clay Model

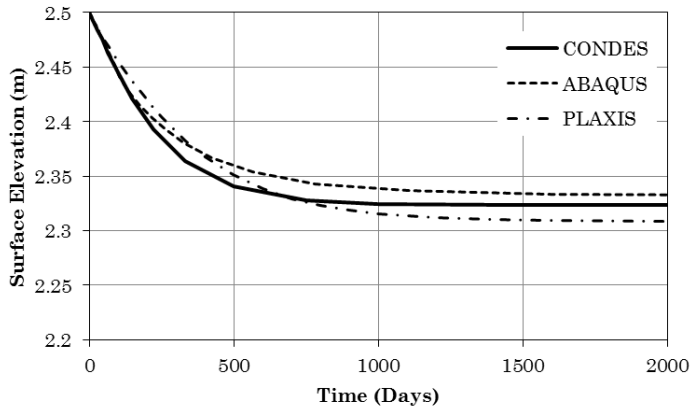

Figure 14: KAO Settlements Predicted by the Capped Drucker-Prager Model

These results show that while both plasticity models match the CONDES predictions reasonably well, the predictions made by the Modified Cam Clay model match the CONDES predictions much more closely. Another feature to note in these plots is the initial slope of the settlement curve, which represents the initial settlement rate. These figures show that the ABAQUS models better predict this rate than the PLAXIS models, regardless of the plasticity model used.

For one-dimensional models with drainage allowed only at the top surface, the initial segment of the curve should be approximately linear. This segment

represents a region in time where consolidation begins at the bottom of the soil column in the form of a distinct consolidation front. This consolidation front is identified as a boundary between two zones in the soil: a lower zone which has undergone a reduction in void ratio, and an upper zone which has not. Upward-draining water from the lower zone creates a critical upward gradient which causes the soil in the upper zone to remain at a state of near-zero effective stress. Linear settlement will occur until the consolidation front reaches the top of the soil column. Within this initial linear segment, the rate of settlement is exactly equal to the linear flow rate of seepage water leaving the soil. Thus, the initial rate of settlement can be predicted analytically by using the critical gradient and the hydraulic conductivity at the initial void ratio to find the Darcy seepage velocity. By the law of conservation of mass, the Darcy velocity must be equal to the initial settlement rate before the consolidation front reaches the top of the soil.

The consolidation front can be easily seen in the void ratio profiles shown in Figure 15 and Figure 16. Figure 15 shows the void ratio profiles predicted by CONDES, which are assumed to be the true void ratios which would be observed in a consolidating soil column. At time 43 days, the consolidation front in the CONDES model had progressed about half way up the soil column. The PLAXIS results in Figure 16 show the consolidation front progressing more slowly. Note that the location of the consolidation front is easily observed in the CONDES results, as the void ratio profile at 43 days shows a clear point at which the void ratios begin to reduce. Both the ABAQUS and the PLAXIS models show some

reductions in the void ratio even above the point where the consolidation front is expected to be. Thus, it can be concluded that the neither PLAXIS nor ABAQUS is able to perfectly define the behavior of the consolidation front. However, the approximations made by these codes are still close enough to the CONDES predictions to be considered accurate.

Also note that the ABAQUS models show some sharp changes in the slopes of the void ratio profiles near the top surface of the soil. It is unclear what causes these variations. One possibility is that the extremely low effective stresses in that region have caused small numerical errors to occur which are compounded with each calculation step. However, this could not be confirmed and the true cause is still unknown.

Also note that the ABAQUS models produce transient profiles which more closely match the positions of the CONDES profiles. All but the PLAXIS Capped Drucker Prager model also predict an accurate steady state void ratio at the bottom of the soil column.

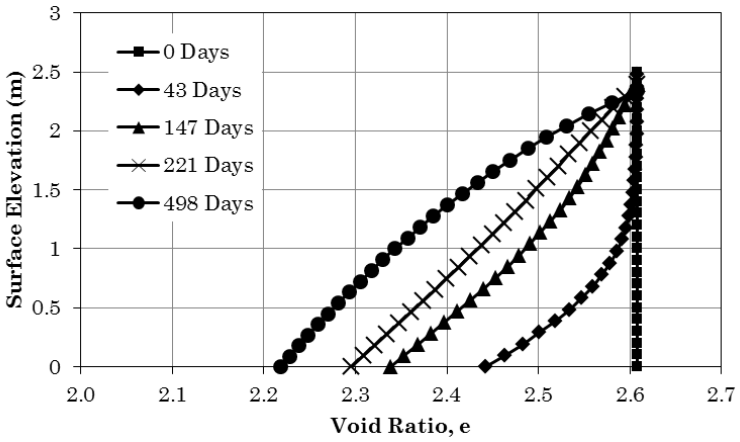

Figure 15: KAO Void Ratio Profiles Predicted by CONDES

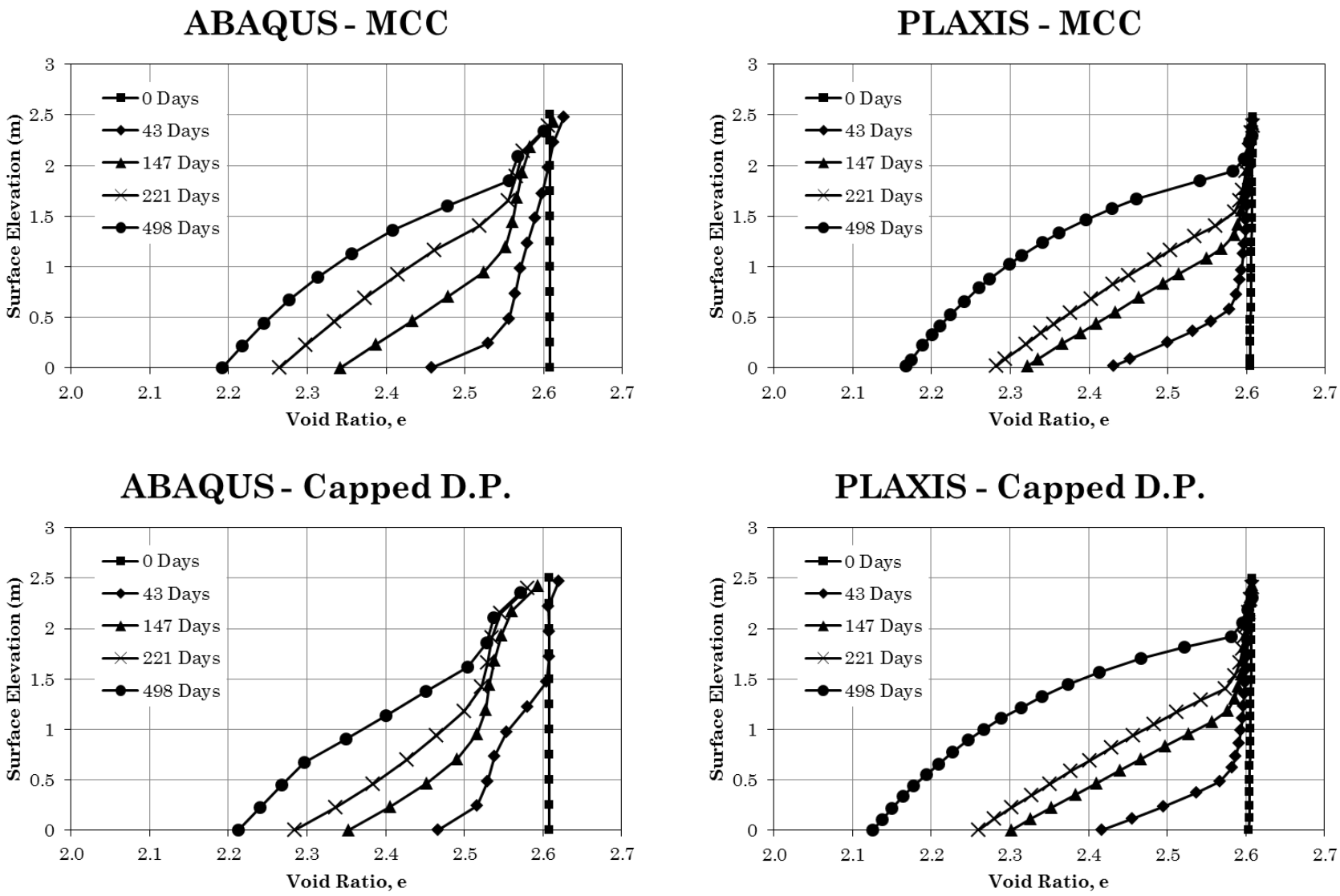

Figure 16: KAO Void Ratio Profiles Predicted by ABAQUS and PLAXIS

From (1) it is known that the void ratio is theoretically a function of the effective stress state. Thus, the effective stress profiles should change in accordance with the changing void ratio profiles. The effective stress profiles predicted by the PLAXIS and ABAQUS models are shown in Figure 17 for comparison. A comparison between Figure 16 and Figure 17 shows that the effective stress profiles change at roughly the same rate as the void ratio profiles, as expected.

Also note that the effective stress profiles in the ABAQUS models at time 0 days (i.e. at the initial condition) are constant with depth and show nearly zero effective stresses, as desired. The PLAXIS models, however, show some deviation from a homogeneous initial effective stress state. PLAXIS clearly uses an automated algorithm to initialize the effective stresses which is independent of the user's inputs, and the result is a small linear increase in the initial effective stress with depth. At the bottom of the soil, the initial vertical effective stress is roughly 0.35 kPa. For the KAO material, this stress state remains on the recompression line of the constitutive model shown in Figure 3 such that the effect on the predicted volume change is negligible.

Theoretically, the steady state vertical effective stress at the bottom of the soil column should be 11.3 kPa (as calculated using the buoyant unit weight of the material in its initial condition multiplied by the initial height of the model, 2.5 m). Both ABAQUS models provide good approximations of this steady state stress state, though the Modified Cam Clay PLAXIS model appears to under-predict this stress.

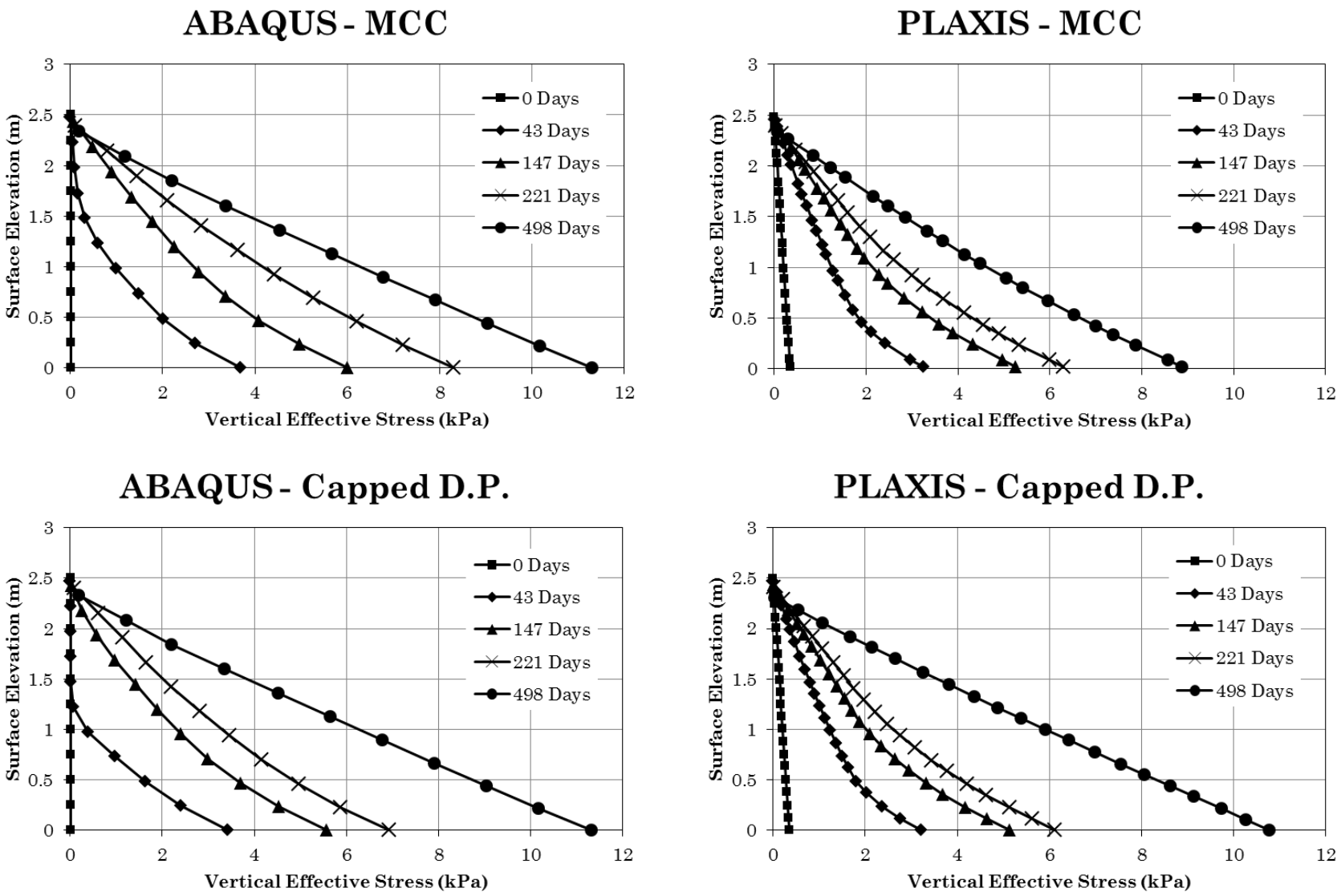

Figure 17: KAO Effective Stress Profiles Predicted by ABAQUS and PLAXIS

Stress paths were also used to assess how well each code adhered to the one-dimensional K_0 assumption. Using the relationship in (5), the K_0 value which was input into these codes was transformed into the q vs. p' stress space. This transformed parameter, η, represents the slope of the K_0 line in this stress plane.

Plots of the stress paths followed by each model are shown in Figure 18. For each model, five nodes were selected at five different elevations within the soil column. The legend in each plot shows the elevations above the bottom of the soil column at which the nodes were located *in the initial geometry*. These nodes were then followed in a Lagrangian fashion throughout the consolidation process, such that stress data was always collected from the same nodes regardless of their positions after consolidation began. Each marker in Figure 18 represents the stress state of the given node at an instant in time.

All stress paths in Figure 18 show a noticeable deviation from the K_0 line at lower stresses. These deviations are present at all locations within the soil column. It was observed that the initial slope of all four of these stress paths are roughly equivalent to the value of M, which is itself the value of η at critical state. Thus, these models appear to predict that the soil is in a near-critical state immediately after it is deposited. As consolidation progresses, the stresses move away from the critical state line and move back towards the K_0 line. Once the soil reaches a K_0 state of stress, the K_0 line is followed through the remainder of the consolidation process.

Here, it should be noted that the stress paths follow the critical state line *while they reside within the elastic zone of the initial yield surface*. Both plasticity models should show zero change in the mean effective stress within the elastic region, such that the stress path should be perfectly vertical. The slant in the predicted stress paths within the elastic region suggests that some algorithm other than the plasticity/elasticity models drives the stress/strain development prior to the point where the soil yields. Recall from sections 3.1.1 and 3.1.2 that both the PLAXIS and ABAQUS codes make use of an uncoupled, nonlinear finite strain approximation algorithm (called "Updated Mesh" in PLAXIS and "NLGeom" in ABAQUS). Likely, these algorithms are active even while the stress state resides within the elastic zone. These algorithms would then cause some elastic strengthening of the soil, and would push the stress state along the critical state line. At some point, the plasticity model would begin to assert control over the soil's behavior. This point is likely coincident with the peak of the deviated region of the stress path. The region where the stress paths move from the peak down toward the K_0 line would then represent a transition from behavior dominated by the finite strain approximation algorithm to behavior dominated by the plasticity model. Once the stress path reached the K_0 line, the plasticity model would have begun to dominate the soil's behavior.

The ABAQUS Modified Cam Clay model shows a peak in the deviated region of the stress path to occur approximately where the stress path encounters the initial yield surface. However, the ABAQUS Capped Drucker-Prager model shows a

peak which occurs outside the initial yield cap/failure line. This may be explained by the fact that the Cap Plasticity model in ABAQUS uses a non-associated plastic potential surface along the failure line, which exists above the failure line (Dassault Systems, 2013). Both PLAXIS models show a peak occurring before the yield surface or the Drucker-Prager failure line are encountered. Thus, PLAXIS must use a unique method to determine when the plasticity algorithm is invoked. The workings of this method and the development of the Soft Soil plasticity model are not clear from the literature provided with the PLAXIS code, nor are they explained in detail on their website. Thus, the criteria for activation of the plasticity model in PLAXIS remain unknown.

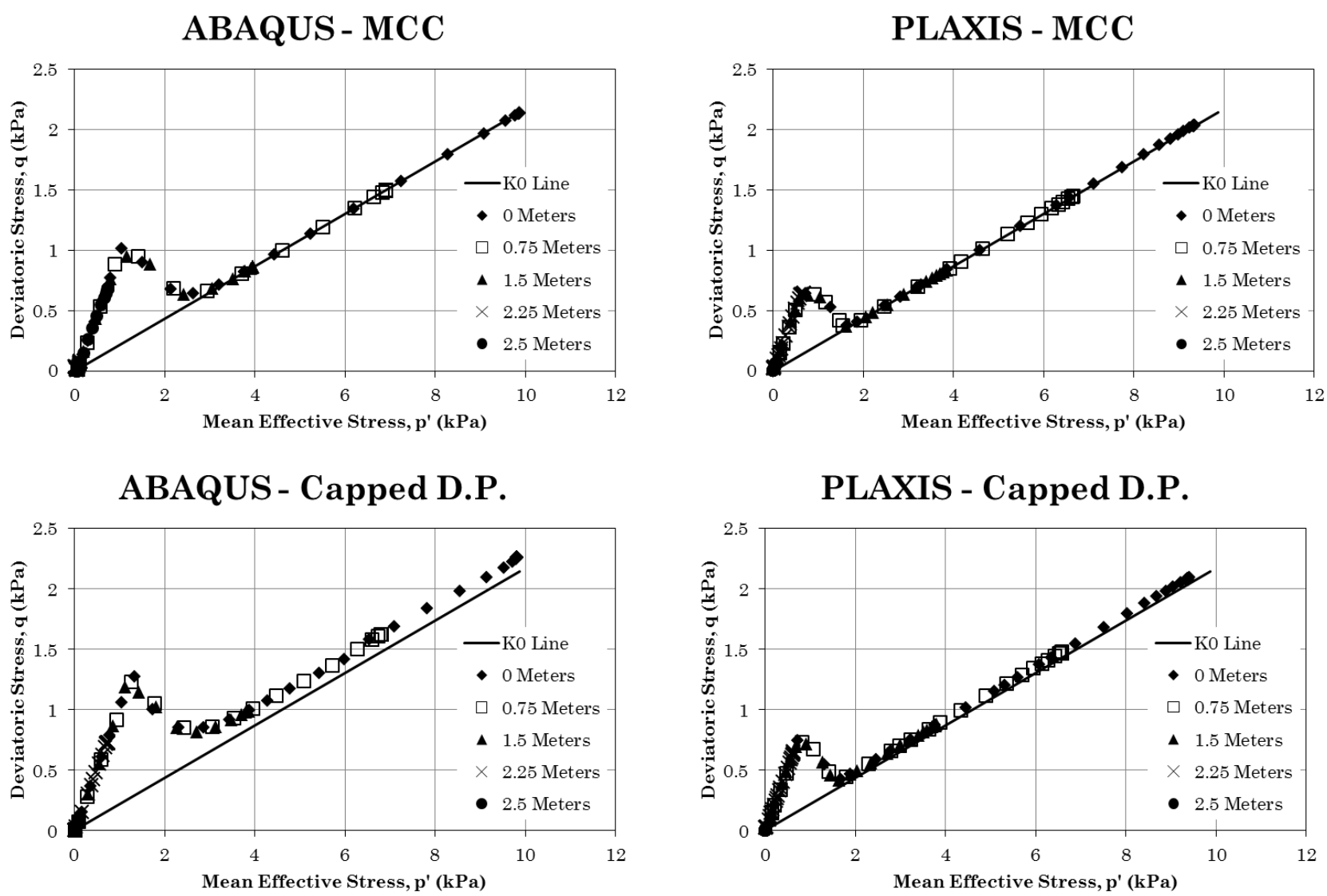

Figure 18: KAO Effective Stress Paths Predicted by ABAQUS and PLAXIS

Figure 19 shows the constitutive behavior of several nodes within each model. The same nodes which were tracked in the stress path plots were also tracked to show the constitutive behavior of each model. The line labeled CONDES in each constitutive plot is a direct representation of the constitutive relationship in (1), which the Modified Cam Clay and Capped Drucker-Prager model parameters were fit to.

All four models show a reasonable match to the desired CONDES behavior. Note that both of the ABAQUS models used an initial effective stress of 0.01 kPa, though the constitutive behavior of both models shows stresses occurring below 0.01 kPa. ABAQUS is thus predicting a stress reduction, particularly near the top of the soil column, which leads to a slight volume increase. The void ratio profiles in Figure 16 corroborate this observation, as the void ratios near the top of the soil column appear to increase slightly for both of the ABAQUS models. Both of the PLAXIS models also show some stress relaxation near the top surface of the soil, as can be seen indirectly by the slight increases in the void ratios at the top of each PLAXIS void ratio profile. However, the effect is much less pronounced in the PLAXIS models. Although the cause of this is unknown, the effect on the void ratio is minimal and the overall effect on the total soil volume is negligible.

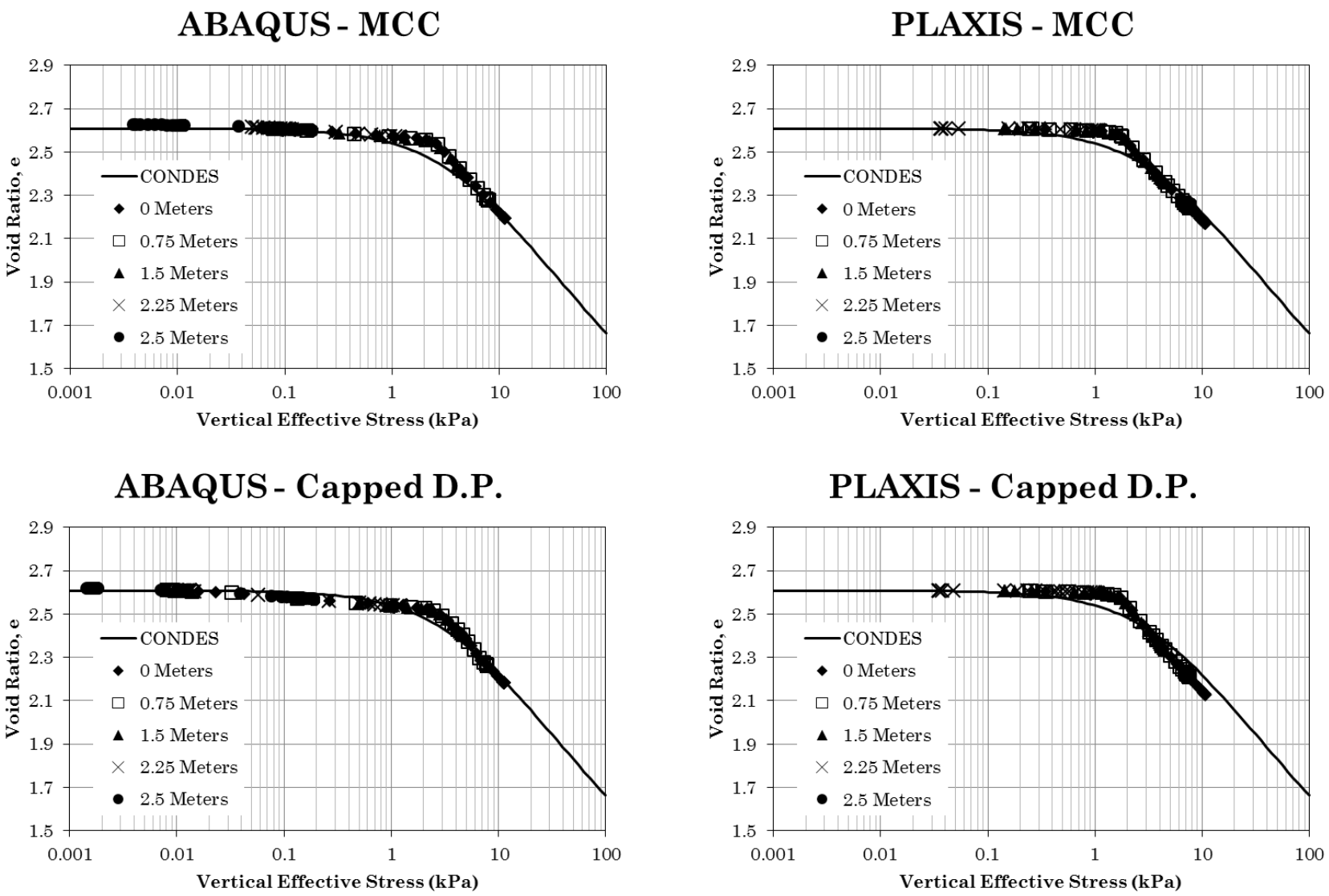

Figure 19: KAO Constitutive Behavior Predicted by ABAQUS and PLAXIS

3.2.2. One-Dimensional Results: Keystone Example Tailing

Keystone example tailing (KEX material) is somewhat softer than kaolin clay, as evidenced by its higher initial void ratio and lower preconsolidation stress. This material was included to represent a tailing slurry produced by a typical thickener used in mining operations. However, the details of the mineralogy and geographical source of this material are not at the liberty of the author to disclose.

Figure 20 and Figure 21 provide the settlement curves predicted by both ABAQUS and PLAXIS. The ABAQUS Modified Cam Clay model provided a good match to the expected settlements predicted by CONDES. The ABAQUS Capped Drucker-Prager model, on the other hand, provided a less reliable match. Both of the PLAXIS models were quite far from the expected settlement. Such a large deviation in the PLAXIS models was caused by an assumption made by PLAXIS that the preconsolidation pressure cannot be less than 1 kPa. Thus, any volume changes occurring at stresses below 1 kPa cannot be captured by PLAXIS without alteration to some of the application's source code input files.

The predicted void ratio distributions from PLAXIS in Figure 23 confirm that the reduction in void ratio predicted by PLAXIS is considerably less than that predicted by CONDES in Figure 22. The ABAQUS Capped Drucker-Prager void ratio profiles show a relatively good fit to the CONDES predictions, though an abrupt change in the slope of the curve at 150 days and a less abrupt change in the curve at 24 days are present in the ABAQUS profiles. The cause of these issues is unknown.

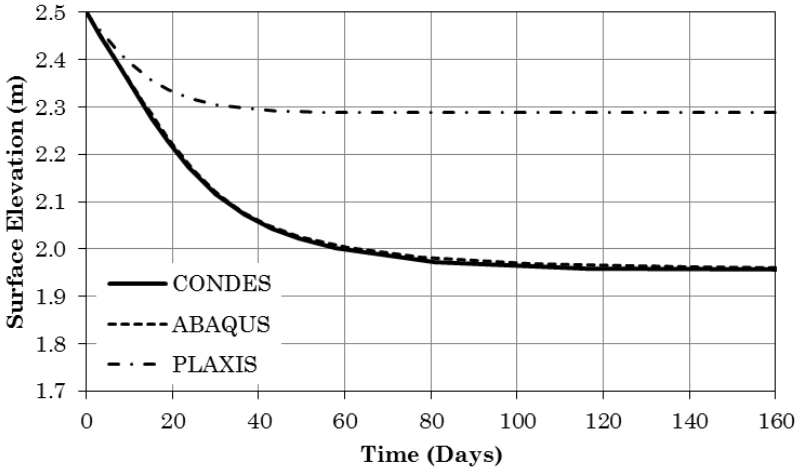

Figure 20: KEX Settlements Predicted by the Modified Cam Clay Model

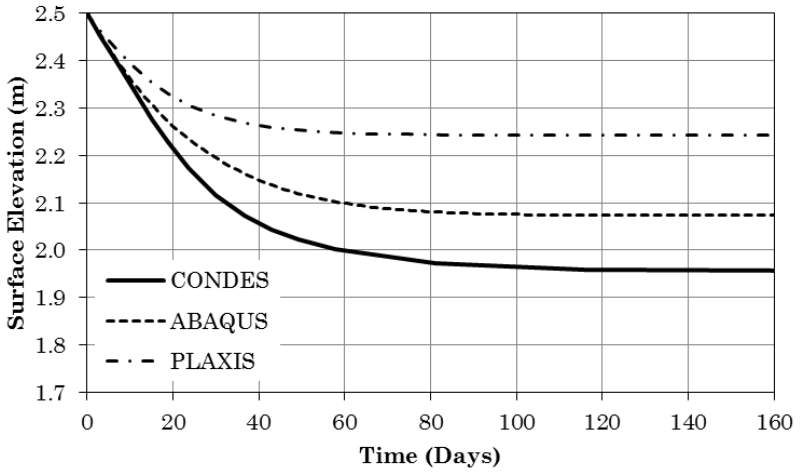

Figure 21: KEX Settlements Predicted by the Capped Drucker-Prager Model

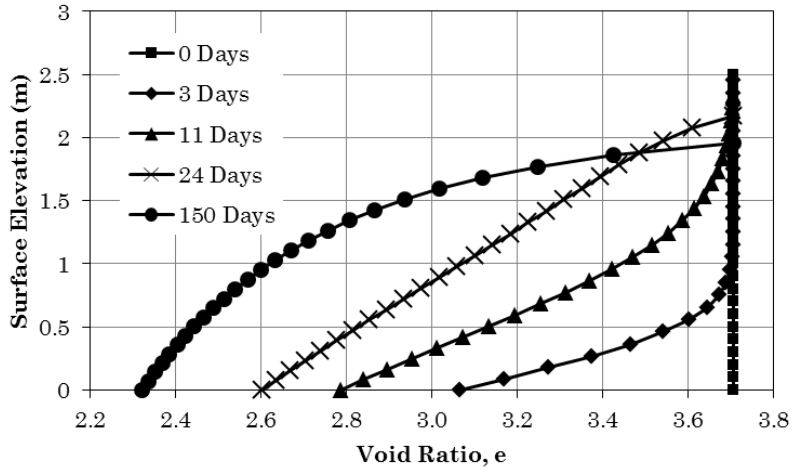

Figure 22: KEX Void Ratio Profiles Predicted by CONDES

Note that the ABAQUS Modified Cam Clay void ratio profiles match very well with those predicted by CONDES. The profiles are similar in both shape and magnitude. However, there again exists a slight increase in the void ratio at the top of the soil column for both of the ABAQUS models. The increase in void ratio is only observed in the steady state profile (i.e. at 150 days). This is different than the increased void ratios observed in the KAO ABAQUS models, which occurred at times earlier in the consolidation process and which did not appear in the steady state profile. Thus, the plasticity models may be predicting some slight dilatancy in the regions of the soil where the effective stresses do not rise appreciably. In these regions, the stress state will always be near either the yield ellipse or the failure line, and some dilatancy would be predicted if the stress state were to encounter the dry side of the yield/plastic potential curves.

The effective stress profiles depicted in Figure 24 are all somewhat similar, though it can be assumed that the ABAQUS Modified Cam Clay profiles represent the true state of the soil due to the close match this model had to the CONDES predictions. Because the effective stress states in the PLAXIS models are similar to those from the ABAQUS models, it can be concluded that the discrepancies in the PLAXIS settlement and void ratio predictions are caused by the 1 kPa minimum preconsolidation pressure used by PLAXIS. This observation is confirmed in the PLAXIS constitutive plots provided later.

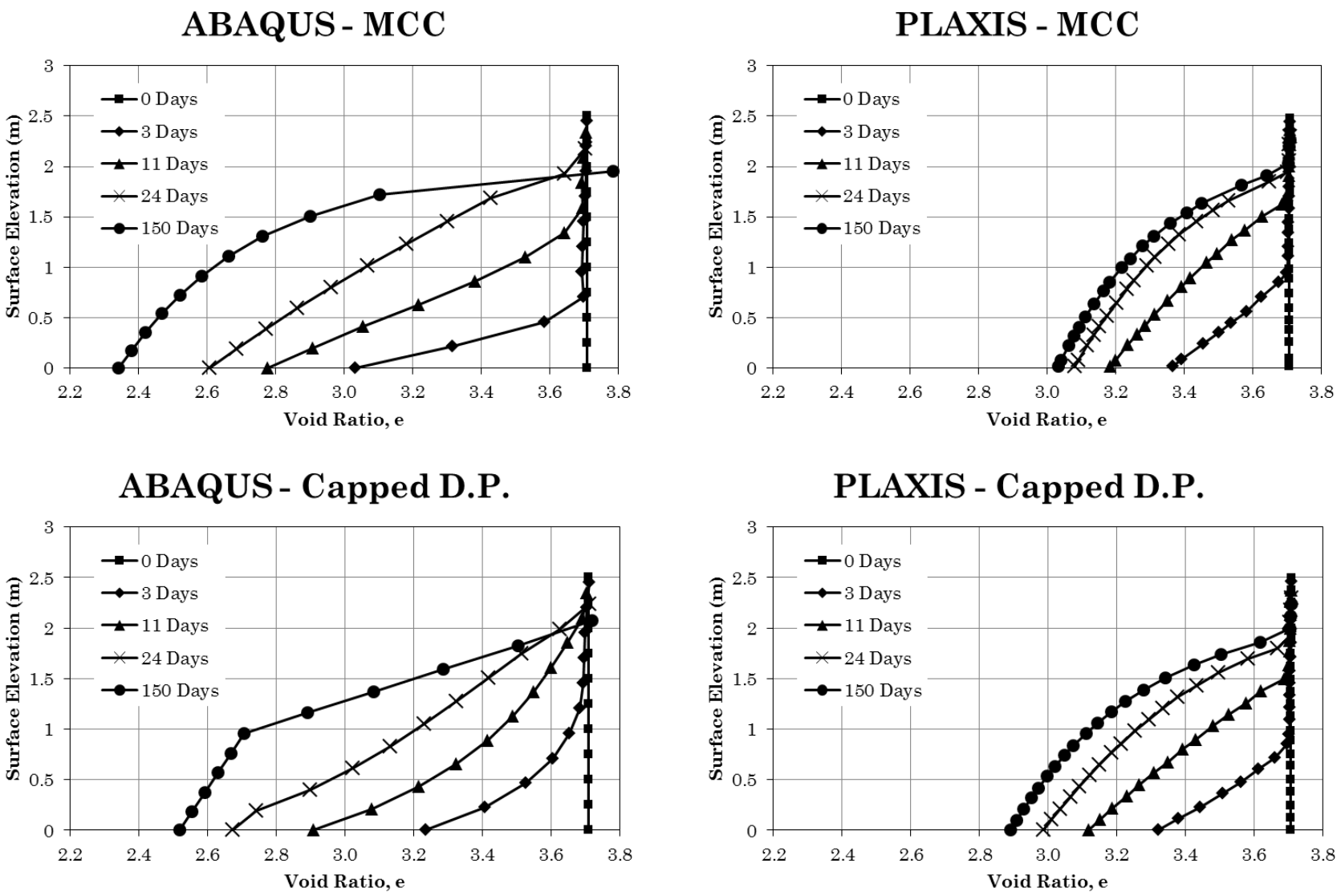

Figure 23: KEX Void Ratio Profiles Predicted by ABAQUS and PLAXIS

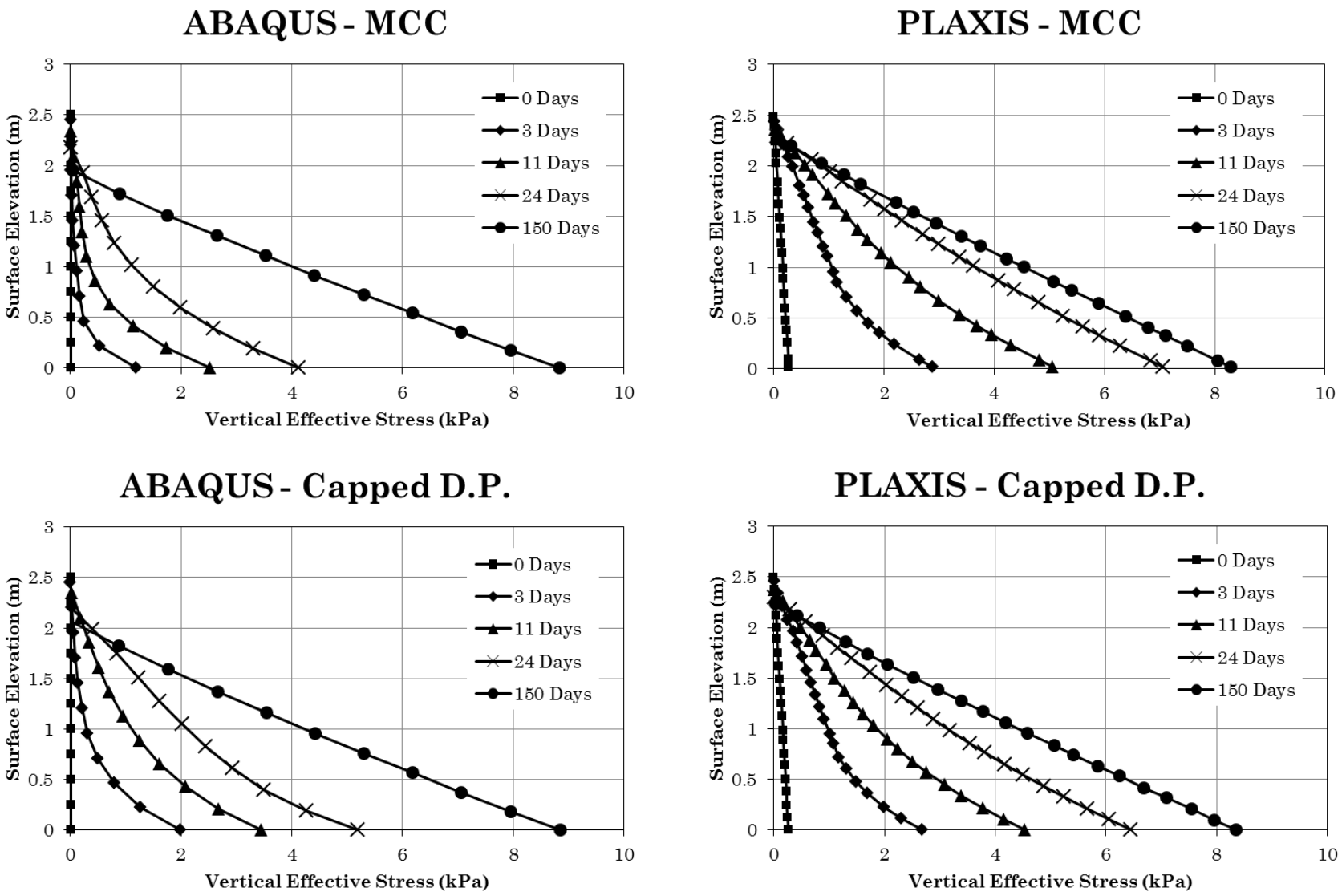

Figure 24: KEX Effective Stress Profiles Predicted by ABAQUS and PLAXIS

The effective stress paths predicted by both of the ABAQUS models in Figure 25 show behavior which closely matches the K_0 line. Here again, a deviation from the K_0 line is noticeable at lower effective stresses, though the deviation is much smaller in magnitude for the KEX material than was observed in the KAO material. The initial yield surface for the KEX material is much smaller than that of the KAO material. As a result, stress paths which follow the critical state line would encounter the yield surface at lower effective stresses. The result would be that the plasticity model would take control from the approximated finite strain algorithm earlier in the consolidation process, resulting in less deviation from K_0 behavior.

Some deviations in the ABAQUS Capped Drucker-Prager model can also be observed at larger stresses. These deviations are not fully understood, but may be a consequence of some slight differences between the cap yield surface and the Modified Cam Clay elliptical yield surface used in ABAQUS. The deviation is small, however, and it is likely not the cause of any discrepancies in the volumetric response of the soil.

Figure 25 shows a larger deviation in both of the PLAXIS models at lower effective stresses. The range of the deviated stresses still falls within the initial yield surface, however, because PLAXIS used a preconsolidation stress of 1 kPa for the KEX models. Thus, this deviation will appear in all PLAXIS models because the initial yield surface for any soil will use a preconsolidation stress of 1 kPa or greater.

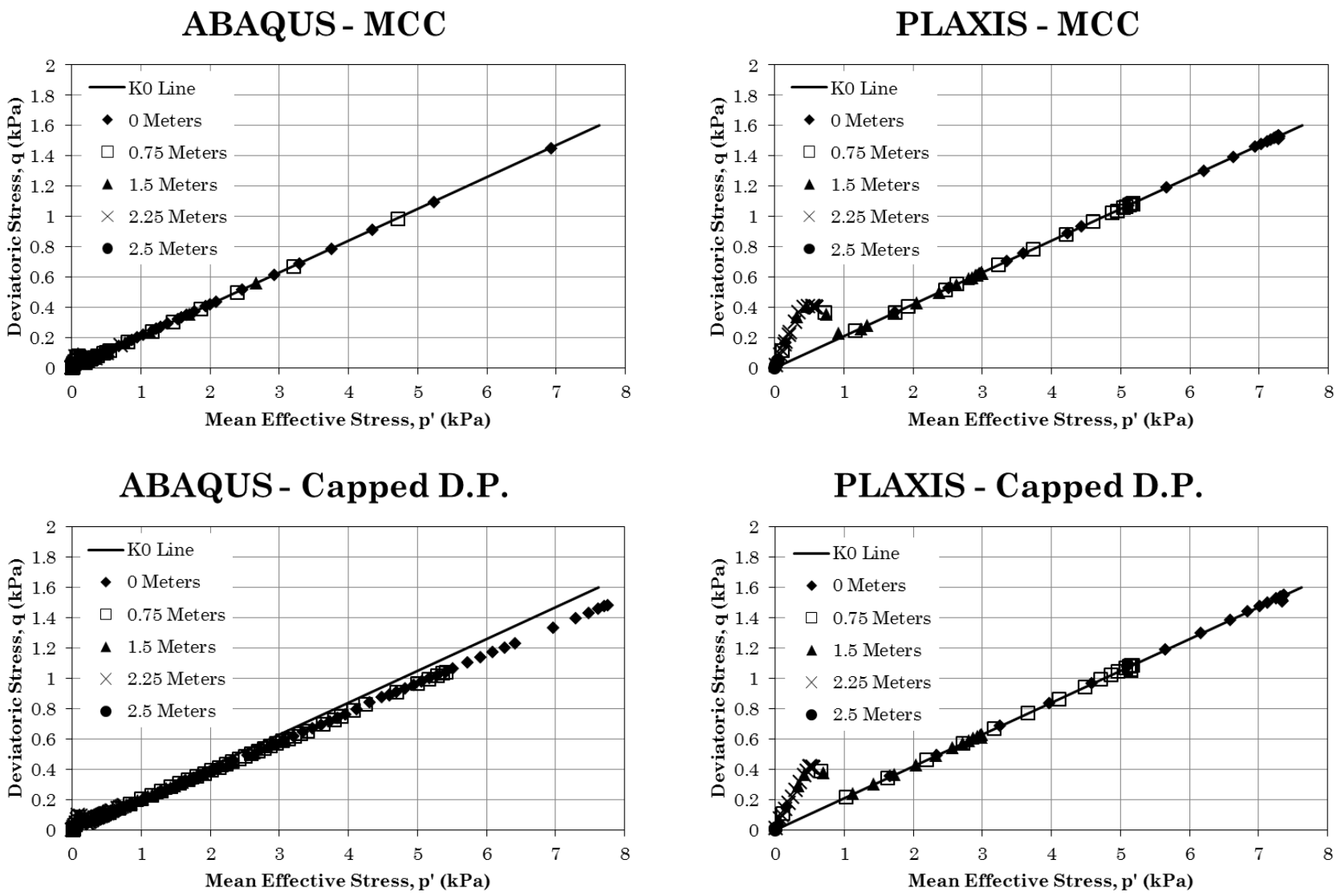

Figure 25: KEX Effective Stress Paths Predicted by ABAQUS and PLAXIS

The constitutive plots in Figure 26 show another, related consequence of the 1 kPa preconsolidation stress used by PLAXIS. Both PLAXIS models predicted constitutive paths which are shifted to the right as compared to the CONDES line. This shift is evidence that PLAXIS used a preconsolidation stress of 1 kPa, as the sharp break in the constitutive path (which represents the intersection of the URL and the NCL) occurs at approximately 1 kPa in both models. The result is that, for any given vertical effective stress, the void ratio predicted by PLAXIS will be greater than expected resulting in less predicted settlement.

Also in Figure 26, the ABAQUS Capped Drucker-Prager model shows more curvature in its constitutive behavior than it did when using the KAO material. This curvature is likely caused by the stress paths encountering the Drucker-Prager failure line instead of encountering the Modified Cam Clay cap. Because the plastic potential is non-associated along the failure line, the development of the stresses and thus the void ratios will be different than those predicted by the pure Modified Cam Clay model. Near an effective stress of 10 kPa, the model appears to revert back to linear behavior at a slope approximately the same as the CONDES line. Thus, for larger models which developed greater effective stresses, the Cap Model in ABAQUS would likely continue along this line and follow the CONDES path.

Note that the ABQUS Modified Cam Clay model showed some dilatancy at lower effective stresses. This observation confirms that the increase in void ratio near the top of the model was somehow the result of the constitutive model, though this deviation from the expected constitutive behavior remains unexplained.

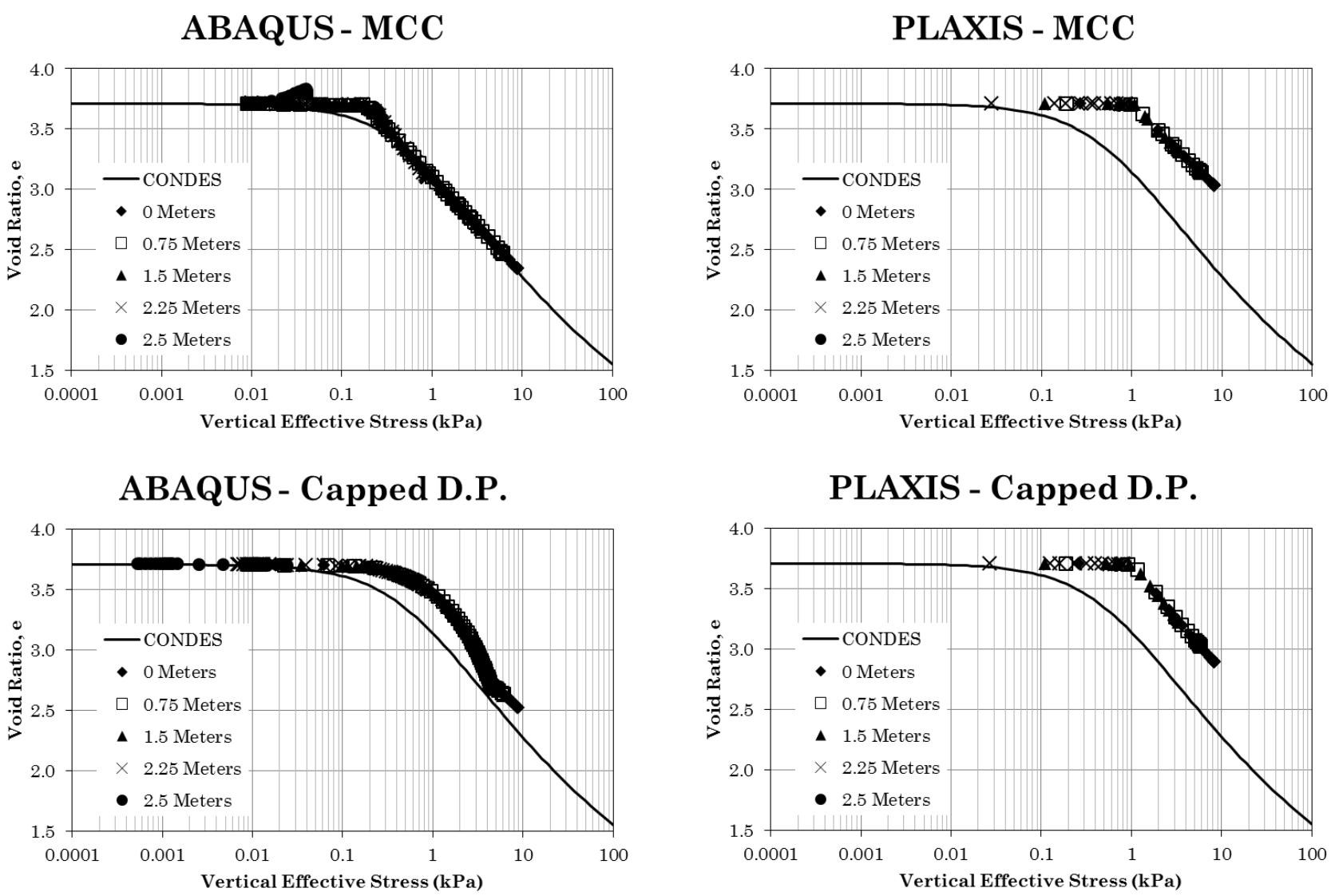

Figure 26: KEX Constitutive Behavior Predicted by ABAQUS and PLAXIS

3.2.3. One-Dimensional Results: Gulf of Mexico Dredged Material

Soil dredged from the Gulf of Mexico (GOM material) was then modeled using ABAQUS and PLAXIS. This material is slightly more compressible than the KEX material, and is representative of the fine-grained material which might be used to fill geotextile tubes in the scenario where no sandy material is economically available. Other than the material parameters presented in Table 1, no details are available concerning the mineralogy or geographical origins of this material.

Settlement curves predicted using the two available plasticity models are presented in Figure 27 and Figure 28. The ABAQUS Modified Cam Clay model again provided a reasonable fit to the expected settlement curve, while the ABAQUS Capped Drucker-Prager predictions were less accurate. Both PLAXIS models again showed substantial deviation from the expected CONDES settlement curve due to the 1 kPa preconsolidation stress assumed by PLAXIS.

A comparison between the CONDES void ratio profiles in Figure 29 with the ABAQUS and PLAXIS predicted curves in Figure 30 then show how the ABAQUS Modified Cam Clay model matched the CONDES profiles quite well, while the ABAQUS Capped Drucker-Prager model provided only a rough match. Again, the PLAXIS void ratio profiles proved to be poor representations of the expected CONDES profiles. Also of interest is the fact that in these models, ABAQUS shows a *reduction* in the void ratio at the top surface of the models as opposed to the dilation observed previously.

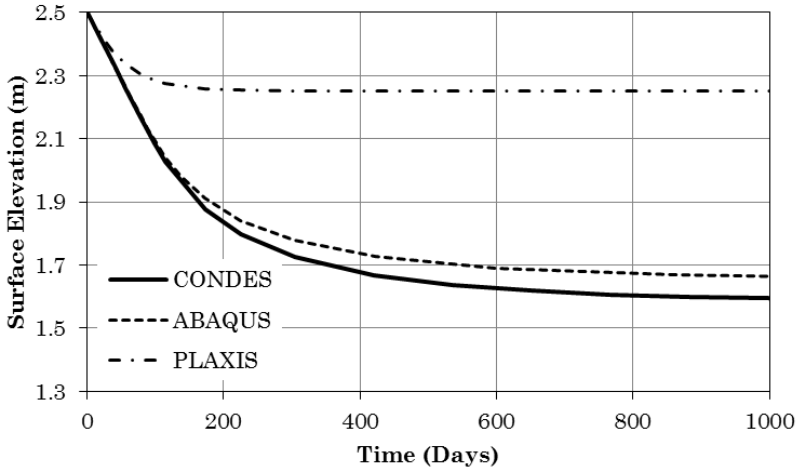

Figure 27: GOM Settlements Predicted by the Modified Cam Clay Model

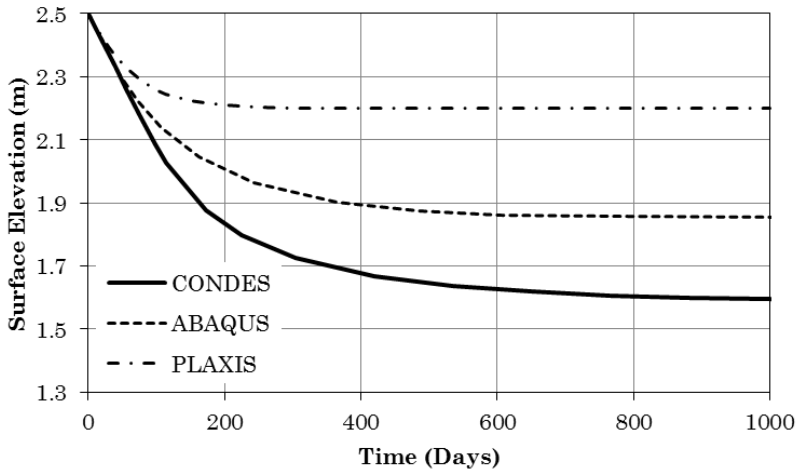

Figure 28: GOM Settlements Predicted by the Capped Drucker-Prager Model

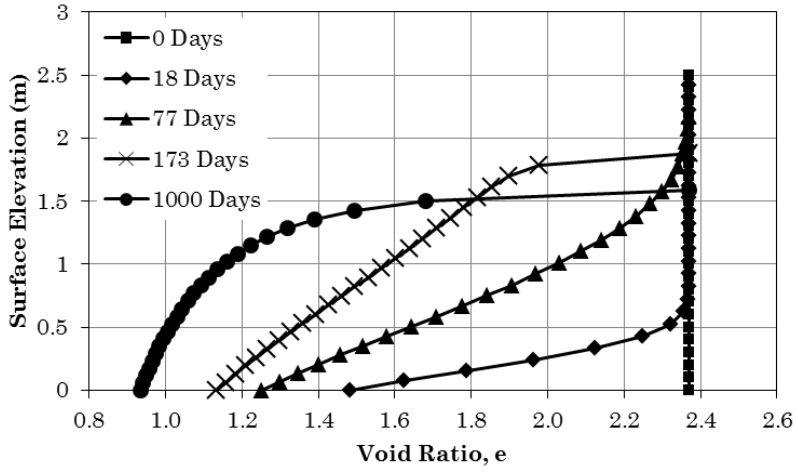

Figure 29: GOM Void Ratio Profiles Predicted by CONDES

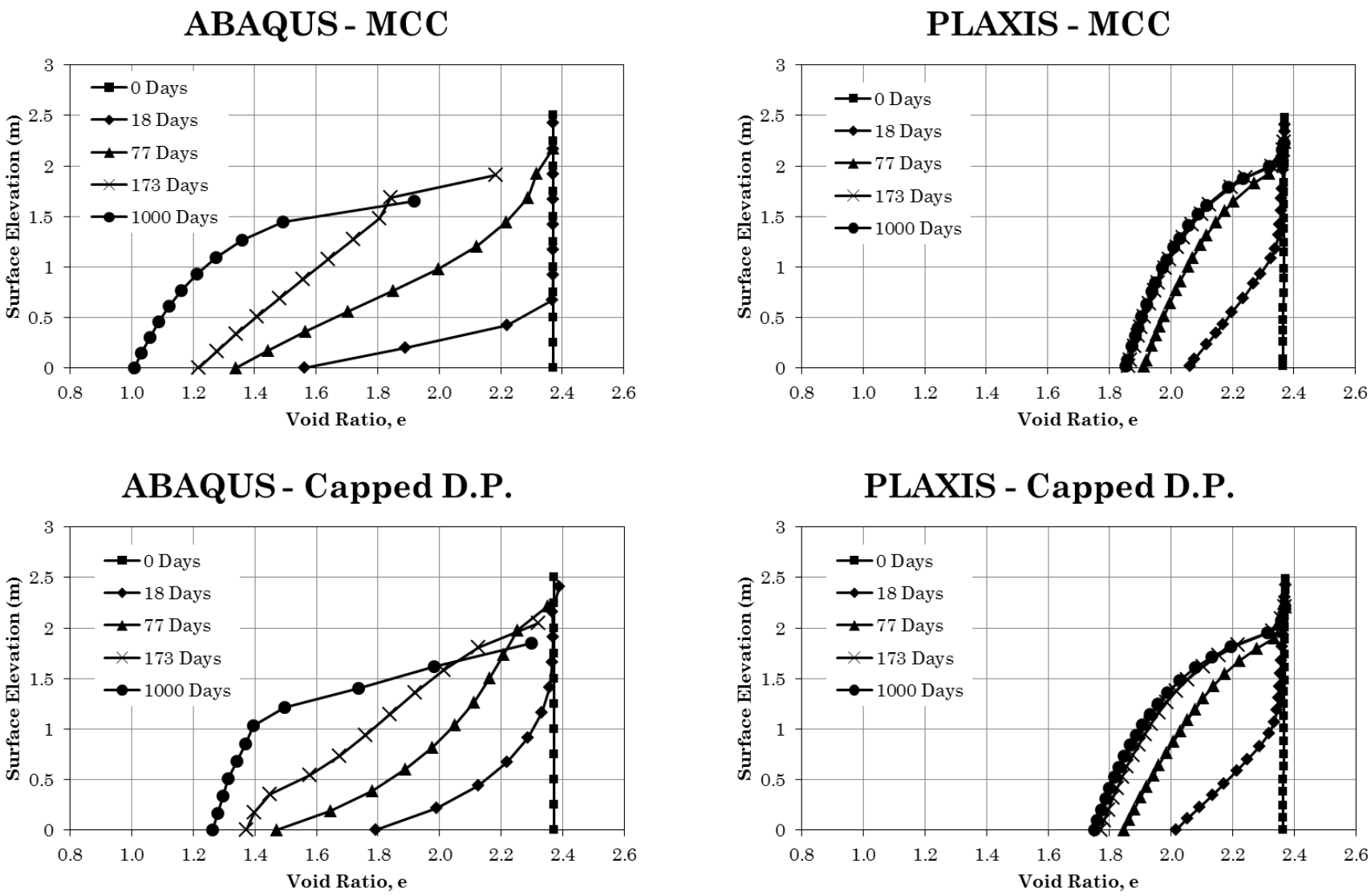

Figure 30: GOM Void Ratio Profiles Predicted by ABAQUS and PLAXIS

The vertical effective stress profiles in Figure 31 show only a minor stress increase at the top surface. However, the GOM material is so highly compressible that even minute changes in the effective stress state would lead to noticeable changes in the void ratio. Here, the void ratio at the top surface predicted by the ABAQUS Modified Cam Clay model at steady state is approximately 1.9. Solving (1) for the vertical effective stress at a void ratio of 1.9 using the GOM properties in Table 1 produces a stress of 0.2 kPa. The stress increase observed in the steady state effective stress profile is roughly equal to 0.2 kPa. Thus, the void ratio reduction observed at the top of the soil is the result of a minor increase in stress which is amplified by the compressibility of the soil. Note that the KAO material showed a similar small stress increase near the top surface of the soil at steady state in the ABAQU S Modified Cam Clay models. The compressibility of the KAO material is substantially less than that of the KEX material, such that the stress increase did not result in a significant change in the void ratio.

Also note that the initial and final vertical effective stress profiles in all four GOM models take on roughly the same shape, though the final heights differ. This same pattern is true of the vertical effective stress profiles in the KAO and KEX models as well. As a result, the PLAXIS and ABAQUS codes can be assumed to correctly compute the stress states within the soil. The differences in the transient vertical effective stress profiles are the result of the abnormally high transient void ratios, which lead to increased hydraulic conductivity, increased rate of excess pore pressure dissipation, and thus increased rate of change in the effective stresses.

The ABAQUS GOM models also show stress paths which align quite well with the theoretical K_0 line. The preconsolidation stress for the GOM material is even smaller than that for the KEX material, such that if any deviations are present in the ABAQUS stress paths at low stress levels they are imperceptibly small due to the small initial yield surface. Again, both of the PLAXIS model stress paths show a larger deviation at lower effective stresses.

The constitutive behavior predicted by the four GOM models in Figure 33 follows similar trends to those established in the KEX models. The ABAQUS Modified Cam Clay model showed a good match to the target CONDES curve, while the ABAQUS Capped Drucker Prager model again showed some excess curvature in its constitutive path which caused it to deviate from the CONDES curve. The 1 kPa preconsolidation stress used by PLAXIS again caused both of the PLAXIS models to shift considerably to the right. As with the KEX PLAXIS models, this resulted in the prediction of less volume change than would be expected.

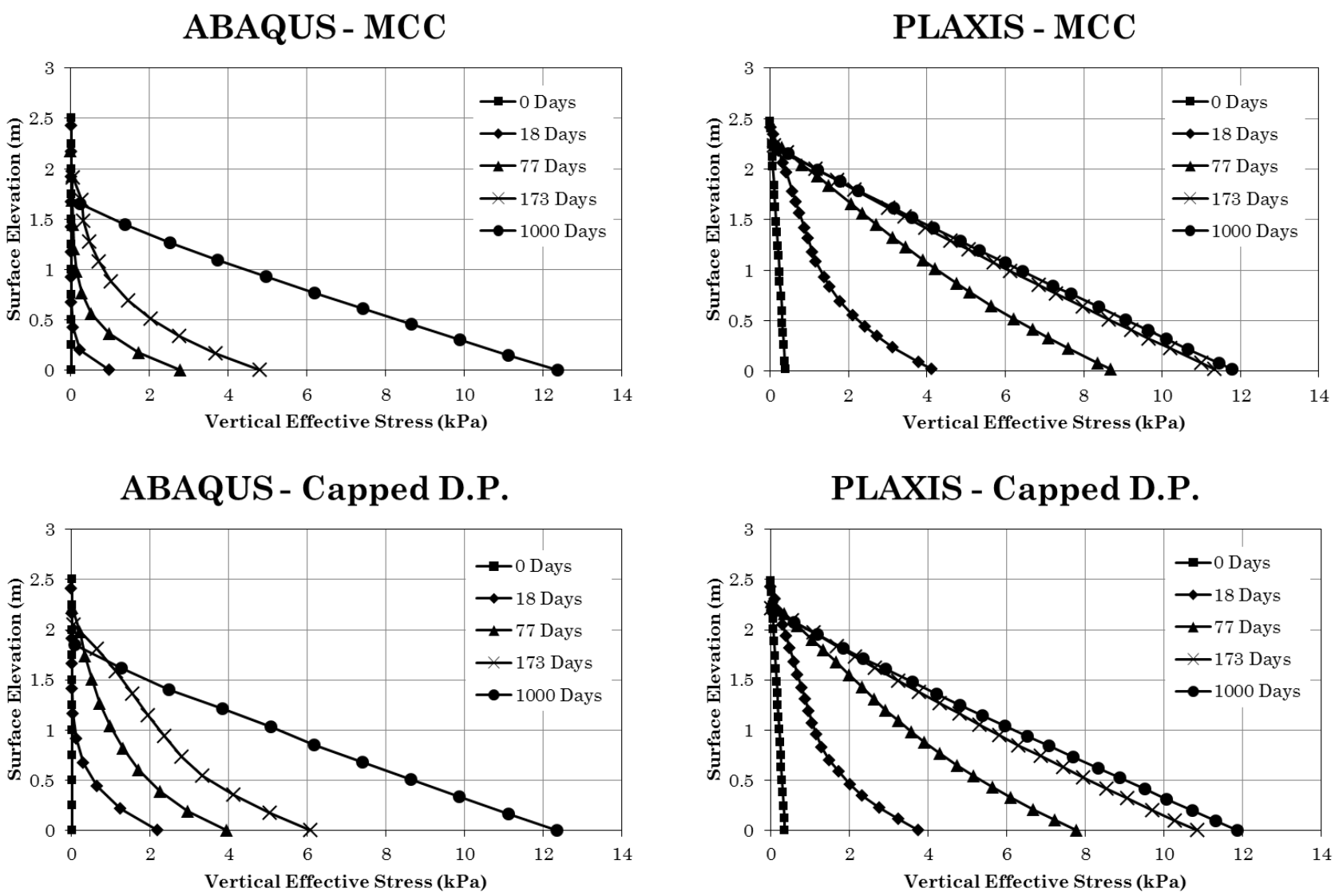

Figure 31: GOM Effective Stress Profiles Predicted by ABAQUS and PLAXIS

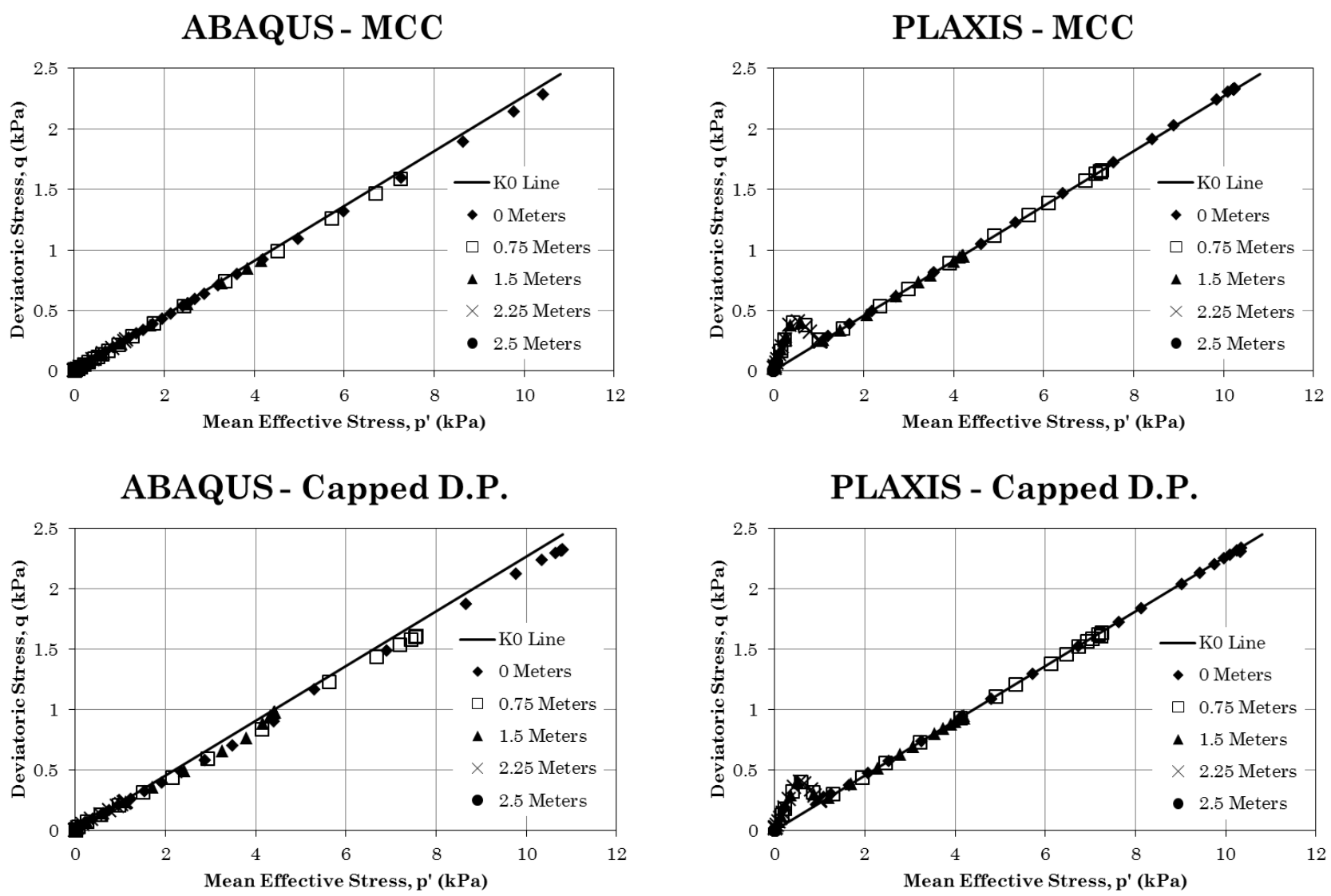

Figure 32: GOM Effective Stress Paths Predicted by ABAQUS and PLAXIS

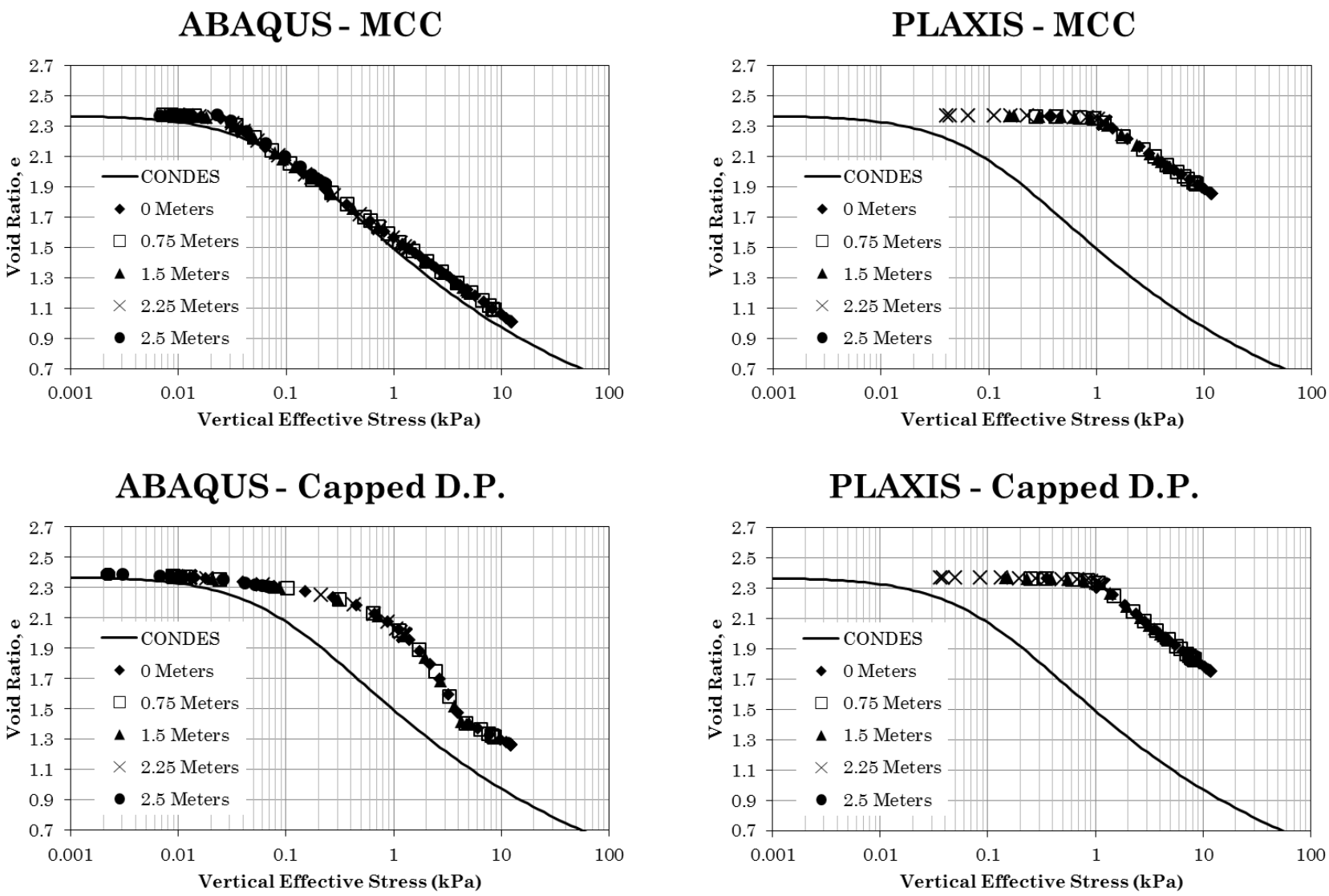

Figure 33: GOM Constitutive Behavior Predicted by ABAQUS and PLAXIS

3.2.4. One-Dimensional Results: East Coast Dredged Material

East coast dredged material (ECM material) is a slurry-type soil which was dredged from the ocean floor. This material represents the most compressible material of the four soils tested. ECM material shows by far the largest initial void ratio, and also the smallest initial preconsolidation stress. From Figure 1 it can be seen that this material undergoes much larger changes in void ratio over the expected range of stresses than any of the other soils. As a result, it was expected that this soil would prove to be the most difficult to model numerically because of how rapidly its volume reduces under very small stresses.

This expectation proved to be correct. The relatively drastic changes in void ratio with relatively small changes in effective stress required noticeably greater computational effort to successfully compute. It was also found that these ECM models were sensitive to the maximum time step allowed during the calculations. When the maximum time step was set too small, the calculations entered a state of numerical oscillation which compounded in each successive time step to the point where the error grew beyond the tolerated limits. Increasing the maximum time step resolved this issue. Note that both PLAXIS and ABAQUS use dynamic time stepping, such that they will automatically reduce the time step if needed to achieve the desired accuracy. Thus, the best practice for simpler, one-dimensional consolidation models is to use a large maximum time step and to allow the automated time stepping algorithm to choose the correct length for each time step.

Here, maximum time steps of roughly ten per cent of the total time interval were specified to allow the model to successfully compute.

Figure 34 and Figure 35 show the settlements predicted by the four ECM models. Here again, the settlements predicted by the ABAQUS Modified Cam Clay model proved to be the most accurate of the four models. With this extremely compressible ECM material, some discrepancy still exists in the ABAQUS Modified Cam Clay predicted settlements, though it is much less than the discrepancies in any of the other three models. Again, the PLAXIS models produced erroneous results due to the 1 kPa preconsolidation pressure assumption.

A comparison of the CONDES void ratio profiles in Figure 36 and the ABAQUS and PLAXIS void ratio profiles in Figure 37 also shows that the ABAQUS Modified Cam Clay model produced the most accurate results. However, even this model showed some error in the predicted void ratio at the bottom of the soil column at steady state (i.e. 20,000 days). A reduction in void ratio at the top of the soil column is also present in the ABAQUS Modified Cam Clay model at steady state. The vertical effective stress profiles in Figure 38 show a stress increase of roughly 0.1 kPa in this model at steady state. According to the CONDES constitutive model in (1), an effective stress of 0.1 kPa relates to a void ratio of 8.23 which roughly matches the void ratio predicted at the top of the soil column in Figure 37. Thus, it can be concluded that the void ratio reductions observed at the top of the soil columns in these ABAQUS models is attributable to a slight increase in effective stress in that region. The effect of slight stress increases on the void ratio is

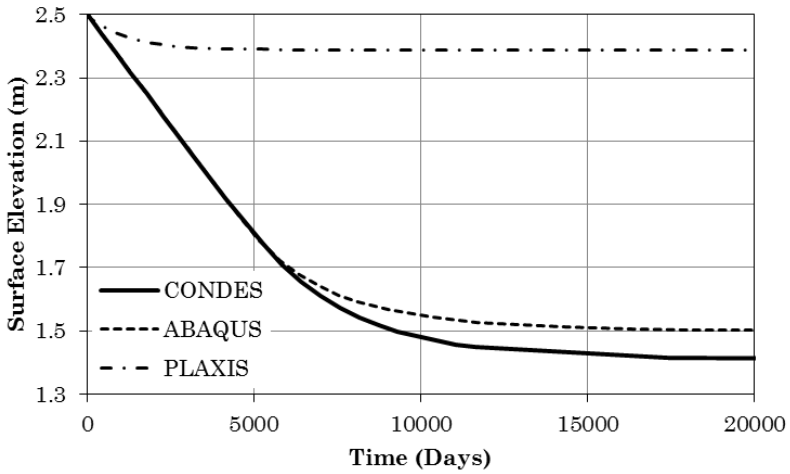

Figure 34: ECM Settlements Predicted by the Modified Cam Clay Model

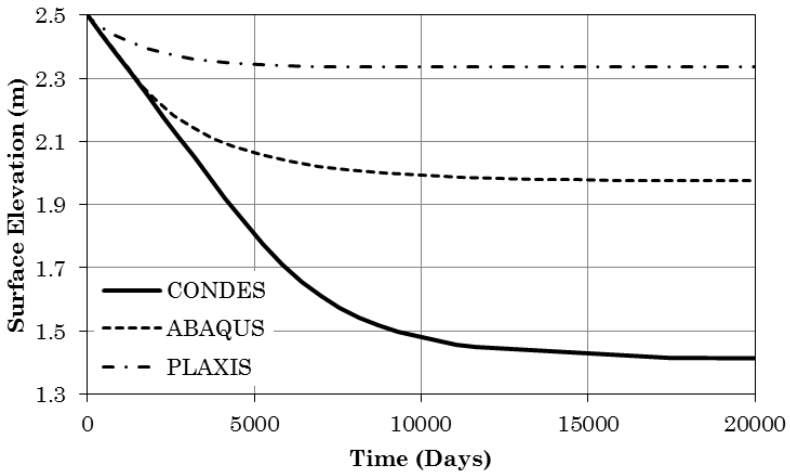

Figure 35: ECM Settlements Predicted by the Capped Drucker-Prager Model

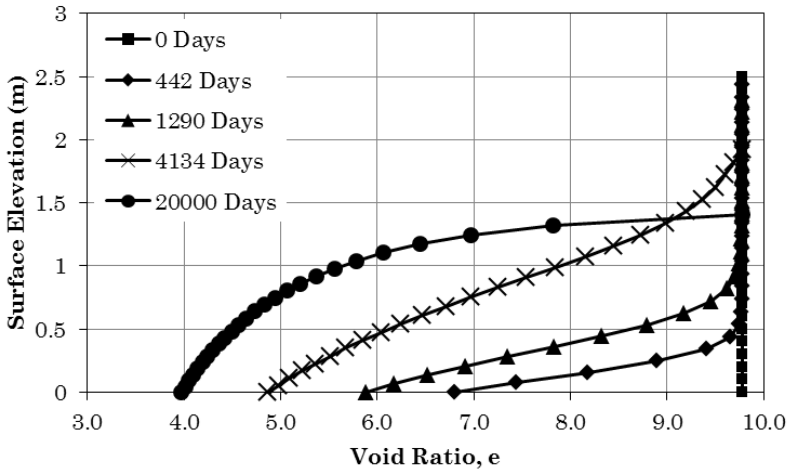

Figure 36: ECM Void Ratio Profiles Predicted by CONDE

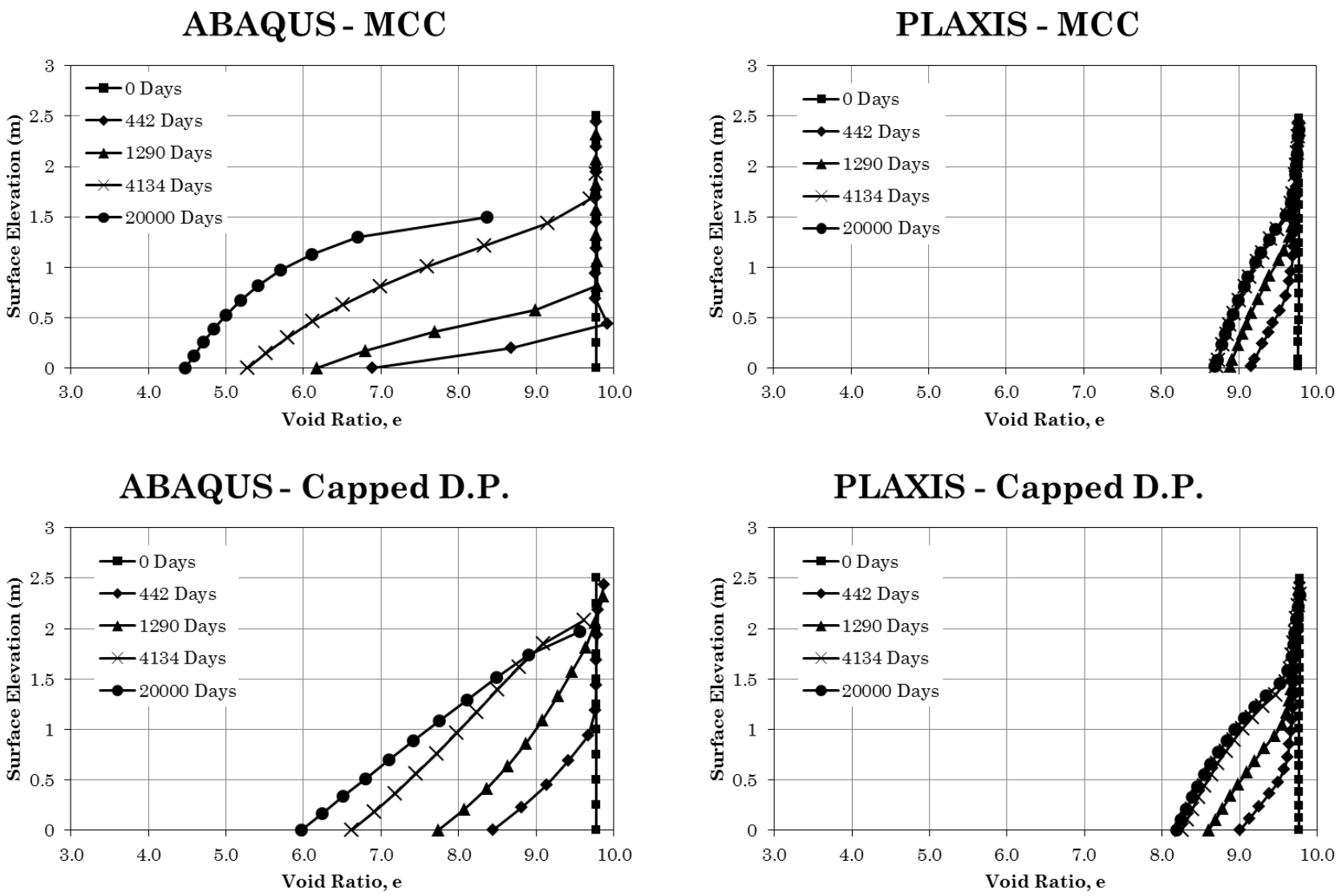

Figure 37: ECM Void Ratio Profiles Predicted by ABAQUS and PLAXIS

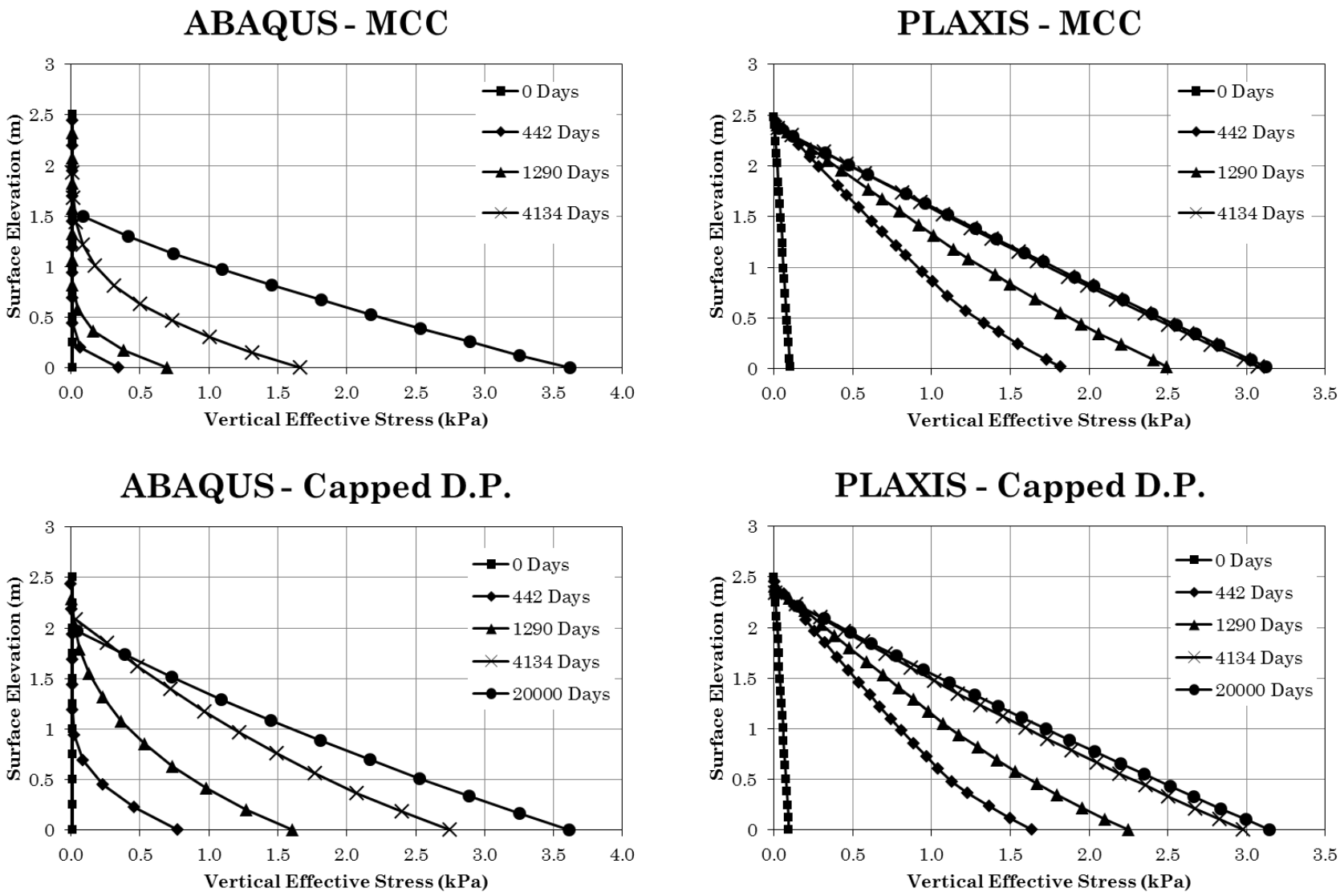

Figure 38: ECM Effective Stress Profiles Predicted by ABAQUS and PLAXIS

amplified in these highly compressible soils because of their tendency to rapidly reduce in volume under small effective stresses. However, the cause of the increased stress at the top of the soil columns remains unknown.

Figure 39 provides the stress paths predicted by each of the four models. As with all previous soils, the PLAXIS models show a noticeable deviation in the stress paths at lower stresses. Of particular interest with the ABAQUS ECM stress paths, though, is the linear deviation from the K_0 line predicted by the Capped Drucker-Prager model. The fact that the stress path remains linear indicates that the K_0 condition is preserved, but that the value of K_0 assumed by the Capped Drucker-Prager model is smaller than that shown in Table 2. Likely, this is a result of imperfect fitting of the Cam Clay cap to the ideal Modified Cam Clay elliptical yield surface through the parameter R. However, a substantially better fit is likely not possible due to the slight differences in the definitions of the cap surface and the Modified Cam Clay yield surface in ABAQUS.

The constitutive behavior of the ABAQUS Capped Drucker-Prager model is also more deviant than was observed in previous models. This is likely the result of two independent issues: an imperfect fitting of the parameter R and the non-associated plastic potential surface along the Drucker-Prager failure line.

Also note that the constitutive path of the ABAQUS Modified Cam Clay model varies somewhat from the CONDES curve. Recall that the fitted parameters used in all of these models were fit for stresses ranging from 0.001 kPa to 50 kPa. The maximum effective stress reached in these ECM models, however, was roughly

4 kPa. Thus, if the constitutive parameters were fit across a range of stresses closer to the range of stresses observed in the ECM models (e.g. 0.001 kPa to 5 kPa), the constitutive behavior of these models would likely match the CONDES curve more closely.

The slight mismatch in the constitutive parameters is also likely the cause of the mismatched settlement curves in the ABAQUS Modified Cam Clay model. Should the constitutive parameters have been better fit, the resulting settlement curves and void ratio profiles would more closely match the CONDES predictions.

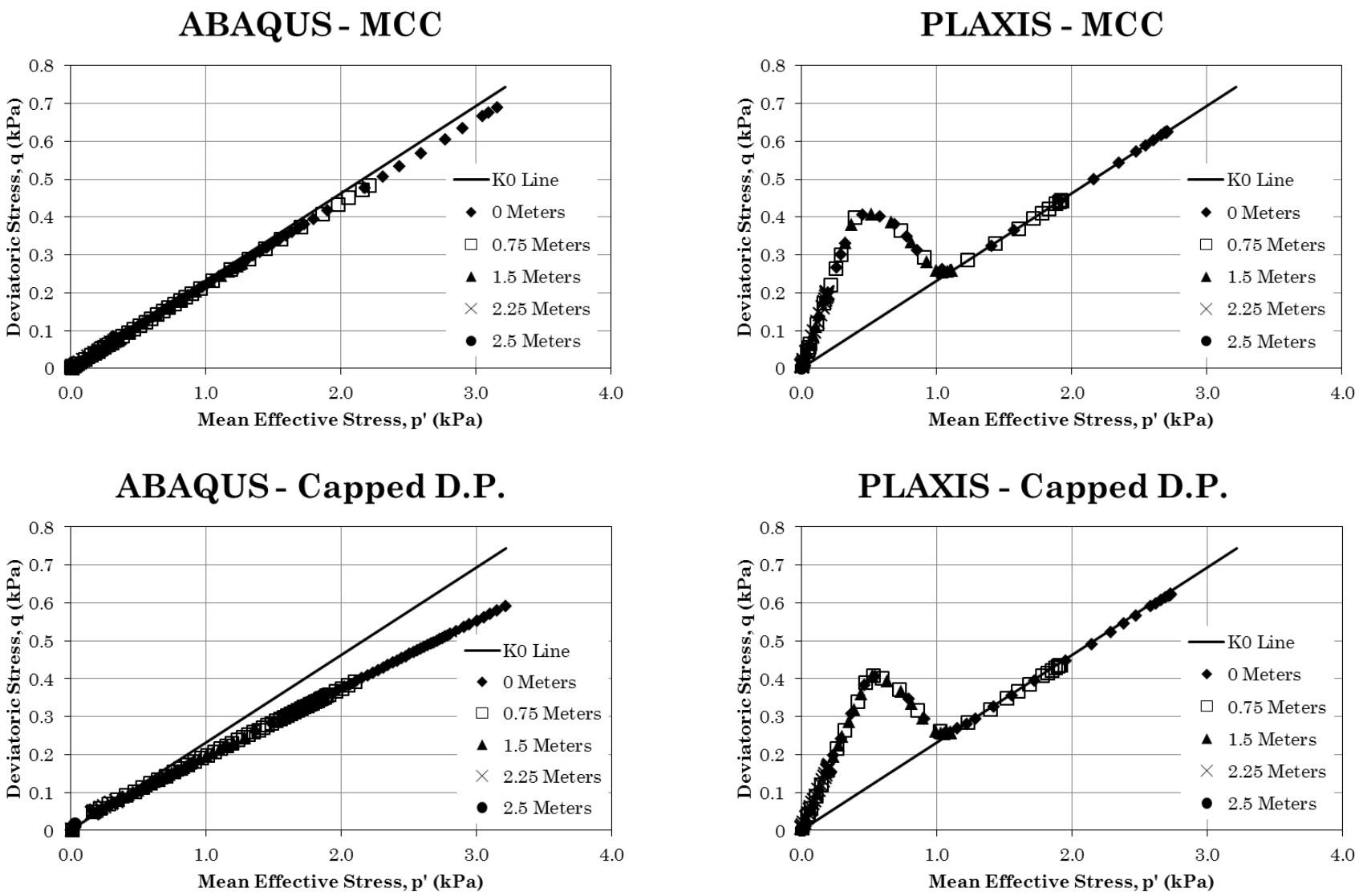

Figure 39: ECM Effective Stress Paths Predicted by ABAQUS and PLAXIS

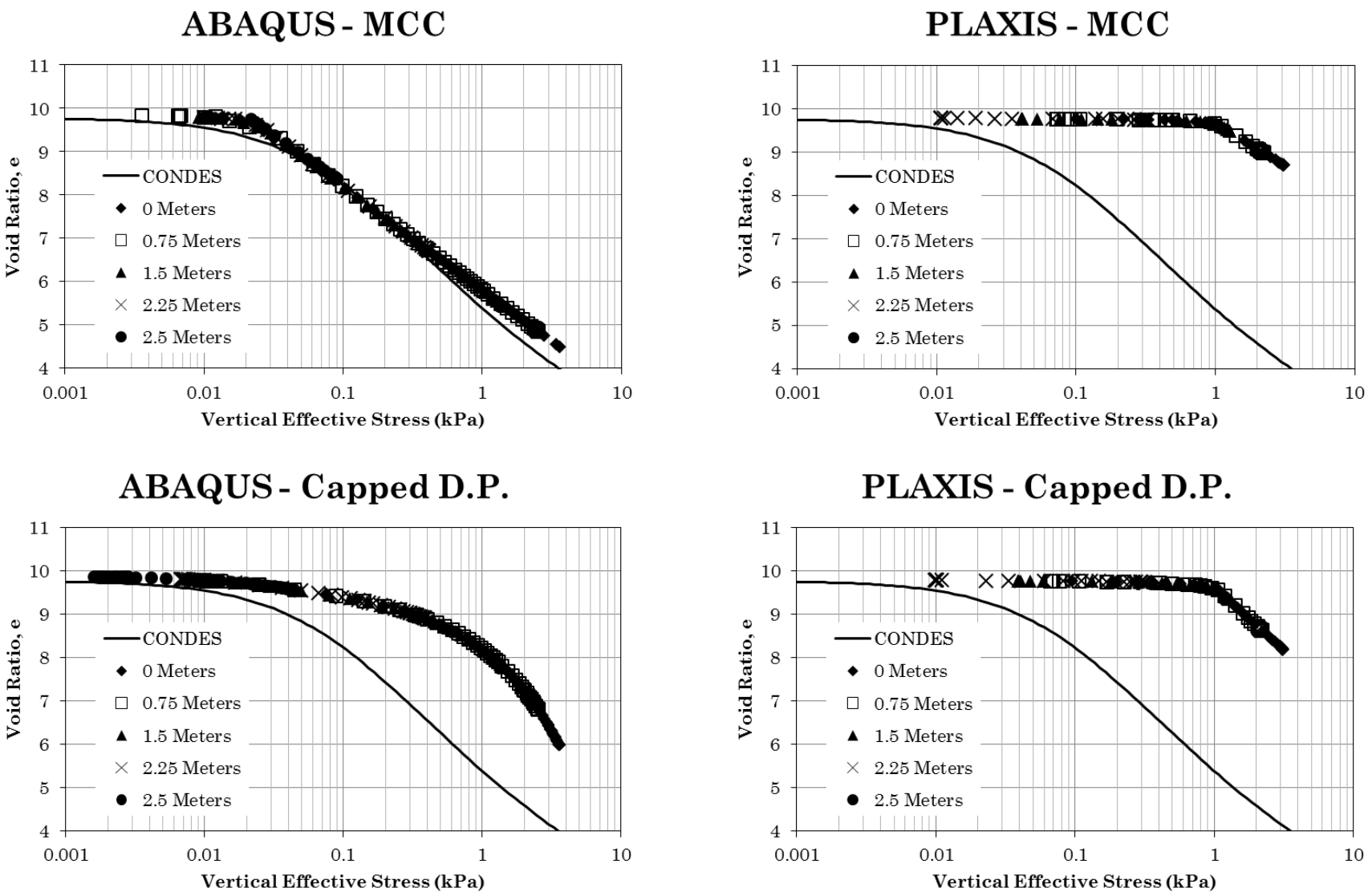

Figure 40: ECM Constitutive Behavior Predicted by ABAQUS and PLAXIS

3.3. One-Dimensional Modeling Conclusions

At the onset of this one-dimensional modeling effort, it was desired that the ABAQUS and PLAXIS codes be validated for use in modeling the consolidation of very soft, hydraulically deposited soils. An additional goal was then to determine if the Modified Cam Clay or Capped Drucker Prager plasticity model would provide a better match to the idealized constitutive model represented by (1).

Results from the KAO models appear promising for both the ABAQUS and PLAXIS codes. However, the PLAXIS code assumes a minimum preconsolidation stress of 1 kPa regardless of the true preconsolidation stress of the soil. This assumption is highly restrictive for materials with preconsolidation stresses significantly less than 1 kPa, as any volume changes which occur below 1 kPa are completely ignored by the code. The result is that PLAXIS will consistently under-estimates the reduction in volume of a highly compressible soil during self-weight consolidation. Results for the KAO material did not show this behavior because the material is relatively stiff with a preconsolidation stress above 1 kPa. Thus, it can be concluded that PLAXIS is only able to produce valid results for hydraulically deposited soils with preconsolidation stresses greater than 1 kPa.

ABAQUS, however, produced reasonable results for all four soils when using the Modified Cam Clay model. ABAQUS allows the user to directly control both the initial effective stress in the model and the preconsolidation stress of the soil. These inputs are still limited by the geometric and numerical complexity of the

models. Highly complex models require greater computational effort, and extreme complexities may lead to singularities in the ABAQUS solver algorithm if the initial stress in the soil is too near zero.

ABAQUS also gives the user more control over the properties of the finite element mesh. For example, either quadrilateral or triangular elements may be used, with the quadrilateral elements being of a lower order and generally less computationally taxing. For highly complex models, or for models which use highly compressible soils (e.g. ECM material), making use of the simpler quadrilateral elements and deactivating the "Reduced Integration" option for those elements greatly reduces the computational effort required to compute the model. By simplifying the finite element mesh, it becomes possible to reduce the initial effective stress to a level which allows the model to properly predict the constitutive behavior.

It was noticed that the void ratio profiles for the GOM and ECM ABAQUS materials showed some reduction in the void ratio at the top of the soil in steady state. The relatively high compressibility of these soils causes their predicted void ratios to be sensitive to relatively small effective stresses. Thus, when the numerical models predict small changes in effective stress at the soil surface, the result is a substantial drop in the void ratio.

Stress paths for the KAO material were also observed to deviate from the expected K_0 stress path at lower stresses. To a smaller degree, this same observation was made with the KEX material. The cause of this deviation was

determined to be the approximated finite strain algorithms in both ABAQUS and PLAXIS, which act independently from the plasticity model. For ABAQUS models, the deviation ceased once the stress path encountered the initial yield surface, at which point the plasticity model presumably dominated the evolution of stresses and strains. Thus, for soils with very small initial yield surfaces, this deviation was not observed in ABAQUS. PLAXIS, on the other hand, showed a similar deviation in all four materials. Likely, this is a result of the 1 kPa preconsolidation stress used by PLAXIS for the KEX, GOM and ECM materials, which would have artificially inflated the initial yield surface.

From this observation, it is clear that the modeling procedures and techniques discussed in this thesis are limited to soft, compressible soils. Soils which are overly stiff, and which have relatively high initial preconsolidation stresses, would show larger deviations in their predicted stress paths due to their large initial yield surfaces. For very stiff soils, the deviated region of the stress path would dominate the stress predictions made by these numerical codes to the point where the K_0 condition would no longer be approximated. Thus, there is conceptually a maximum stiffness for which these modeling techniques are applicable. KAO material may encroach on that theoretical stiffness boundary as indicated by the stress paths in Figure 18. Soils with initial preconsolidation stresses much greater than that of KAO may produce inaccurate results when modeled using the techniques discussed here.

Results from the KEX, GOM and ECM models show that the Modified Cam Clay model generally provides more accurate results than does the Capped Drucker-Prager model for softer soils. The Capped Drucker Prager model produces a noticeably curved constitutive path which deviates from the desired constitutive path of softer soils. As a result, the void ratios predicted by the Capped Drucker-Prager model are noticeably smaller than those predicted by CONDES. Additionally, the stress paths produced by the Capped Drucker-Prager Model deviate from the K_0 path as a result of an inability to perfectly match the elliptical cap in the Capped Drucker-Prager model to the Modified Cam Clay ellipse. As a result of these observations, it was concluded that the Modified Cam Clay plasticity model provides more accurate results than the Capped Drucker-Prager model. Therefore, all two-dimensional modeling was conducted using only the Modified Cam Clay plasticity model.

For all materials except KAO, the PLAXIS code produced results of underwhelming accuracy. The restriction imposed by PLAXIS that the preconsolidation stress of a soil must be greater than 1 kPa imposes severe restrictions on its ability to model soft soils. Because PLAXIS was unable to correctly model the softer soils KEX, GOM and ECM, it was decided that PLAXIS would not be used in the two-dimensional modeling effort.

4. TWO-DIMENSIONAL CONSOLIDATION MODELING

Having shown both the strengths and limitations of the numerical codes ABAQUS and PLAXIS via simple one-dimensional consolidation models, it was desired to develop modeling procedures for simplified two-dimensional consolidation scenarios. Here, the term "simplified" denotes models with minimal geometrical complexity. These simplified models used the same square geometries which were employed in the one-dimension models. Details concerning the development of these models are given in the next section.

These simplified two-dimensional consolidation models were intended to act as an intermediate step between the previously discussed one-dimensional models and the more realistic (and thus more complex) geotextile tube and TSF models. Two materials were selected for this modeling effort: KEX and GOM. These materials represent an intermediate range of compressibility as compared to the KAO and ECM materials. Additionally, the KEX and GOM materials are representative of the real-world materials which may be encountered by engineers in practice. KEX is a mine tailing which provides a close approximation to tailing materials deposited in a TSF. GOM is then representative of the fine-grained alluvial sediments which are commonly dredged from the ocean floor near the coast and which may be used as fills for geotextile tubes when coarser fills are not available.

The goal of this intermediate modeling stage was to discover how hydraulically deposited soils behave under two-dimensional seepage conditions. Classical consolidation theory is typically implemented using oedometric assumptions which do not provide allowances for two-dimensional flow or compression (Craig, 2004). When two-dimensional flow occurs the resulting excess pore pressures are no longer easily calculable using analytical methods. Even when stiff, highly overconsolidated soils are considered, two-dimensional seepage scenarios often require the use of numerical codes to provide accurate predictions. Hydraulically deposited soils, which have been shown to be highly sensitive to small changes in effective stress (and thus to small changes in pore pressure) were expected to be equally sensitive to the two-dimensional seepage forces at work in these models. Thus, the complexities introduced through two-dimensional seepage are two-fold: the two-dimensionality itself requires more complex numerical tracking of the seepage flows, and this two-dimensionality is amplified by the high compressibility of these hydraulically deposited soils.

4.1. Model Creation and Execution

Simplified two-dimensional models were created using the same initial geometries as the one-dimensional models discussed previously (i.e. square models with side lengths of 2.5 m). Additionally, these simplified two-dimensional models made use of the same mechanical boundary conditions as the one-dimensional models. In this way the soil was externally constrained so that it could not push

past the left, right or bottom boundaries. However, the soil was allowed to compress laterally within the confines of the external boundaries.

The two-dimensionality of these models was introduced through the seepage boundary conditions, where both lateral and vertical drainage was allowed. Figure 41 shows these boundary conditions, where zero flux was specified at each black boundary and zero pore pressure was specified at each grey boundary. These boundary conditions correspond to a soil which is exposed to dry air during consolidation.

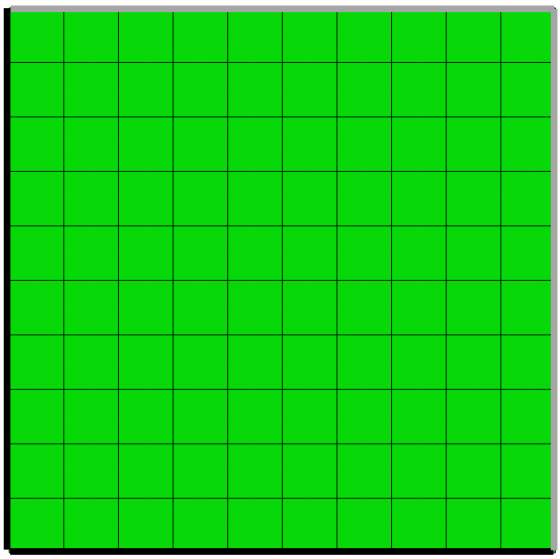

Figure 41: Initial Geometry and Seepage Boundary Conditions for Simplified Two-Dimensional Models

The generation of these models in ABAQUS followed nearly the same procedure described in section 3.1.1. In fact, each two-dimensional model was created by modifying a one-dimensional model and adding a zero-pore-pressure boundary condition to the right vertical face of the soil body.

Through trial and error it was discovered that an instantaneous change in the pore pressures at the right boundary caused errors to occur in ABAQUS. To overcome those errors, the pore pressure boundary condition on the right face was ramped from the undrained pore pressure distribution to zero pore pressure over 100 seconds. In this way the numerical marching scheme was able to gradually adjust to the new boundary condition.

The boundary condition at the right face took on the following components. A tabular amplitude function was first defined which ranged from an amplitude of 1.0 at time zero to an amplitude of zero at time 100 seconds. Then, within the pore pressure boundary condition editor window, this amplitude function was specified under the Amplitude drop-down box. The same analytical field used to create the initial (undrained) pore pressure distribution was then selected under the Distribution drop-down box. A magnitude of 1.0 was then specified, such that the combination of the amplitude function and analytical field function would control the boundary condition.

By applying this boundary condition directly to the right face of the soil body, it would cause a pore pressure boundary condition to be specified twice for the node in the top-right corner of the body (by the top and right face pore pressure boundary conditions). Instead, a node set was created which included all nodes on the right face of the model except the node in the top-right corner. The right-face pore pressure boundary condition was the applied directly to that node set. Note that a node set can only be created *after* a finite element mesh has been generated.

The mesh selected for these models was the same used in the one-dimensional models. It consisted of a grid of 10 by 10 quadrilateral elements of type CAX8P. Although the mesh could have been refined in the vicinity of the drained boundaries, it was left as a 10 by 10 grid for use in visual inspection of the model results later on. A uniform grid allowed for easier detection of soil deflections as the consolidation process progressed.

These models were calculated in the axisymmetric condition with the line of symmetry coinciding with the left vertical face of the soil. The model parameters shown in Table 2 were also used as inputs for these simplified two-dimensional models. All other properties of the two-dimensional models remained the same as those of the one-dimensional models with the exception of the initial effective stress. Due to the added complexities of the two-dimensional models, the specified initial effective stress was required to be larger than that used in the one-dimensional models. Specifically, an initial effective stress of 0.30 kPa was specified in the KEX model and a stress of 0.40 kPa was specified in the GOM model.

Note that these initial stresses are larger than the preconsolidation stresses for both materials. Within ABAQUS, the specified preconsolidation stress was not changed (i.e. the p_c' value in Table 2 was still entered into the Clay Plasticity material model). When this condition is encountered, ABAQUS automatically hardens the initial yield surface so that the specified initial effective stress value represents the new preconsolidation pressure of the soil (Dassault Systems, 2013). An equally viable alternative would be to manually specify a new preconsolidation

stress, though this extra step is not necessary so long as the user is aware of the automatic change to the initial yield surface.

The consequence the altered initial yield surface is that the constitutive behavior predicted by ABAQUS is also altered. More specifically, any volume changes which should have occurred at stresses below the specified initial effective stress are no longer captured by the ABAQUS model. In this way, the ABAQUS results begin to experience the same issues that PLAXIS showed when modeling softer soils, i.e. that the constitutive path is pushed to the right in the compression plane. Ultimately the additional complexities within these two-dimensional models lead to some degradation of their accuracy. The accuracy of these models will be discussed further after the model results are presented.

4.2. Two-Dimensional Modeling Results

Herein, results from the two-dimensional consolidation models are provided. Pursuant to the findings from the one-dimensional modeling effort, only the Modified Cam Clay plasticity model in the ABAQUS code was used in the two-dimensional models.

Results from the one-dimensional models were shown as a function of elevation. However, two-dimensional models vary spatially with both horizontal and vertical distance, such that results from these models are shown as a function of vertical and horizontal distance. Each of the results plots provided below summarizes the state of the model at a specified distance from the left side. This

distance is represented by the variable X (i.e. distance in the x-direction from the origin in the bottom left corner of the model). Results are provided at X distances of 0, 1.5, 2.25 and 2.5 m.

CONDES does not have the ability to model two-dimensional seepage scenarios, and so CONDES results are not be displayed for these two-dimensional models. Constitutive behavior plots continue to show the CONDES curve, however, because this curve represents the desired constitutive relationship given in (1) and is not actually an output from the CONDES code. Here, it should be noted that (1) was developed using a one-dimensional stress state parameter, i.e. vertical effective stress. Because the soil in these two-dimensional models has the ability to compress both horizontally and vertically, this relationship may not be matched perfectly by the ABAQUS predictions. Some variation from the CONDES curves in the following constitutive behavior plots were expected as a result.

4.2.1. Two-Dimensional Results: Keystone Example Tailing

The consolidation process for a vertically and laterally drained soil is much more irregular than that for a one-dimensional soil column.
Figure 42 shows how the laterally drained KEX soil deforms through time.

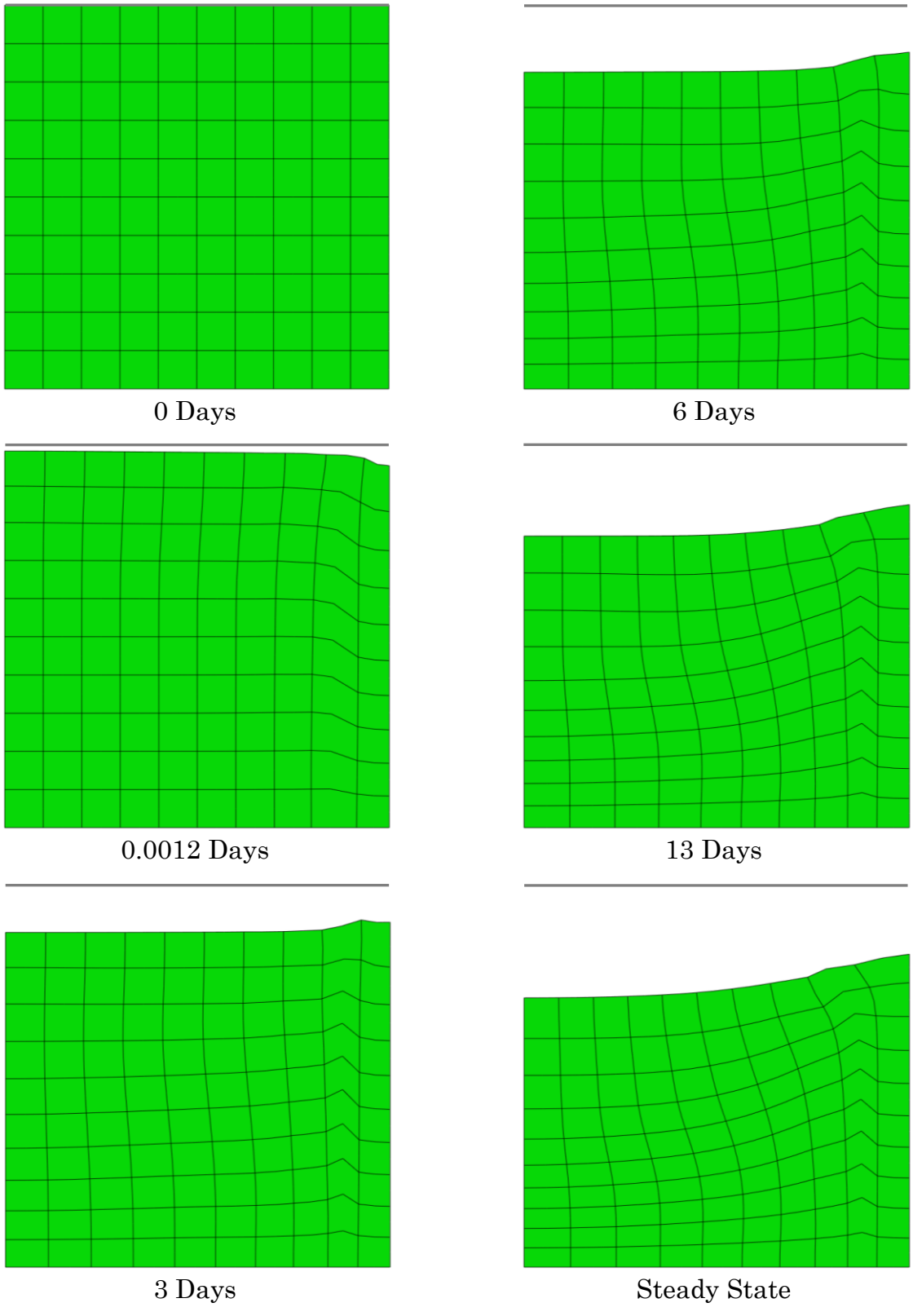

Figure 42: KEX 2D Consolidation Progress with Time

Note that all images in Figure 42 are equally scaled and that grey lines are shown above each image. These grey lines show the location of the top surface of the soil in its undeformed condition. Using these lines as a reference, it becomes readily apparent that the settlement occurring in this model is not at all uniform across the width of the geometry. Recall that the mechanical boundary conditions used in these models were the same as those from the one-dimensional models. Only the seepage boundary conditions were altered to allow both lateral and vertical drainage. Clearly, the differences between the settlements depicted in Figure 42 for a two-dimensional model and those depicted in Figure 12 for a one-dimensional model are caused by differences in the drainage condition and are not the result of any other mechanical stimulus.

The sensitivity of hydraulically deposited soils to the direction of drainage is a direct result of their high compressibility. Lateral drainage results in the imposition of non-vertical seepage forces on the soil, which in turn cause changes in the effective stress state and thus changes in the volumetric response of the soil. The high compressibility of hydraulically deposited soils amplifies the effect of these seepage forces, as these soils have been shown to be quite sensitive to relatively small changes in the effective stress state.

Figure 42 shows how the soil quickly responds to the imposed zero-pore-pressure boundary on the right side of the soil, as the soil along that boundary quickly consolidates. However, as drainage begins to occur in the horizontal direction at day 3, the soil near the bottom of the model can be observed to shift

slightly to the right under the influence of lateral seepage forces. Here, the soil along the right side of the model continues to consolidate at a relatively rapid rate though its reduction in volume is offset by the increase in density caused by the rightward movement of soil from elsewhere in the model. At day 3 (and at all times greater than day 3) the result is that the vertical settlement of the soil near the right (drained) boundary is actually less than the vertical settlement of the soil near the left (undrained) boundary.

As consolidation continues the soil continues to migrate towards the right drained boundary such that, at steady state, the vertical settlement near the right boundary is always less than the settlement across the remainder of the soil surface. The rightward displacement of the soil is quite evident in Figure 42 at the steady state condition. It should also be noted that the majority of the rightward displacements occur in the lower half of the soil body, while the elements in the upper half are actually pushed to the left somewhat. Likely, as the soil in the lower portions of the body are pushed to the right, the soil near the top-right surface is pushed upward and is caused to move leftward to maintain stability of the small slope which is formed.

Figure 44 through Figure 47 then show the graphical results for the KEX material in a similar fashion to the results shown for the one-dimensional models. Note that the horizontal scales in Figure 45 are variable in order to show greater detail at the lower effective stresses for the profiles closer to the undrained vertical boundary. Here, each plot is labeled with an X-position, corresponding to the

distance from the left side of the model. The dashed lines in Figure 43 show the approximate locations of each profile as an example. Note that for the void ratio and effective stress profiles, the profiles lines were *not* allowed to deform with the mesh, such that the X-values reported in each image are the absolute distance from the left side of the model at all time values. For these results plots, the profile lines in Figure 43 represent the location of each profile at all points in time. The stress path and constitutive plots, however, tracked specific nodes through time such that the profiles for those plots are not represented by Figure 43 except at zero days (i.e. the undeformed geometry).

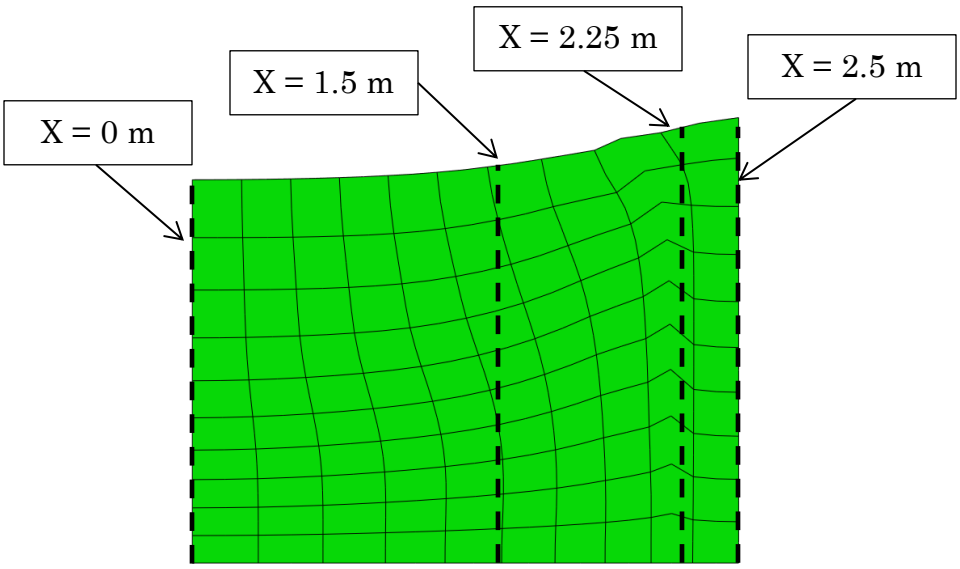

Figure 43: Location of Results Profiles for Void Ratio and Effective Stress

For the stress path and constitutive path plots, the distances reported in the legends represent elevations above the bottom of the model *in the model's undeformed geometry*.

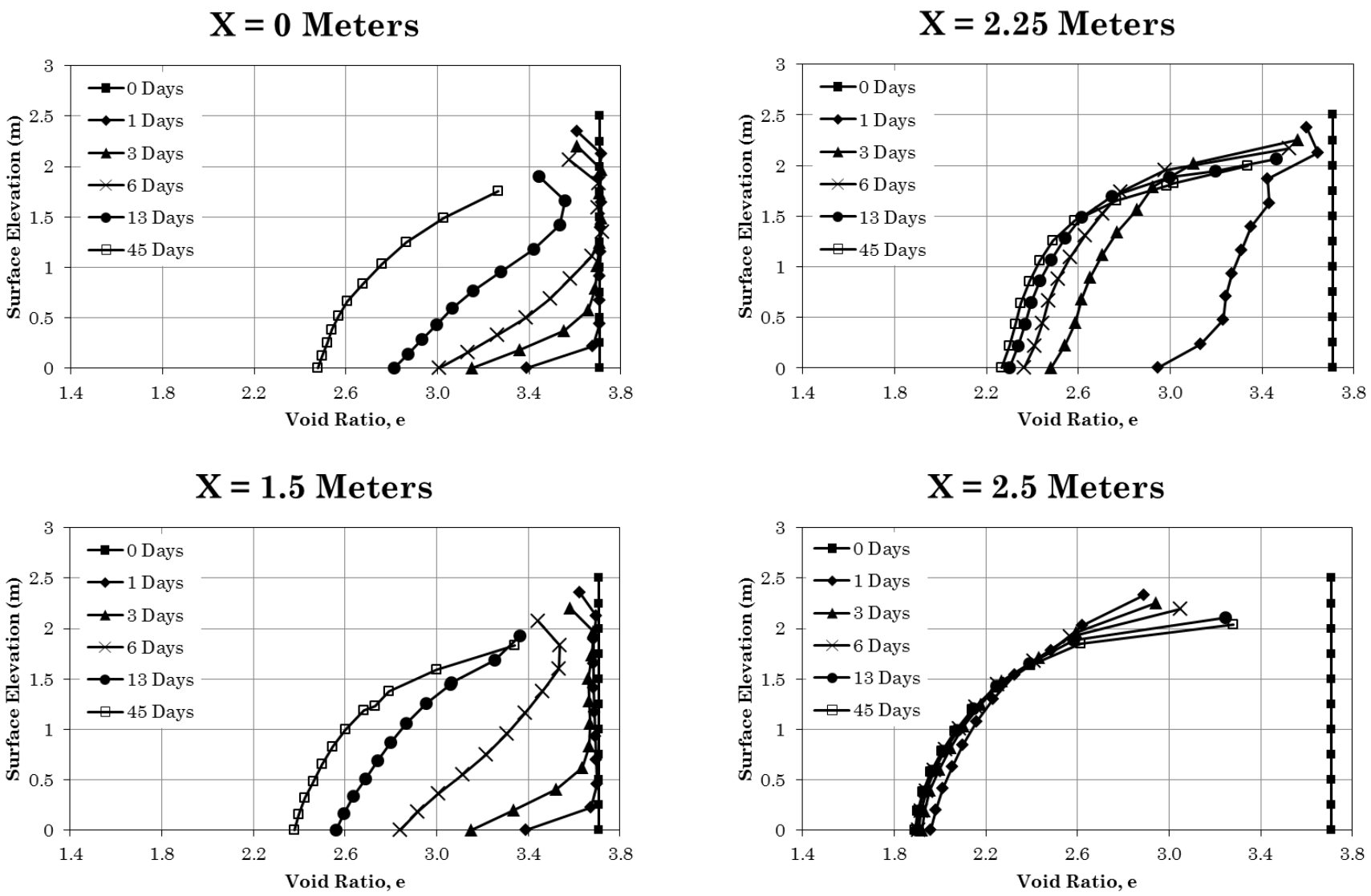

Figure 44: KEX 2D Void Ratio Profiles at Various Locations

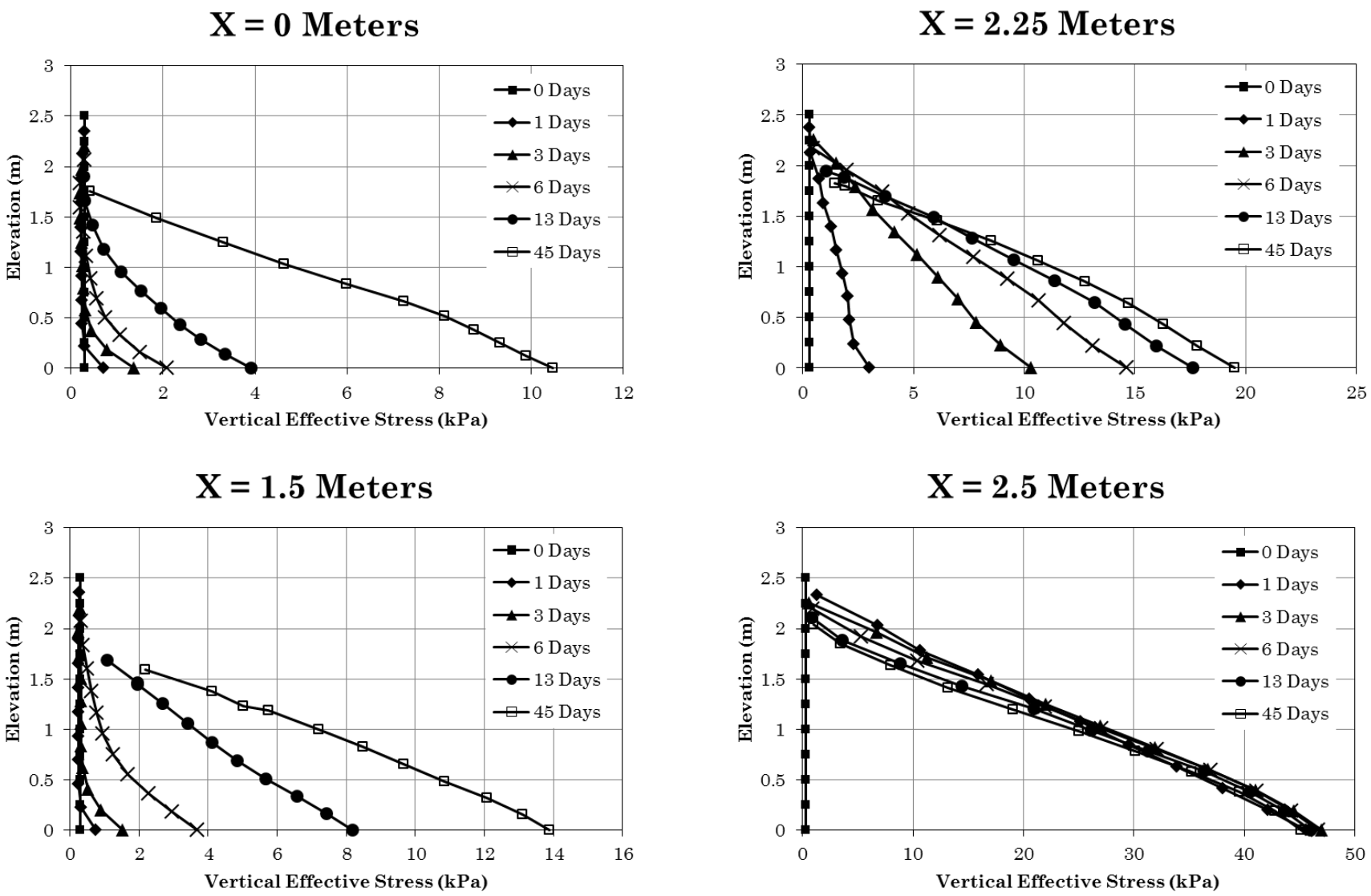

Figure 45: KEX 2D Effective Stress Profiles at Various Locations

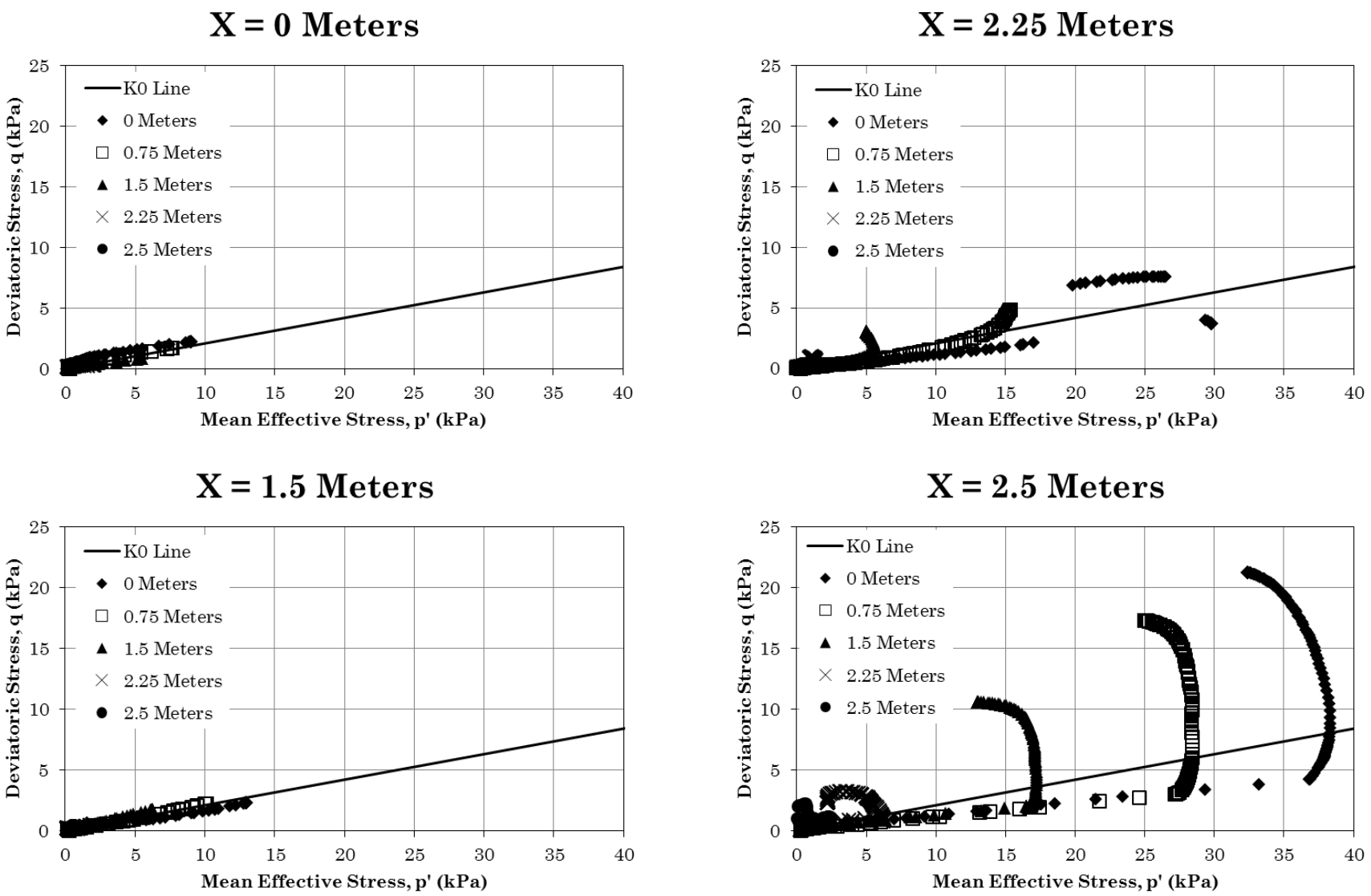

Figure 46: KEX 2D Effective Stress Paths at Various Locations

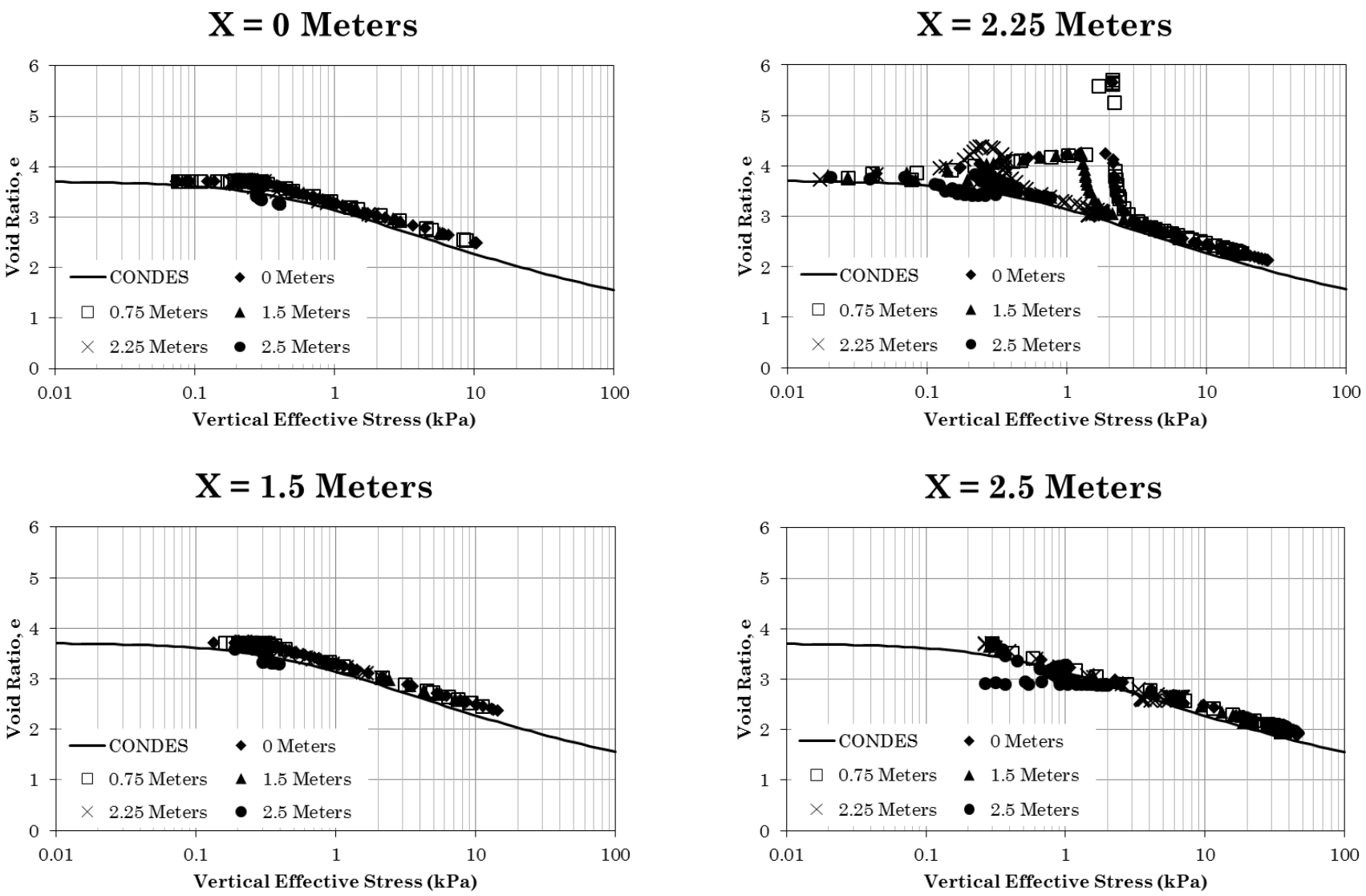

Figure 47: KEX 2D Constitutive Paths at Various Locations

Plots of both the void ratio and vertical effective stress profiles show how consolidation progresses at different rates for different horizontal positions within the soil. The rate of consolidation may be conceptually understood by comparing the positions of the transient profiles to the profiles in the initial and steady state conditions (i.e. at times of 0 and 45 days). Profiles clustered near the initial state profile indicate that consolidation occurs more slowly, as more time is required for the profile to be pushed towards the steady state condition. The void ratio and effective stress plots in Figure 44 and Figure 45 at the X = 0 m position show this type of trend. Conversely, profiles clustered around the steady state profile indicate more rapid consolidation, as less time is required for the consolidation process to complete. The void ratio and effective stress profiles at the X = 2.5 m position show this type of behavior.

An interesting trend is revealed by looking at the changes in void ratio at the top surface of the soil over time. The void ratio profiles at X = 0 m, 1.5 m and 2.25 m show the void ratio at the top surface decreasing with time, which indicates a small increase in the effective stress at those points. However, at X = 2.5 m (i.e. at the right edge of the soil), the void ratio is shown to *increase* noticeably over time which indicates a *reduction* in the effective stresses at that location.

Increases in the vertical effective stress near the top surface at X = 0 m, 1.5 m and 2.25 m are easily observed in Figure 45, though the vertical effective stress near the surface at X = 2.5 m remains relatively constant through time. However, the two-dimensionality of this model requires that the constitutive behavior be a

function of both vertical and horizontal effective stresses. The result is that the reduction in void ratio at the top-right corner of the soil is likely the result of decreased horizontal effective stress, which in turn is the result of the soil in that area being pushed upward by the soil below.

Also of interest is the fact that the vertical effective stresses generally increase with distance from the left side of the model (i.e. as the profiles approach the right drained boundary). The height of the soil is not variable enough to account for such large changes in the vertical effective stress with horizontal distance. Instead, this observation is the result of a more complex steady state pore pressure distribution. The soil near the left (undrained) edge of the soil shows steady state vertical effective stresses which are similar in magnitude to those observed in the one-dimensional models as the drainage in that region is less affected by the right drained boundary. However, nearer to the right drained boundary the pore pressures drop well below the one-dimensional steady state pore pressures, such that the effective stresses are caused to increase relative to the one-dimensional model results. The pore pressure is zero everywhere along the right drained boundary, such that the effective stresses are equal to the total stresses.

Here, it is important to note that the scales on the abscissas of the plots in Figure 45 are not consistent. This was done intentionally so as to provide greater resolution for the stresses near the top surface at locations closer to the left side of the model.

Another direct consequence of these lateral seepage forces is that the major principal stresses are no longer oriented in the vertical direction, and the K_0 condition is no longer a valid approximation of the soil behavior. These trends can be observed in Figure 46 and Figure 47. The effective stress paths at X = 0 m and 1.5 m approximate the K_0 condition, the stress paths at X = 2.25 m and 2.5 m show much more substantial deviations from the K_0 line. These deviations are the direct result of the two-dimensional seepage allowed in these models. At these two locations a linear stress path is followed which lies below the K_0 line, indicating that the lateral effective stress is still linearly related to the vertical effective stress. At some point in time, however, the lateral and vertical effective stresses take on a highly nonlinear relationship as the deviatoric stress climbs rapidly.

Deviations in the constitutive behavior were also observed, especially at X = 2.25 m. Upon closer inspection of the graphical settlement results in Figure 42, a region of noticeably less settlement can be observed near X = 2.25 m. This is likely a consequence of the observed rightward movement of soil, causing the density of the soil to increase in that region. Recall that ABAQUS uses a finite strain approximation algorithm in tandem with, but independent from, the Modified Cam Clay plasticity model. As the soil densified, the finite strain algorithm likely predicted an increase in the void ratio to compensate. Thus, the large deviations from the CONDES line at X = 2.25 m may be caused by this finite strain algorithm.

Also in these constitutive plots, the void ratio decrease at the top-right corner of the model can be observed. Here, a series of several data points lie noticeably

below the CONDES line at X = 2.5 m. Here again, the CONDES line and the observed data points are reported in terms of the vertical effective stress and not the mean effective stress, such that changes in the horizontal effective stress are not accounted for.

4.2.2. Two-Dimensional Results: Gulf of Mexico Dredged Material

The two-dimensional model created for the GOM material followed many of the same trends discussed previously for the two-dimensional KEX model. In particular, the rightward migration of soil (towards the right drained boundary) was confirmed in this model, as well as rapid consolidation of the soil along the right drainage boundary followed by the stiffening of the soil in the region near X = 2.25 m.

Figure 48 shows how the consolidation progressed through time in this GOM two-dimensional model. Note that only slight differences exist between the KEX and GOM consolidation processes. Figure 49 through Figure 52 then show the plotted results from the GOM model in the same fashion as those shown for the KEX model. The profile positions for the void ratio and vertical effective stress plots are the same here as those shown in Figure 43 above. Again note that the abscissa scales for the vertical effective stress plots are not constant, and that they were reduced for the X = 0 m and 1.5 m in order to show more detail.

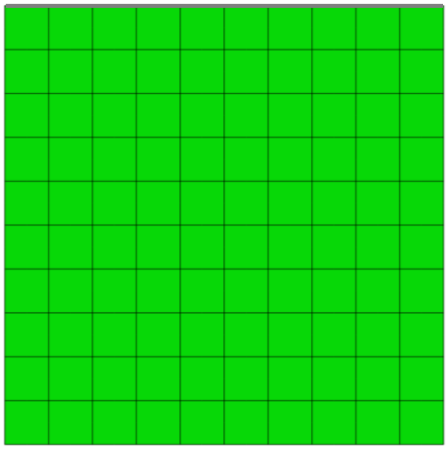

0 Days

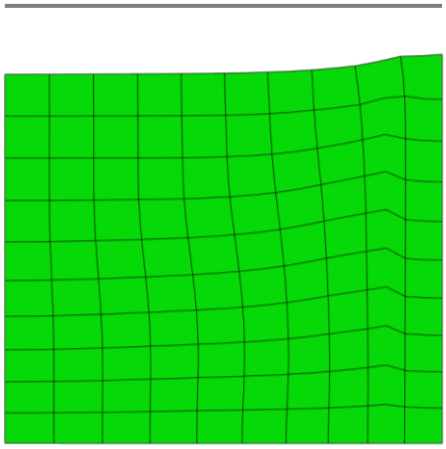

20 Days

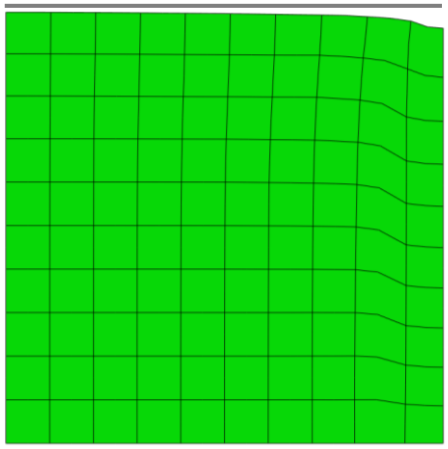

0.0012 Days

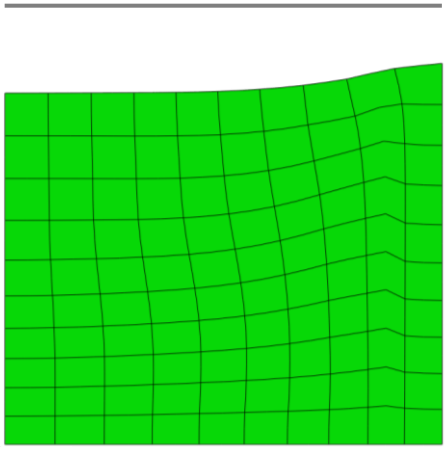

35 Days

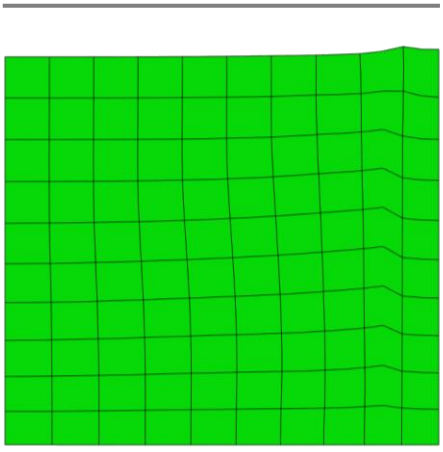

9 Days

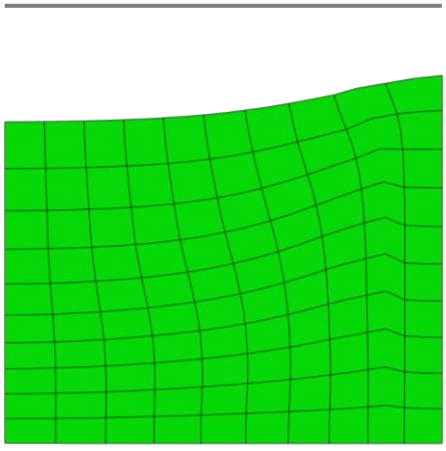

200 Days

Figure 48: GOM 2D Consolidation Progress with Time

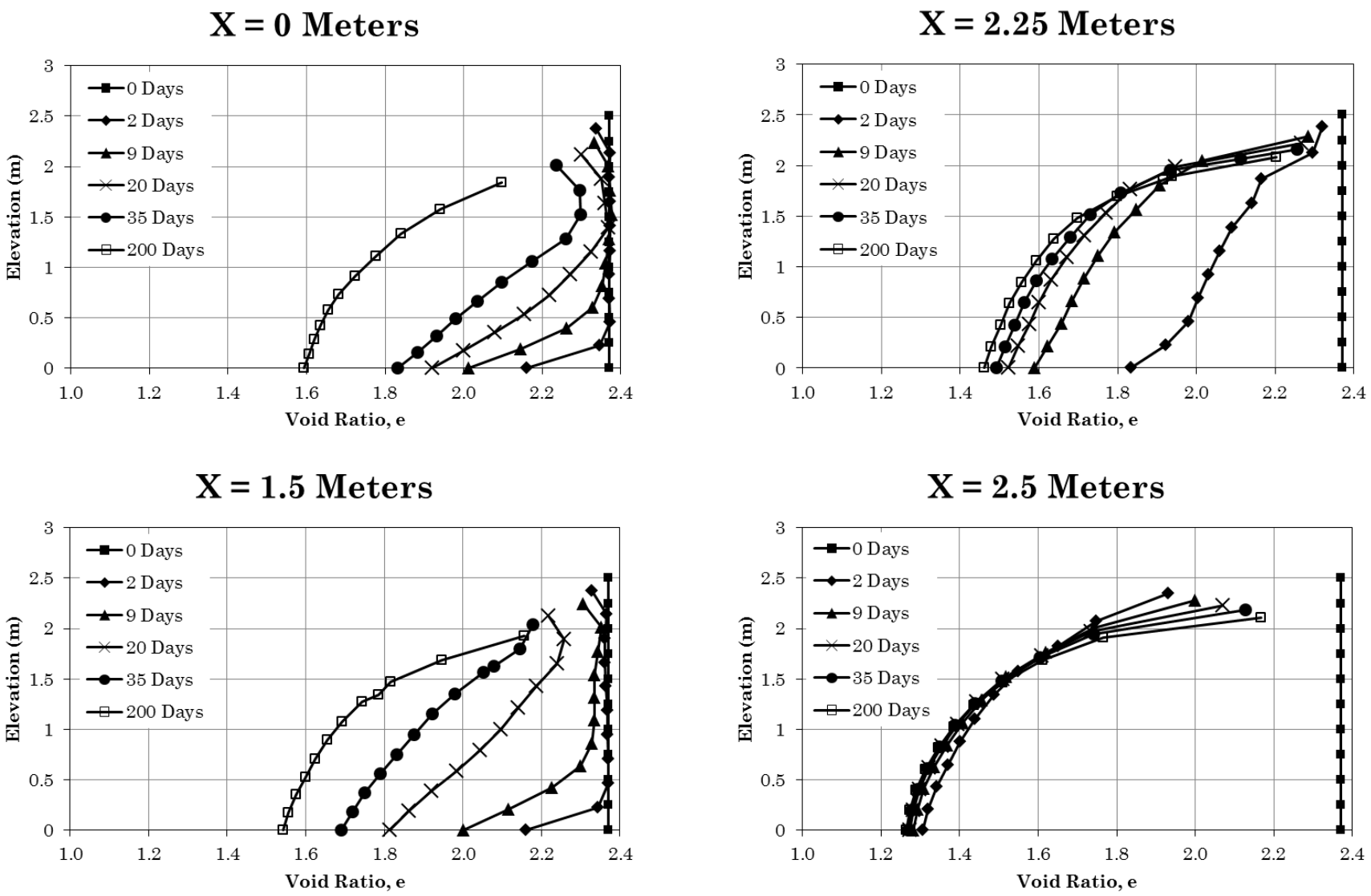

Figure 49: GOM 2D Void Ratio Profiles at Various Locations

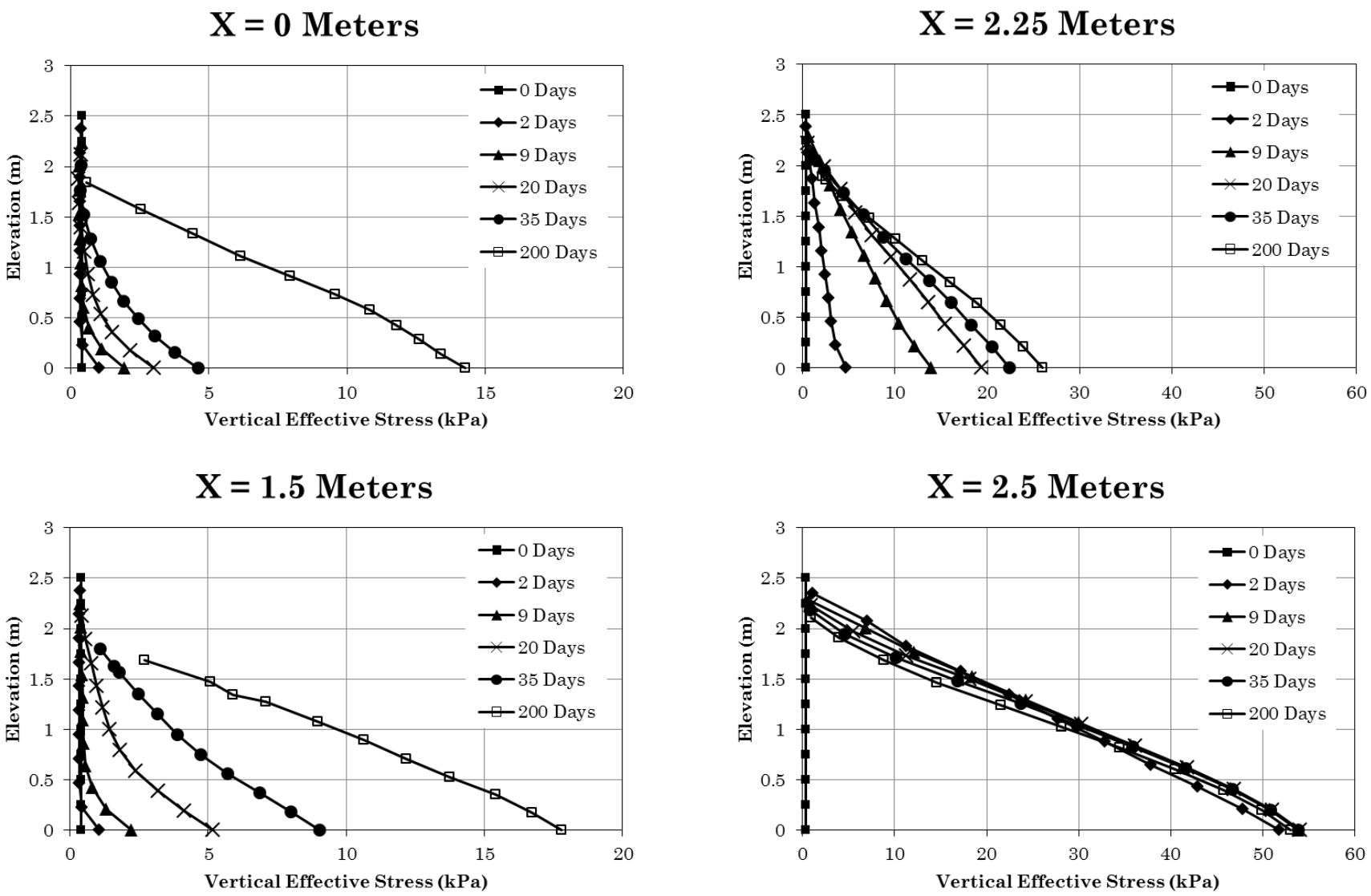

Figure 50: GOM 2D Effective Stress Profiles at Various Locations

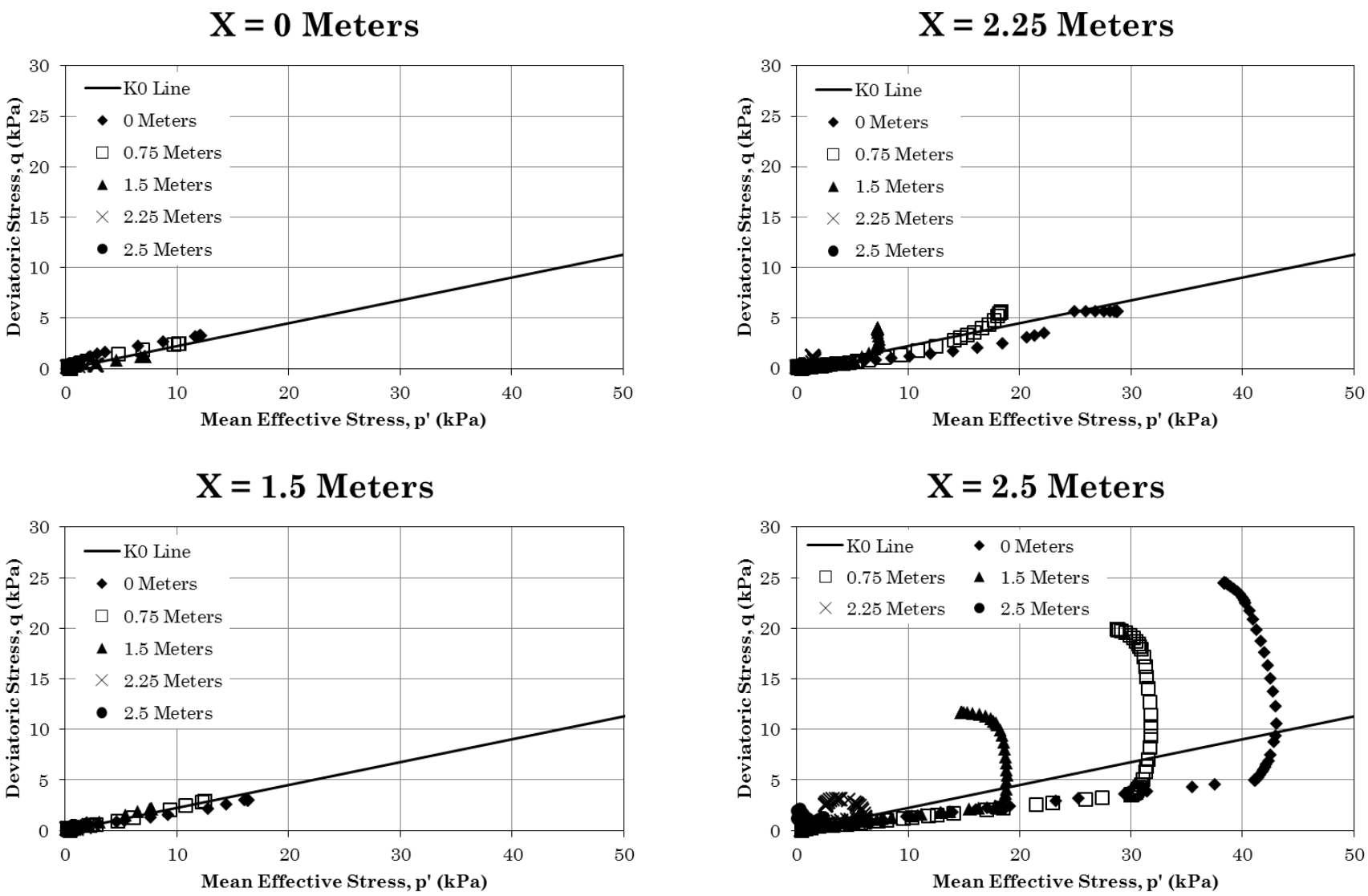

Figure 51: GOM 2D Effective Stress Paths at Various Locations

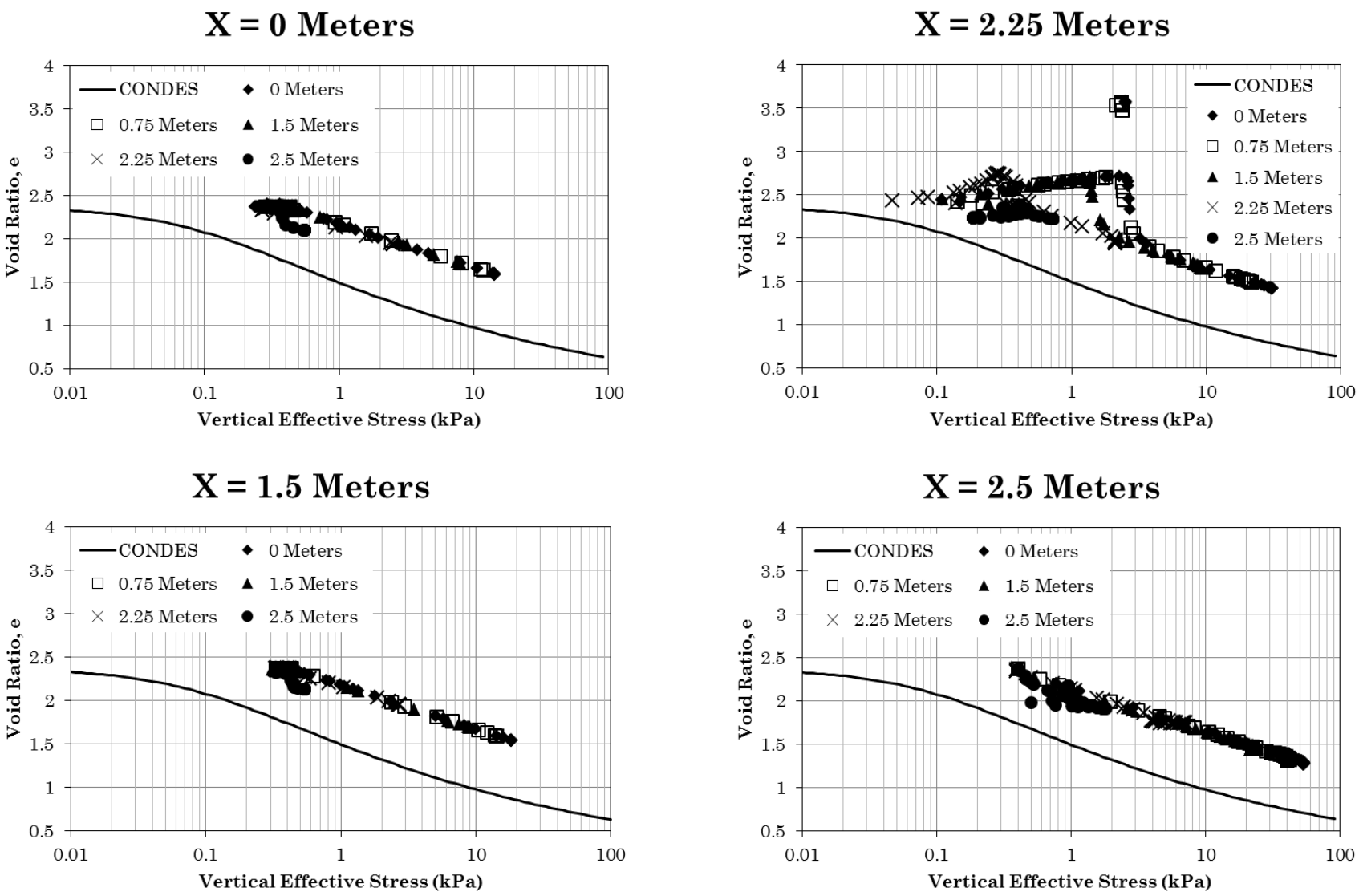

Figure 52: GOM 2D Constitutive Paths at Various Locations

The plotted results in Figure 49 through Figure 52 are remarkably similar (in form, not in magnitude) to those from the KEX two-dimensional model. These two models thus provide a good representation of the behavior of a hydraulically deposited soil under two-dimensional drainage conditions.

One noteworthy exception to this observation is the fact that the GOM constitutive paths lie slightly apart from the theoretical CONDES curve. This discrepancy is not purely a consequence of the fact that the CONDES curve was developed using a one-dimensional stress state assumption, but is in fact the result of the increased initial effective stress specified for this model. Recall that the initial effective stress could not be set lower than about 0.40 kPa in ABAQUS without causing the model calculation to fail. As a result, the preconsolidation stress used by ABAQUS was assumed to be 0.40 kPa, which is several times larger than the 0.02 kPa preconsolidation stress defined in Table 2. Thus, the GOM model results show less settlement than the material would actually undergo.

4.3. Two-Dimensional Modeling Conclusions

As anticipated, these models which made use of two-dimensional drainage conditions produced results far different than those from the one-dimensional models. One major conclusion from this modeling effort was that the high compressibility of hydraulically deposited soils causes them to be sensitive to the non-vertical seepage forces which develop as a result of the laterally drained boundary. Initially, the soil along that boundary consolidates quickly due to the

nearby zero pore pressure boundary condition. However, the large seepage gradient which develops as a result causes the soil to compress horizontally as well as vertically. This leads to a rightward movement of the soil in the lower and middle elevations, which in turn pushes the soil near the top right corner of the model upwards. The soil near the top-right corner then experiences a relaxation of the horizontal effective stress, causing an increase in the void ratio in that region.

Two-dimensional seepage introduces additional complexities into the model relative to the one-dimensional models. As a result, the user-specified initial effective stress must be increased to allow the calculation to complete successfully. For soils such as the KEX material with an initial effective stress of 0.30 kPa, the increased initial effective stress is near enough to the soil's true preconsolidation stress that the errors introduced are negligible. However, the GOM material has a lower preconsolidation stress and is more highly compressible than the KEX material such that the initial effective stress specified in ABAQUS (0.40 kPa) was even greater than that used for the KEX material. The mismatch between the initial effective stress specified in ABAQUS and the true preconsolidation stress of the GOM material resulted in at least some error in the volumetric strain which is not negligible. The magnitude of this error can be conceptually estimated by comparing the ABAQUS constitutive paths to the relationship in (1). However, because (1) was derived using one-dimensional consolidation assumptions, it does not represent the true theoretical behavior of the soil and so the magnitude of the error caused by the increased initial effective stress remains unknown.

Also recall that the Modified Cam Clay parameters listed in Table 2 were fit to the one-dimensional relationship in (1). Thus, these fitted parameters are likely not perfectly matched to the true two-dimensional behavior of the soil. However, the parameters in Table 2 were still used in these two-dimensional models because a theoretical constitutive relationship using two- or three-dimensional stress state parameters was not readily available. Any error resulting from the improperly fit Modified Cam Clay parameters is not measurable without a true two- or three-dimensional theoretical constitutive model to compare the ABAQUS results against.

Overall, though, these two-dimensional results have shown that ABAQUS is capable of providing accurate results for many hydraulically deposited soils, so long as the initial effective stress specified in ABAQUS is not substantially greater than the soil's preconsolidation stress. With that conclusion, the KEX and GOM materials were then used to develop example ABAQUS models. These example models include a consolidating geotextile tube filled with fine-grained material and a tailing storage facility filled with a fine tailing.

5. EXAMPLE APPLICATIONS FOR HYDRAULICALLY DEPOSITED SOILS

Hydraulically deposited soils are encountered in engineering practice in several forms. Among the most common forms are dredged sediments and mine tailing. Dredged sediments may be used in any number of applications such as deepening or widening river channels, removing contaminated sediments, deepening shipping ports, etc. The application of interest to the author is how dredged sediments consolidated when used as fill for a geotextile tube.

Mine tailing is another very common engineering application where hydraulically deposited soils are encountered. Geotechnical and mining engineers are constantly confronted by the challenge of estimating the capacity of a TSF. Many critical mine processes depend upon those predictions to develop life-of-mine schedules which allow the mine to plan for its future operations. Here, a simplified TSF model is considered which provides an example of how a full TSF could be modeled.

5.1. Geotextile Tube Example Application

Geotextile tubes have been successfully implemented around the globe for several purposes, including shoreline protection and slope protection, slurry dewatering (Howard and Trainer, 2011) and the creation of embankment structures

(Tyagi, 2005). The Saemangeum Development Project in South Korea has made extensive use of geotextile tubes in an effort to reclaim approximately 280 km^2 of land from a river estuary near the city of Kunsan. As part of this effort, containment dikes will be used to partition the areas to be reclaimed, and the partitioned areas will be backfilled with dredged alluvium to create new land. Many of these containment dikes will be shrouded with geotextile tubes as a means of protection from wave action, while other dikes will be constructed entirely of stacked geotextile tubes.

Geotextile tubes have historically been filled with sandy materials whose relatively high hydraulic conductivity allows them to quickly drain and consolidate. However, scenarios exist where only fine-grained fills are readily or economically available. These fills require substantially longer to consolidate due to their reduced hydraulic conductivity. An extended consolidation period may have substantial impacts on project scheduling and may result in substantial increases in overall project cost if the project is delayed due to inaccurate prediction of the consolidation time.

Very little is presently known about the consolidation behavior of geotextile tubes filled with fine-grained, hydraulically deposited soils. The exact nature of this consolidation process must be understood before fine-grained fills can be implemented in construction projects. Specifically, the rate of consolidation, the time required for the fill to fully consolidate, and the final consolidated height of the geotextile tube are all parameters which are of interest to geotechnical engineers.

Significant attention has been given to the external stability of stacks of geotextile tubes, both in marine and dry-land applications. Examples of studies on external stability of geotextile tube embankments include the papers published by Tyagi and Mandal (2005) and Yiming et al. (2010). Some focus has recently been given to the consolidation and strength of geotextile tubes as well, including a numerical analysis study conducted by Beemsterboer, et al. (2012). This study used the PLAXIS code to analyze a system of hydraulically filled geotextile tubes inside an embankment. Geotextile tubes were not modeled discretely, however. Instead, zones within the embankment containing geotextile tubes were modeled as single discrete sections in the PLAXIS model. Thus, the interactions between geotextile tubes and the consolidation process inside each geotextile tube were ignored.

Numerical modeling may help engineers to accurately predict the behavior of geotextile tubes for design purposes. The modeling techniques and procedures developed for the one- and two-dimensional models can be applied to predict the consolidation of geotextile tubes in the field. Several differences exist from the simplified one- and two-dimensional models discussed previously, but many of the conclusions drawn from those models were used to help create a geotextile tube model.

5.1.1. Geotextile Tube Model Creation and Execution

The GOM material was selected for use in the geotextile tube model because it is the most similar to fine-grained materials which may be encountered in a dredging operation. Although the ECM material is also a dredged material, its

compressibility is so high that likely could not be successfully modeled in a highly complex geotextile tube model. Recall that as the geometric complexity and the material compressibility increase, the initial effective stress specified in ABAQUS must also increase. Thus, the initial effective stress required to represent the ECM material in a geotextile tube model would be potentially hundreds of times greater than the preconsolidation stress for that material. The resulting volumetric strain predictions would be highly erroneous and would not provide a good representation of the modeling process used for geotextile tubes.

Before creating a numerical model in ABAQUS, the initial geometry of a geotextile tube had to be developed. Several methods are available to predict the shape of a geotextile tube immediately after filling. For this research, a method proposed by Carroll (1994) was implemented. Here, the slurry fill was assumed to act as a Newtonian fluid with zero shear strength. Although it is known that hydraulically deposited soils do exhibit some shear strength immediately after sedimentation, this strength is assumed to be negligible. It was also assumed that the fill slurry was deposited instantaneously such that no consolidation occurs during filling and the soil remains in a state of zero effective stress. The geosynthetic itself was assumed to be thin, weightless, and to have no ability to carry moments or to interact frictionally with the slurry. The geotextile tube itself was assumed to be very long in the axial direction, such that plane strain conditions exist.

With these assumptions, a simple force balance was performed on each differential arc length of the geotextile tube using a linearly increasing internal pressure with depth below the maximum elevation of the geotextile tube. The result is a system of nonlinear differential equations which require numerical solutions. A $4^{th}/5^{th}$ order Runge-Kutta ordinary differential equation solution technique was implemented in the program MATLAB to provide solutions to these differential equations. This solver provided the geotextile tube geometry for any soil as a function of the soil's unit weight, geotextile circumference, pumping pressure at the top of the geotextile tube, and maximum height and width of the geotextile tube cross-section. Because not all of these parameters were known a priori, a series of nested iterative procedures were used to solve for the unknowns. Commonly, the geotextile circumference, pumping pressure and soil unit weight were used as known inputs, while the remaining parameters were solved for numerically along with the geotextile tube geometry.

The numerical solver was also given the ability to model scenarios where two different fill materials were used. Scenarios such as these may arise if the dredging operation encounters two different soils while filling a single geotextile tube. The resulting layered soil inside the geotextile tube could then be modeled using this solver. Another scenario may exist where the lower portion of a geotextile tube is submerged, while the upper portion is not. In this case, the unit weight input for the lower (submerged) section of the geotextile tube would be the buoyant unit weight of the soil, while the total unit weight would be input for the upper section.

Results from this numerical code were validated against the predictions by Carroll (1994), as well as several predictions made by a software package titled GeoCoPS 3.0. The calculation method used by this program is similar to that used in the MATLAB code described above, with some minor variations in its implementation. This program and its calculation methods are described in the publication by Leshchinsky et al. (1996). Geometry calculations from the MATLAB code and from GeoCoPS for the GOM material are compared in Figure 53. Here, the geotextile circumference was assumed to be 15 m and the pumping pressure to be 0.3 kPa. A total unit weight of 14.76 kN/m^3, thus assuming the geotextile tube was not submerged. It can be seen that these calculation methods produce nearly identical results.

It was desired to use as small of a pumping pressure as possible to calculate the ABAQUS model geometry, as the model would be more nearly in equilibrium at the initial condition. However, GeoCoPS does not allow the pumping pressure to drop below 0.3 kPa. Thus, only the MATLAB solver was used to compute the ABAQUS geometry, which is shown in Figure 54.

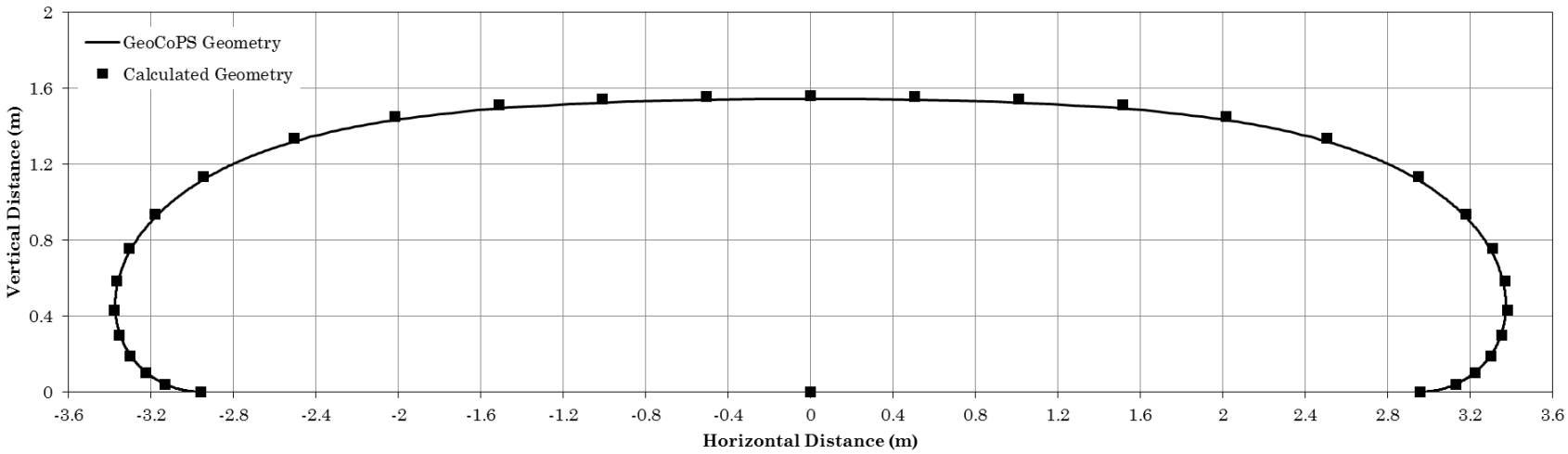

Figure 53: Comparison of Initial Geotextile Tube Geometries for GOM Material using 15 m Circumference and Pumping Pressure of 0.3 kPa

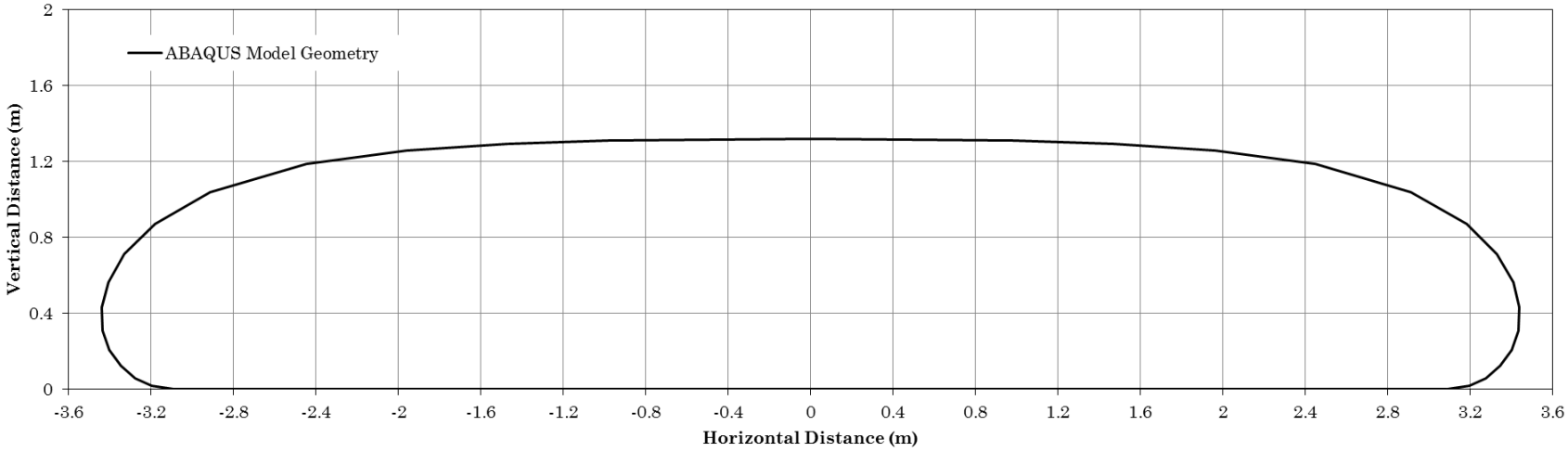

Figure 54: GOM Geotextile Tube Geometry Used in the ABAQUS Model with 15 m Circumference and Pumping Pressure of 0.1 kPa

Within ABAQUS, the geotextile tube model was created using many of the same procedures discussed in section 3.1.1 for one-dimensional models. This model also made use of the Modified Cam Clay parameters for the GOM material in Table 2. However, several additional steps were required to create the more complicated geometry of a geotextile tube.

First, the ABAQUS model used three parts instead of just one: a soil body, a geotextile fabric, and a rigid foundation on which the geotextile tube could deform. Symmetry about the center of the geotextile tube cross section was assumed such that only the right half of the cross section was modeled in ABAQUS.

The geotextile was modeled as a two-dimensional, plane strain wire part with geometry matching the right half of that shown in Figure 53. Note that the geotextile must extend completely along the bottom of the geotextile tube to maintain continuity of the geotextile. The geotextile part was assigned to a truss section with cross-sectional area equal to 0.001 m^2/m. A truss section was chosen so as to ensure that no moments could be carried by the geotextile. The material assigned to this section was given to behavioral properties: a negligible density of 1 kg/m^3 and an elastic mechanical property with an elastic modulus of 1,100,000 kPa and a Poisson's ratio of 0.49. This elastic property correlates to the polyethylene material which is used in the construction of most woven geotextiles. The geotextile part was meshed using truss elements of type T2D3. Truss elements were again chosen to prevent bending moments from developing in the geotextile.

The rigid foundation was created using a discrete rigid part, which took the form of a straight line (i.e. a wire part) along the base of the geotextile tube. Note that discrete rigid parts require that a reference point be created as well. All boundary conditions for the discrete rigid part are applied to the reference point instead of the part itself. The foundation was then meshed using discrete rigid elements of type R2D2. Discrete rigid parts are not assigned material properties or sections.

The soil part was then created using the geometry shown in Figure 53. The geometry of the soil exactly matched the geometry of the geotextile such that the two parts would be in contact with each other. Here, the soil's material model was exactly the same as the models used in the one- and two-dimensional models. A higher order triangular mesh was used for the soil, however, due to the large lateral strains which were expected in the material. Elements of type CPE6MP were chosen.

The meshed geotextile tube model is shown in Figure 55 for reference, including the rigid foundation. Although the geotextile part is present, it is not easily visible as it exactly conforms to the soil body.

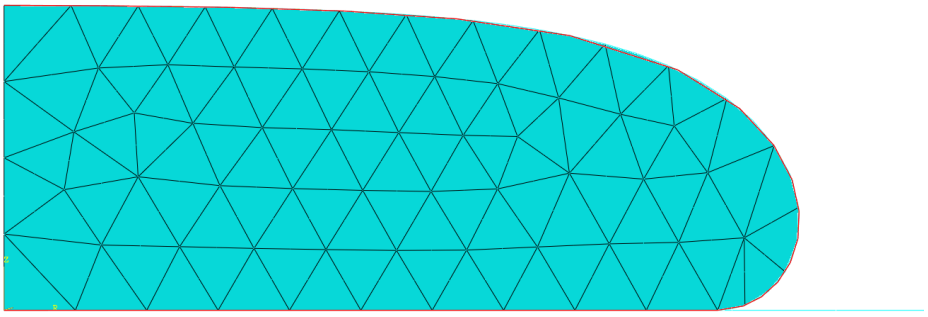

Figure 55: GOM Geotextile Tube Model Setup in ABAQUS

As with the one- and two-dimensional models, two calculation steps were used: an initial step and a consolidation step. Undrained pore pressures were again manually specified in the initial step using an analytical field input to create the pressure distribution based upon the soil's total unit weight and the model height. An initial effective stress of 0.30 kPa was specified, and an external pressure of 0.30 kPa was applied to the curved section of the soil body (i.e. not to the left vertical edge or the bottom horizontal edge of the model) to equilibrate the initial effective stress. A gravity load and an initial void ratio predefined field were also applied to the model.

Boundary conditions for the geotextile tube model were then applied. Along the left vertical edge, a mechanical boundary condition was used to impose zero horizontal displacement. This boundary condition was applied directly to a node set which consisted of all nodes along the left edge excluding the node in the bottom left corner of the model. The bottom left node was excluded to prevent overlap with the interaction specified between the soil and the foundation which will be discussed later. Another mechanical boundary condition was then applied to the reference point of the foundation, which imposed zero displacements in the vertical and horizontal directions, as well as zero rotation about the reference point. Finally, a drainage boundary condition was applied along the curved section of the soil part which imposed zero pore pressure. The pressure was ramped from the undrained pressure distribution to a state of zero pressure using the same technique discussed in section 4.1 for the two-dimensional models. Here, the pressure was ramped over

1,000 seconds. Note that this boundary condition corresponds to a geotextile tube consolidating on dry land. However, one could easily adapt this boundary condition to ramp to a hydrostatic pore pressure distribution which would correspond to a geotextile tube submerged below water.

Interaction properties were then specified for the soil/geotextile and soil/foundation interfaces. Although the geotextile physically interacts with the foundation, it was found to be less computationally demanding to model the soil itself interacting with the foundation. This minor change does not introduce any error, as the soil, foundation and geotextile never move relative to each other along the foundation. The interaction properties for both contacts made use of a tangential behavior with friction coefficient of 1.0 and a normal behavior which specified "hard contact" pressure overclosure. A surface-to-surface contact interaction was then specified between the soil body and the geotextile. This interaction was applied to all surfaces where the geotextile interacts with the soil body, and the default interaction options were used with the exception of the discretization method. There, the "node-to-surface" option was selected because the nodes in the contacting surfaces would not perfectly align with each other.

The interaction between the soil and the foundation was slightly more complicated, however. Two independent surface-to-surface interactions were specified: one interaction between the soil and the foundation along the horizontal base of the soil body (i.e. where the soil and foundation are initially in contact) and one along the curved face of the soil body (i.e. where the deformed soil may

eventually come into contact with the foundation as the soil deflects). These contacts were separated so that different contact options could be specified to each. The contact interaction along the horizontal bottom edge of the soil was allowed to adjust the position of the soil body slightly to bring the soil into immediate contact with the foundation. This option was enabled so as to allow ABAQUS to automatically correct for any numerical error encountered by the contact interaction algorithm. The interaction along the curved soil surface was then applied between the foundation surface and a node set which included all nodes along the curved soil surface excluding the node at the intersection of the horizontal bottom surface and the curved surface of the soil. This node was included in the first soil-foundation interaction, and thus it cannot be included in the second interaction as well. Both of these interactions also made use of the "node-to-surface" discretization method.

All other analysis options were created in the same manner that the one- and two-dimensional models were created. With that, the geotextile tube model was complete and ready to be run.

5.1.2. Geotextile Tube Model Results

Plotted or numerical results from the geotextile tube model would be difficult to interpret, and so no plotted results are presented here. Instead, results are presented graphically as shaded contour plots overlain on top of the deformed geometry of the geotextile tube. Void ratio results are presented in Figure 56 and vertical effective stress results are presented in Figure 57. Effective stresses are given in units of Pascals, with compressive stresses being negative.

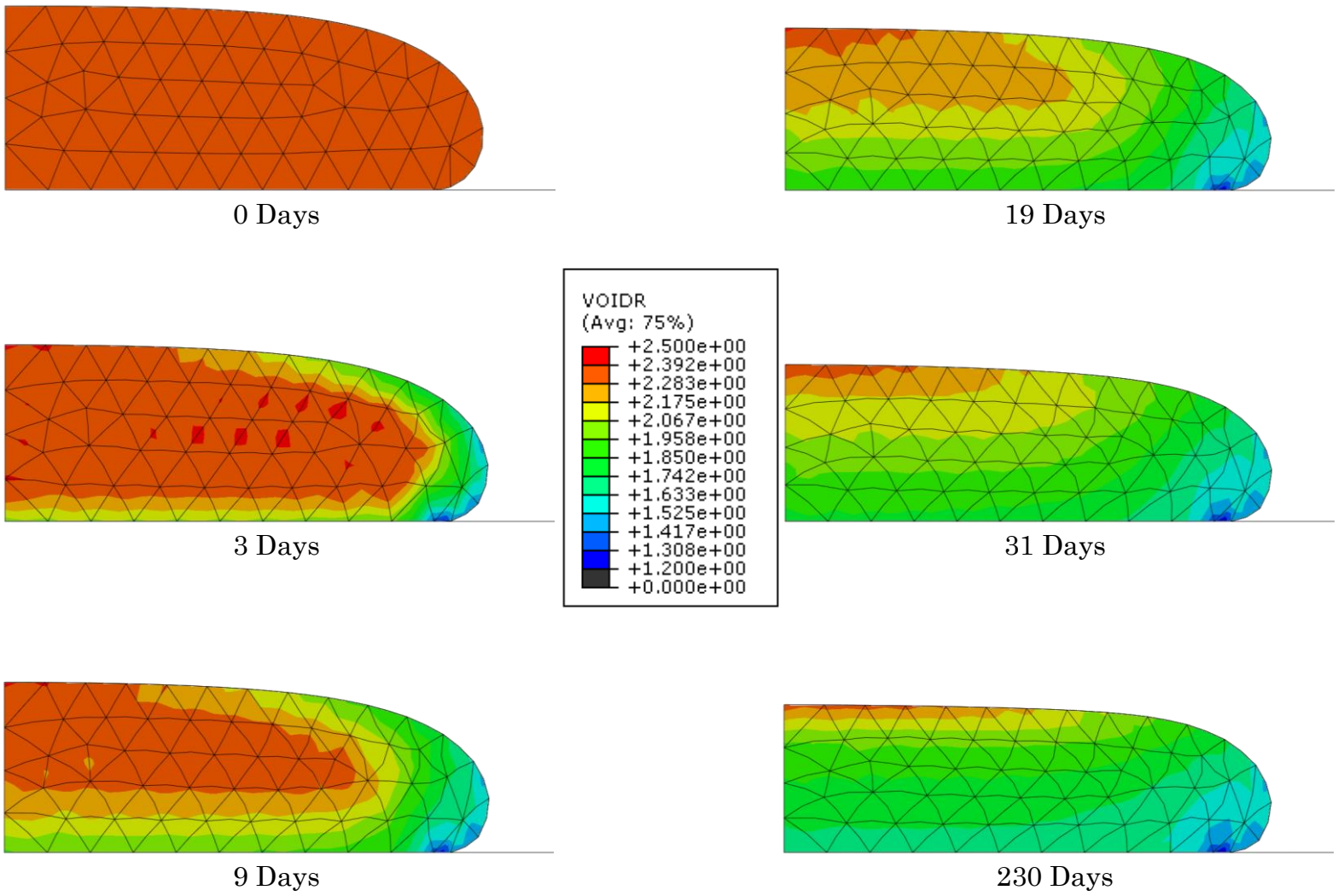

Figure 56: GOM Geotextile Tube Void Ratio Predictions

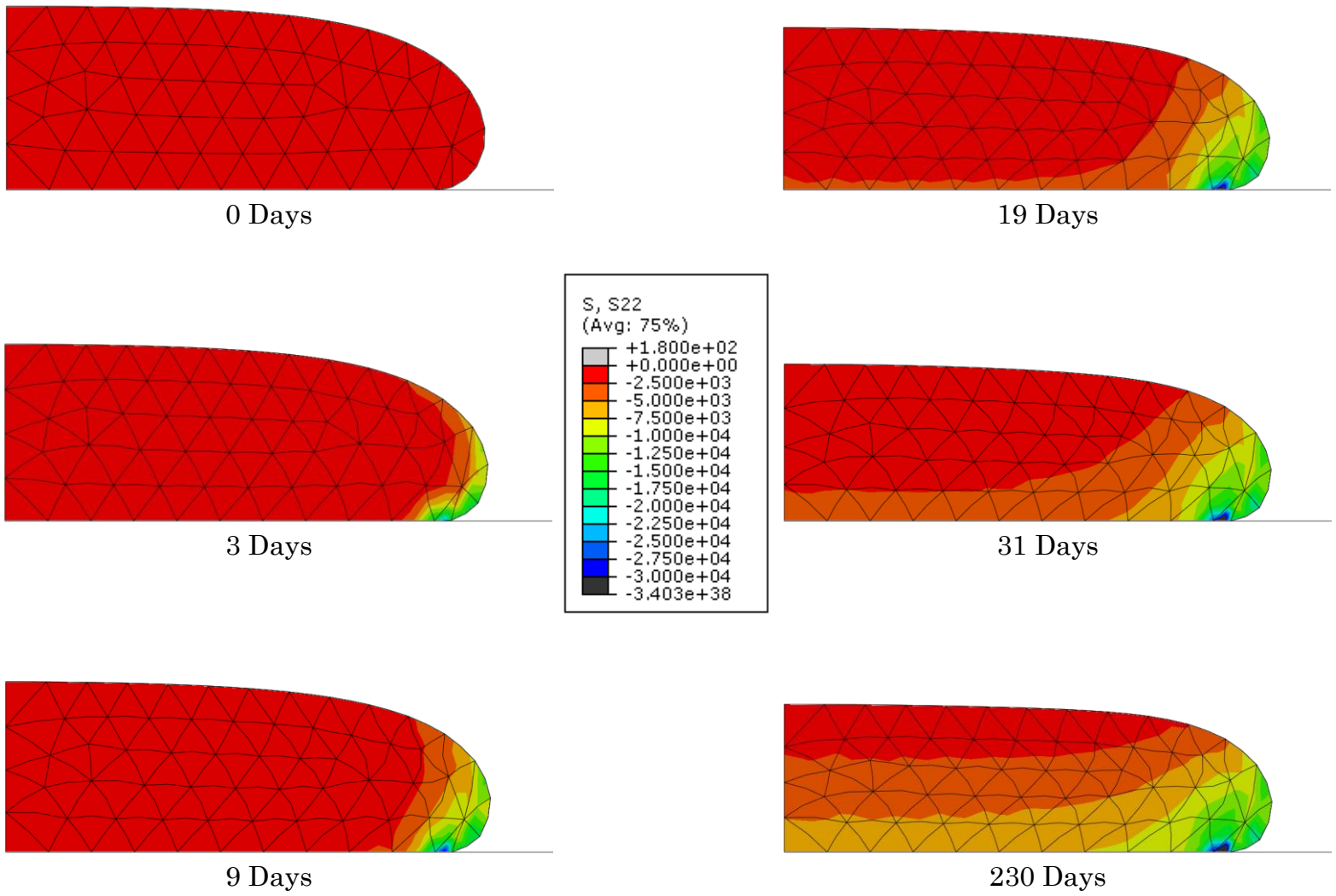

Figure 57: GOM Geotextile Tube Vertical Effective Stress Predictions

The void ratio results in Figure 56 show the formation and progression of a distinct consolidation front. Near the bottom of the model, the consolidation front is predicted to form in much the same way as the front shown in the one-dimensional models, where consolidation begins at the bottom of the soil body and then progresses upward through time. Here, the consolidation front also wraps around the interior of the curved edge of soil body. This portion of the front is driven by its proximity to the zero pore pressure boundary condition. Through time, the consolidation front can be seen to penetrate towards the center of the geotextile tube from all sides. After 19 days, the consolidation front has reached the top of the geotextile tube and the consolidation process has penetrated into all areas of the soil.

The vertical effective stresses in the soil do not follow the same trends as the void ratios. Here, the vertical effective stress begins to increase first in the toe of the geotextile tube instead. The void ratios, however, began to decrease all around the perimeter of the geotextile tube. This is likely a consequence of the two-dimensionality of the stresses which develop inside a geotextile tube. Although the vertical effective stresses increase first in the region of the toe, the horizontal effective stresses (and thus the mean effective stress) likely increase all along the perimeter of the geotextile tube so as to match the trends shown in the void ratio images.

Also noteworthy is the fact that a large stress concentration can be observed in the soil at the point where the geotextile first makes contact with the foundation.

This region shows a vertical effective stress of nearly 30 kPa at the end of the consolidation process, which is significantly greater than would be predicted by simply taking the product of the soil height and its buoyant unit weight. Two possible explanations exist for this observation, and the true cause is likely a combination of them both. First, some numerical error is likely occurring at that point because of the sharp change in angle of the geometry. Sudden, jagged corners like that often cause the numerical solver to over-estimate the stresses because of the discontinuity in the boundary. However, some stress increase is expected at that point because the weight of the soil which is elevated above the foundation surface to the right of that point is transferred to the foundation through that point. Thus, there is likely to be some noticeable stress increase in that region, thought the true stress increase is likely less than is predicted here.

Constitutively, the model performed as shown in Figure 58. The legend in this figure shows the coordinates of each node which was tracked, given as the nodal position *in the initial condition*. Here, it appears that the soil generally follows the expected trend represented by the CONDES curve. Again, the CONDES curve is a direct representation of the one-dimensional constitutive relationship given by (1). The ABAQUS constitutive paths are pushed somewhat to the right by the 0.30 kPa initial effective stress, though some additional discrepancies likely exist due to the two-dimensionality of the stress states within the soil. Also note that the constitutive path at coordinates (3.1 , 0) (i.e. at the node where the geotextile first makes contact with the foundation) shows a drop and then a sudden

rise in the void ratio. The void ratio likely drops as the stresses begin to concentrate about that node. Then, once the soil closer to the toe makes contact with the foundation, the horizontal stresses in the soil are likely relaxed slightly causing the void ratio to increase again.

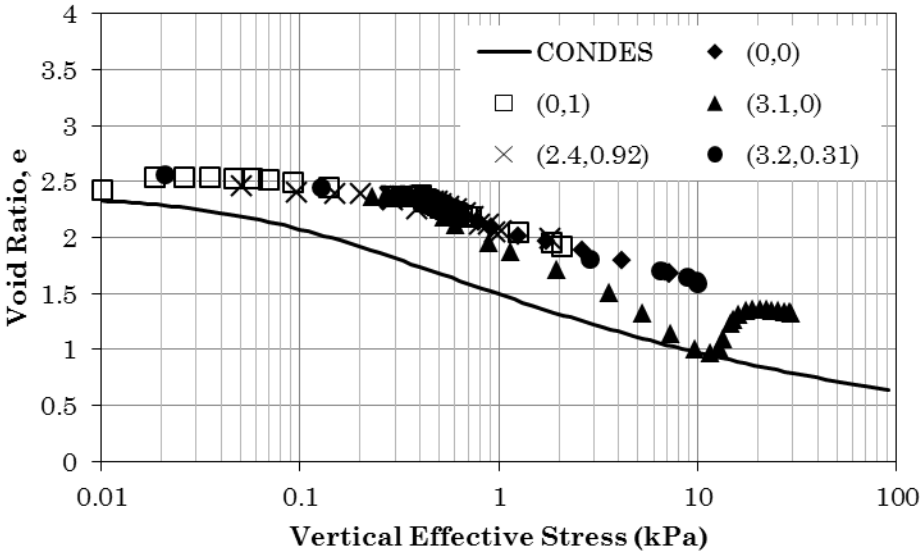

Figure 58: GOM Constitutive Behavior of Soil at Various Locations within the Geotextile Tube

5.1.3. Geotextile Tube Model Summary

Clearly, ABAQUS has the ability to model the highly complex geometry of a geotextile tube. This complexity is due not only to two-dimensional drainage, but also to the fact that the geotextile tube is allowed to spread laterally as a result the flexibility of the geotextile shell. The geotextile tube model also accounted for the interactions between soil, geotextile and foundation which again added complexity to the model. Despite these added complexities, the initial effective stress specified

for this model was reduced to a minimum value of 0.30 kPa, which is 0.10 kPa *lower* than the initial effective stress specified in the GOM two-dimensional model.

Additional modeling efforts revealed that the maximum height of a model plays a significant role in determining the minimum allowable initial effective stress. This topic is given greater attention in the discussion of tailing storage facility models. For now, it can be concluded that the smaller height of the geotextile tube model relative to the height of the two-dimensional model caused the minimum initial effective stress to drop in magnitude more than the added complexities of the model caused it to rise. As a result, the ABAQUS model showed constitutive behavior which was similar in form to the ideal behavior predicted by the relationship in (1).

However, when compared directly to the relationship in (1), the ABAQUS constitutive paths plotted noticeably to the right of the CONDES curve. The two-dimensionality of the geotextile tube model is at least partially the cause of this difference, such that if the ABAQUS constitutive paths were compared to a two-dimensional theoretical constitutive relationship the agreement would be better. However, the initial effective stress of 0.30 kPa also plays a role in causing this discrepancy in constitutive behavior. The GOM material has a preconsolidation pressure of 0.02 kPa, such that initial yield surface was forced to prematurely harden by a substantial amount due to the specified initial effective stress. This premature hardening caused the ABAQUS constitutive paths to be pushed to the right relative to the idealized CONDES curve. The result is that the true reduction

in volume of the geotextile tube should actually be greater in magnitude than ABAQUS predicted.

Thus, it can be clearly shown that ABAQUS, like all numerical models, has limitations which restrict its ability to perform numerical analyses involving very soft, hydraulically deposited soils. In particular, soils with preconsolidation stresses well below the specified initial effective stress should not be modeled using ABAQUS. Instead, models specific to hydraulically deposited soils should be sought out. Commercially, the availability of such models is limited, and further research is needed in order to develop a two- or three-dimensional soft-soil consolidation model.

5.2. Tailing Storage Facility Example Application

A tailing storage facility (TSF) is one of the more common applications where geotechnical engineers may encounter hydraulically deposited soils. Often, the process of milling ore produces tailing material in the form of a slurry. Even after conventional thickening the tailing often remains in slurry form so that it can be pumped to its disposal site. Typical disposal involves pumping the tailing slurry into a reservoir where it is allowed to consolidate and where it will permanently remain. Life-of-mine planning for these conventional mining operations is critically dependent upon the predicted capacity of the TSF, as the TSF must have the ability to store all tailing produced by the mine. Should the TSF prematurely reach its

maximum capacity, the mining operation would be forced to shut down until additional storage space could be discovered.

Several software packages exist which may be used to estimate the capacity of a TSF. However, these software packages may be prohibitively expensive to the engineer. If the engineer had access to a numerical code like ABAQUS, it is possible that they could develop a simplified numerical model which would predict the consolidation time of the tailing and ultimately the total capacity of the impoundment with a reasonable degree of accuracy.

5.2.1. Model Creation and Execution

For the purpose of this thesis, a simplified TSF model was generated in ABAQUS using KEX material properties as an example of how such a full-scale model could be created. This model is intended to be used as a brief example, as TSF modeling is not the focus of this thesis. Thus, it is not a fully functional model which could accurately predict the capacity of a TSF. Instead, this example is intended to give the reader a set of guidelines which could be used to create a more advanced TSF model.

In creating this model, it was first assumed that the tailing was instantaneously deposited instead of depositing the tailing over time. Although this assumption does not represent the true operation of a TSF, it will still allow the model to show how tailing settlement can be predicted using commercially available numerical codes like ABAQUS. The geometry of the TSF was developed from a stage-storage curve by assuming that each segment of the curve represented a

truncated conical prism, such that the areas specified in the stage-storage curve could be converted to radii. The model was then created in the axisymmetric condition so that the two-dimensional cross section would properly represent these conical segments.

The stage-storage curve used for this model is given in Table 5, along with the equivalent conical radius at each elevation. Here, the radius values were input as the x-coordinates in the ABAQUS model, and the elevation values were input as the y-coordinates. The result is the two-dimensional profile of the impoundment bed which is shown in Figure 59. When rotated about the y-axis an approximate three-dimensional representation of the TSF is achieved. An ABAQUS model was then created using this geometry, with a quadrilateral mesh of type CAX8P. The meshed ABAQUS model is shown in Figure 60. It should be noted that the ABAQUS model required the sharp corner at the far right side of the model to be rounded slightly to prevent numerical errors. Rounding of this corner was accomplished by splitting the final segment of the bed profile into two segments. The right segment was made to be fairly short (about 2.5 m long) and was angled down much more steeply than the original bed profile called for. The left segment was then used to connect the right segment to the original bed profile.

Table 5: Stage-Storage Curve for Example TSF Model

Elevation (m)	Area (m²)	Radius (m)
0	1500	22
10	7000	47
20	24000	87
30	61000	139
40	104000	182
50	159000	225
60	226000	268
70	300000	309
80	382000	349
90	473000	388
100	568000	425
110	683000	466
120	800000	505

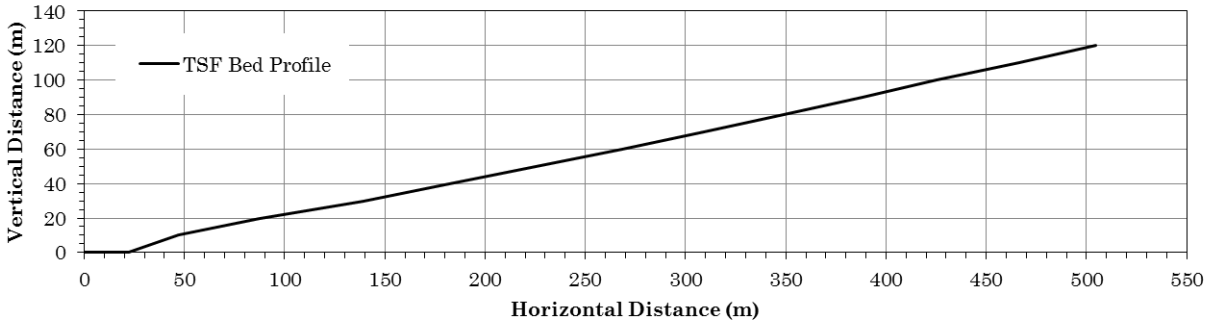

Figure 59: TSF Equivalent Conical Bed Profile

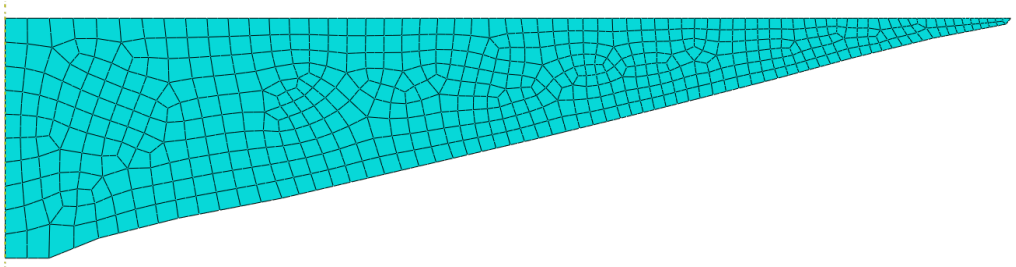

Figure 60: TSF Model in ABAQUS

To simplify the model, the foundation along the bed of the TSF was represented by a mechanical boundary condition which fixed the vertical and horizontal displacements. The horizontal displacements were then fixed along the left vertical face of the model. The node at the bottom left corner of the model was excluded from this boundary condition as it was already included in the boundary condition applied to the bed of the TSF.

Unlike the previously discussed models, the TSF model required that the gravity load be slowly ramped from zero to 9.81 m/s^2 at the beginning of the consolidation step. Ramping of the gravity load took place over a time interval of one day. Sudden application of the gravity load was found to cause the ABAQUS solver to encounter errors, and so a ramped gravity load was instead selected. Because the gravity load was not instantaneously added after the initial step, no initial undrained pore pressure distribution was specified. Without the gravity load, an undrained pore pressure distribution applied at the beginning of the consolidation step would cause the model to no longer be in equilibrium. Instead, the solver was allowed to compute the undrained pore pressures as the gravity load was applied. The relatively low hydraulic conductivity of the soil provided sufficient seepage resistance to approximate the undrained condition during the time period over which the gravity load was applied.

An initial effective stress of 1.50 kPa was required for the model to successfully compute. Multiple factors contributed to the requirement of such a large initial effective stress. As discussed previously, the high compressibility of the

material and the two-dimensional nature of the model both lead to increases in the minimum allowable initial effective stress. Additionally, this model is physically much larger than any of the other models discussed in this thesis. It was discovered that as the height of a model increases, the minimum allowable initial effective stress increases as well. This observation was found to hold true for one-dimensional models as well as the more complex two-dimensional models. Likely, this height dependency arises from the increased stresses present in taller models which lead to larger changes in volume. The ABAQUS solver likely requires some additional stabilizing factor to prevent numerical oscillations when computing these large volume changes, and the larger initial effective stress provides that stabilization.

Other than the steps mentioned above, the ABAQUS TSF model was created using the same procedures as those described for the one-dimensional models in section 3.1.1.

5.2.2. TSF Model Results

Void ratio and vertical effective stress results from the TSF model are provided in Figure 61 and Figure 62. Note that the stress values listed in the legend are given in units of Pascals, using the convention that compressive stresses are negative.

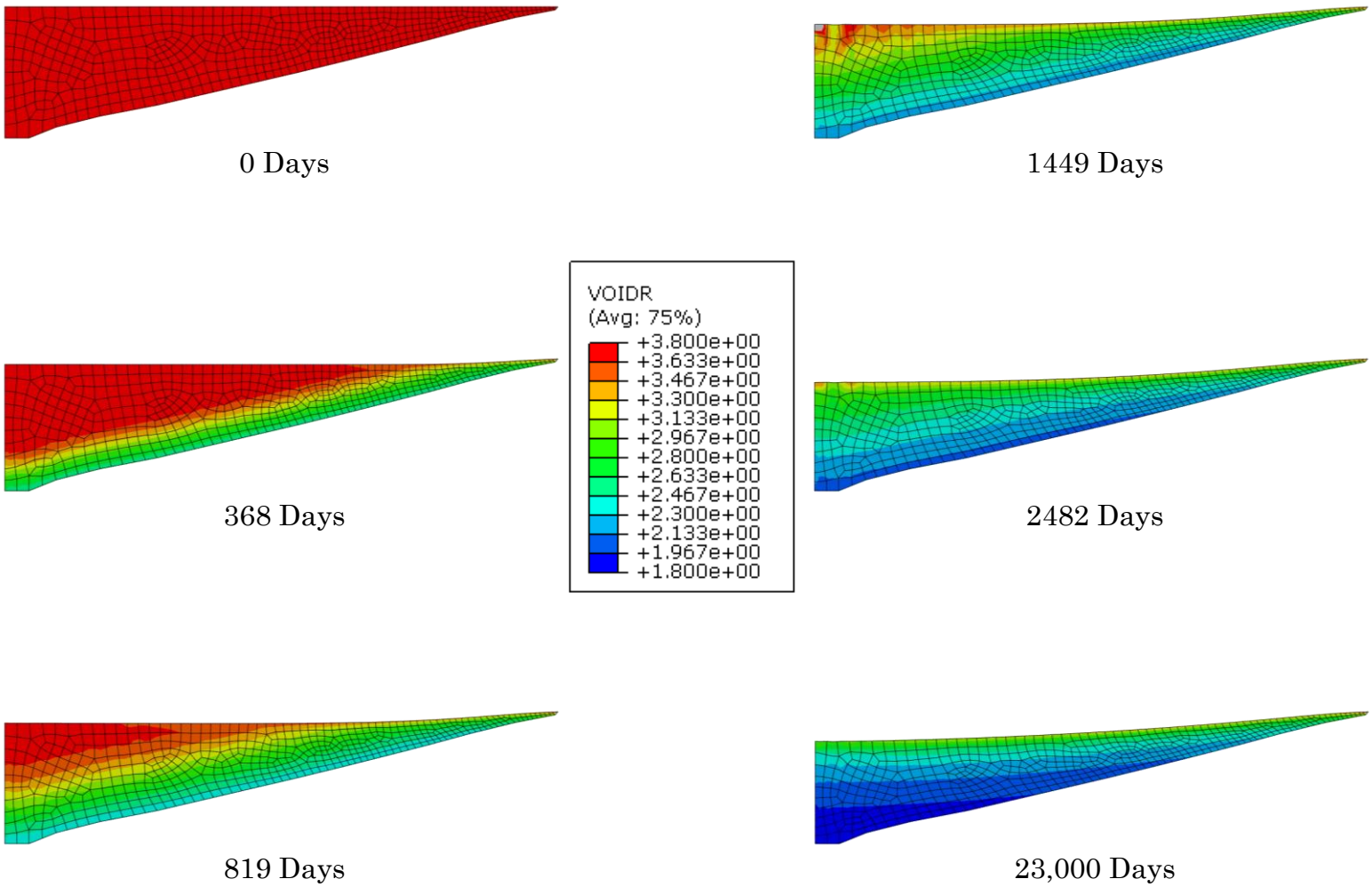

Figure 61: KEX TSF Void Ratio Predictions

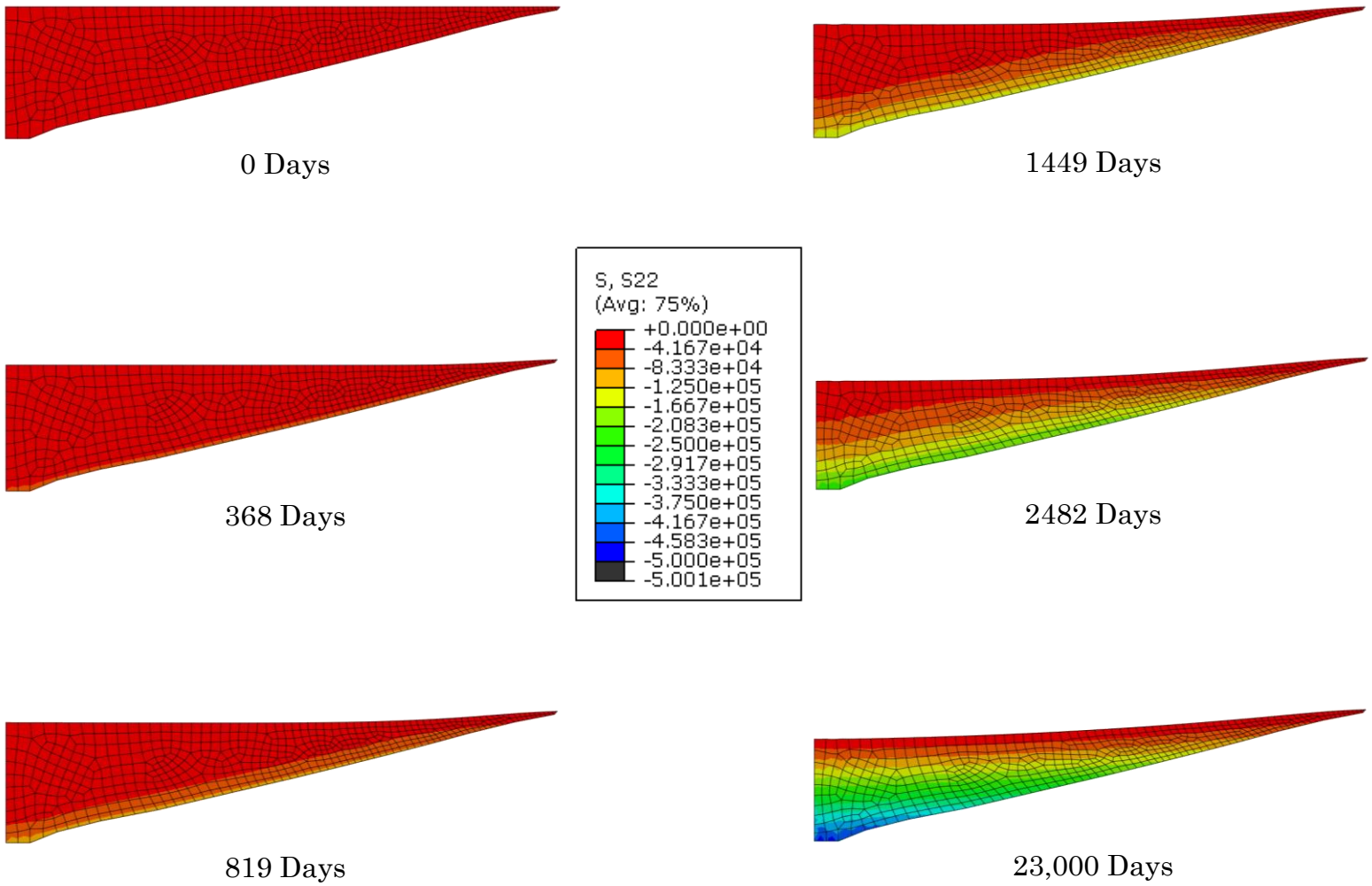

Figure 62: KEX TSF Vertical Effective Stress Predictions

Here, both the void ratio and vertical effective stress plots show a distinct consolidation front beginning along the bed of the impoundment, such that consolidation begins at the base of the soil and progresses upward through time. This observation is quite similar to the one-dimensional models which use similar drainage conditions. Here, though, some lateral displacement of the soil is created by the sloped impoundment bed. Thus, the two-dimensionality of this TSF model is introduced through the geometry and not through the drainage conditions.

A product of this lateral movement of soil is that the stresses at the very bottom of the model increase well above those predicted by the unit weight of the soil which was originally above it. The product of the soil's buoyant unit weight (3.54 kN/m^3) and the soil's initial height (120 m) produces an estimated 425 kPa of effective stress at the bottom model in its fully consolidated state. However, the ABAQUS model predicts at least 500 kPa effective stress at that location. Likely, the soil which shifts to the left adds to the effective stress of the soil below it, causing this discrepancy.

Due to the large initial effective stress specified in this model, the constitutive paths predicted by ABAQUS were again shifted to the right by a noticeable amount. As a result, the model under-predicts the total settlement of the tailing. This shift is shown in Figure 63. However, it is also noteworthy that the constitutive paths at all points in the soil follow the basic one-dimensional trends represented by the CONDES curve. Thus, the consolidation process inside this TSF model is likely predominantly one-dimensional. Although some lateral shifting of

the soil occurs, it does not appear to be substantial enough to cause significant deviations from the one-dimensional constitutive relationship described by (1). Additional evidence for this theory is found in Figure 64 which shows the horizontal displacements predicted by ABAQUS. Here, it can be seen that only the soil near the top of the model shifts noticeably, and even the soil in that region does not shift a great deal relative to the overall width of the model. Thus, consolidation of a soil in an idealized conical TSF is shown to behave predominantly one-dimensionally with only slight horizontal displacements in the soil.

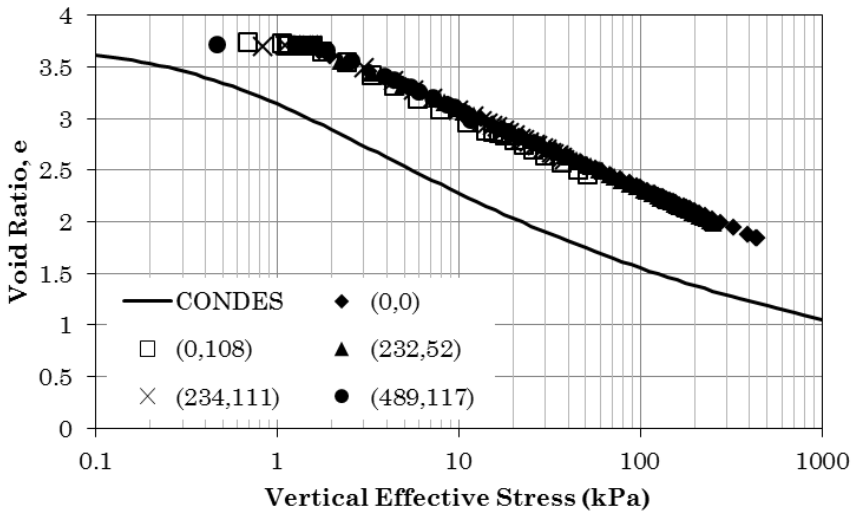

Figure 63: KEX TSF Constitutive Paths Predicted by ABAQUS

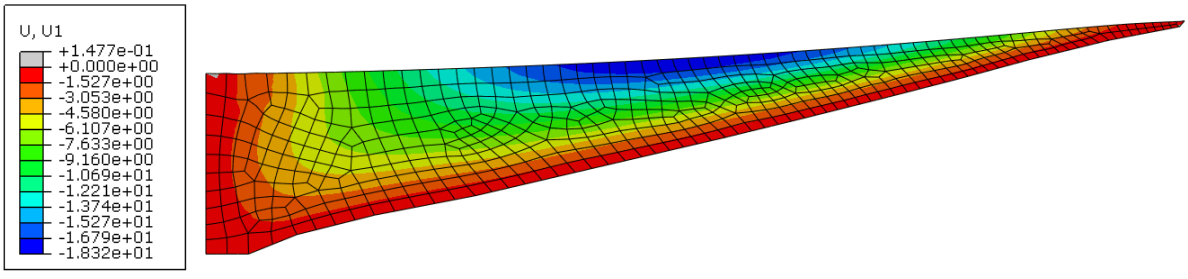

Figure 64: KEX TSF Model Horizontal Displacements

5.2.3. Tailing Storage Facility Model Summary

Tailing storage facilities represent a unique challenge in numerical modeling. Specifically, the physical size of these impoundments causes numerical issues, particularly when the overall height of the model is excessive. Models of excessive height require substantially larger initial effective stresses than do models of smaller size, which is likely due to the greater volume reduction observed in larger models. As a result, the initial yield surface of these larger models is often prematurely hardened in order to account for the larger initial effective stress. Such hardening causes the ABAQUS constitutive paths to be pushed noticeably to the right, which in turn causes ABAQUS to under-predict the volumetric strain of the soil.

The plot in Figure 63 show this rightward shift of the ABAQUS constitutive paths which lead to an unconservative prediction of the volume reduction in the TSF. Should a smaller TSF be modeled, the result would likely be a more accurate prediction of the volumetric strains. Here, the two-dimensionality of the model likely did not contribute significantly to the discrepancies between the ABAQUS constitutive paths and the idealized one-dimensional CONDES line. As a result, the error in the constitutive behavior is likely not recoverable without somehow reducing the initial effective stress specified in the ABAQUS model.

Although the ABAQUS model described in this section was a simplified example, it still provides useful details which may be used to better understand the consolidation processes which occur in a TSF. Most noteworthy is the fact that the

consolidation process was shown to be primarily one-dimensional, with only limited and localized lateral displacements occurring near the soil's top surface. The one-dimensionality of the consolidation process is also confirmed by the existence of a distinct consolidation front which begins along the bed of the TSF and progresses upward in the same manner as was observed in the one-dimensional models.

6. CONCLUDING REMARKS

Hydraulically deposited soils represent a unique challenge to geotechnical engineers, as they may deform substantially under relatively small loads. Classical consolidation theory fails to represent these deformations due to the assumption that the material compressibility and hydraulic conductivity remain constant. Hydraulically deposited soils may experience changes in compressibility and hydraulic conductivity of several orders of magnitude over the course of the consolidation process. Finite strain consolidation theories provide a more realistic predictive framework, though most of these theories are mathematically expressed in only one dimension.

Two- and three-dimensional consolidation scenarios are much more commonly encountered in engineering practice than are one-dimensional scenarios. When these multi-dimensional scenarios arise, numerical codes are often the only reliable means of predicting the soil behavior. Commercial codes like ABAQUS and PLAXIS are commonly found in engineering firms across the globe, and it was the goal of this research to determine if these codes have the capability to model the complex behavior of hydraulically deposited soils.

First, both codes were tested using simple one-dimensional models. Four different soils were modeled, covering a wide range of compressibilities. Additionally, two plasticity models were implemented: the Modified Cam Clay

model and the Capped Drucker-Prager model. The goal was to determine which plasticity model would provide the most accurate prediction of the constitutive behavior of each soil. Both codes make use of an optional finite strain approximation algorithm which is independent of the plasticity model, and which is required to properly account for the stiffening of the soil as it undergoes reduction in volume.

Through these one-dimensional models, it was found that the Modified Cam Clay plasticity model provides the most accurate constitutive predictions in one-dimensional consolidation scenarios. It was also found that the PLAXIS code assumes a minimum preconsolidation stress of 1 kPa. For stiffer soils with preconsolidation stresses greater than 1 kPa, this assumption is valid. However, many hydraulically deposited soils show a preconsolidation stress well below 1 kPa, such that the volumetric predictions offered by PLAXIS become highly unconservative. It was discovered that the 1 kPa assumption can be altered in PLAXIS, though doing so requires making changes to the base code input files. Such a procedure was considered to be too advanced for most practicing engineers to use on a regular basis, and so it was ultimately concluded that results from the PLAXIS code would not be produced for the remaining modeling efforts.

ABAQUS, on the other hand, allows the user to directly manipulate both the initial effective stress and the preconsolidation stress used by the code. Complexities in the models introduced by two-dimensional seepage and by increasing model height were shown to cause the minimum allowable initial stress

to increase. When the initial effective stress specified in an ABAQUS model becomes greater than the preconsolidation stress of the soil, ABAQUS automatically hardens the initial yield surface so that the initial effective stress becomes the new preconsolidation stress. In this way, ABAQUS models may potentially be limited by the same issues which cause the PLAXIS code to provide unconservative predictions. This effect was observed to some degree in the two-dimensional model using GOM material, and also in the geotextile tube and TSF example models.

Two-dimensional modeling revealed a great deal about how hydraulically deposited soils respond to lateral drainage. More specifically, hydraulically deposited soils were found to be sensitive to the existence of lateral seepage forces, which result in lateral compression of the soil as well as vertical compression. Both of the two-dimensional models produced results which took on a nearly identical form, and which showed the importance of accounting for the horizontal stress component when assessing the constitutive behavior of the soil. Because the idealized constitutive relationship in (1) uses only the vertical effective stress and not the mean effective stress, its applicability to two-dimensional drainage scenarios is limited. However, to the author's knowledge a theoretical two-dimensional constitutive relationship has not yet been developed, such that one-dimensional relationships must be used to approximately judge the accuracy of two-dimensional consolidation models.

Examples of real-world scenarios involving hydraulically deposited soils were then given, including geotextile tubes filled with dredged material and tailing

storage facilities which impound tailing slurries. Both of these models introduced additional complexities including the potential for lateral drainage, lateral soil compression and/or increased model height. The result of these added complexities was an increase in the initial effective stress, resulting in a loss of accuracy in the ABAQUS constitutive predictions.

Ultimately the premature hardening of the initial yield surface represents the greatest limitation of these numerical codes when used to model hydraulically deposited soils. Any time that the initial yield surface is prematurely hardened, the constitutive behavior predicted by the code will contain errors in the volumetric strain predictions which are proportional to the amount of hardening which occurred. For very soft soils whose preconsolidation stress is substantially smaller than the initial effective stress assumed by the code, the constitutive predictions will be too inaccurate to be of use in engineering designs. However, these codes provide highly accurate constitutive predictions for soils in which the preconsolidation stress is greater than or only slightly less than the initial effective stress assumed by the code. Thus, the limitations of the PLAXIS and ABAQUS codes (as well as other numerical codes) when modeling hydraulically deposited soils are contingent upon the relationship between the initial effective stress used by the code and the preconsolidation stress of the soil. Despite the limitations of these codes with very soft hydraulically deposited soils, they may still provide an accurate representation of the consolidation of hydraulically deposited soils so long as the initial effective stress and the soil's preconsolidation stress are in agreement.

Modifications to the Modified Cam Clay parameter calibration process would result in a more accurate representation of the three-dimensional stress states which occur in more complex real-world scenarios. Here, Modified Cam Clay parameters were fitted to the relationship in (1) by assuming the soil remains in an at-rest lateral earth pressure condition. By generalizing the relationship in (1) to account for full three-dimensional stress states, the Modified Cam Clay parameters could be better fit to match the true constitutive behavior of the soil.

Additional issues exist with the geotextile tube models which were not addressed in this research. These issues stem from the fact that geotextile tubes may need to be refilled after they have partially consolidated so that they maintain desirable dimensions. The refilling process would introduce a new layer of soil on top of the existing partially consolidated soil, and would cause the void ratios, pore pressures and effective stresses in the existing soil layer to change suddenly. In ABAQUS, two (or more) parts may be used to represent the soil body. The first part would take on the shape of the partially consolidated soil which was already present in the tube, and the second part would take on the shape of the new soil layer above the original soil layer.

Adding fill to a geotextile tube would drastically alter the shape of the tube, however. If the void ratios in the partially consolidated soil layer were assumed to remain constant across the width of the geotextile tube, then the MATLAB code described in section 5.1.1 could be used to estimate the shape of the refilled geotextile tube. The soil unit weights in both soil layers, which are a function of the

void ratios, could be input into the MATLAB code as a piecewise function which varied with height. The output would then be representative of a multi-layered fill. However, this assumption is highly restrictive as it assumes the void ratios in the soil layers are uniformly distributed in the horizontal direction. This approach would also implicitly assume that the refilling process would not disturb the partially consolidated soil layer as the geotextile tube geometry changed. Clearly this is not the case, and so additional steps would need to be taken to assess whether the errors introduced through this assumption would be of consequence.

The TSF model described in section 5.2 assumed that the tailing was instantaneously deposited for the purpose of providing a simplified example. To further generalize this model and to make it more representative of the gradual filling process which actually occurs in a TSF, several soil parts could be used to split the soil into horizontal layers representing the soil deposited over a discrete time interval. A gravity load could then be applied to each soil part independently and at different times so as to better represent gradual filling. The height of each layer would be dependent upon the estimated mine throughput, the equivalent radius of the impoundment at the elevation where the layer is anticipated to reside *in its steady state condition*, and other factors as well. Clearly this is an imperfect solution which would likely the engineer to first assume some of the characteristics of the fully consolidated tailing, then to adjust those assumptions based upon the model results. The logistics of implementing such a model in ABAQUS may prove difficult as well, such as allowing the upper soil layers to deform with the lower soil

layers while maintaining constant volume (and thus maintaining the proper initial void ratio). The interactions between soil layers would add additional complexities to the models which may require the initial effective stress to be increased even further, which would cause the settlement to be under-predicted by an even greater degree.

Additional modeling steps could clearly be taken with all of these models. However, those steps lie outside the scope of this thesis. Further research is still needed in these areas to provide geotechnical engineers with the tools they need to predict the behavior of hydraulically deposited soils in real-world scenarios using commercially available numerical codes. This research has shown both the potential for such commercially available codes in this area, as well as their limitations. If specific engineering scenarios fall within the limits of accuracy of these codes, then these codes can be successfully and reliably used to predict the consolidation behavior of hydraulically deposited soils. However, these codes are still nothing more than tools to be used by engineers, and engineering judgment must always be applied when using these codes and interpreting their results.

7. BIBLIOGRAPHY

Abu-Hejleh, A.N.; Znidarcic, D. and Barnes, B.L. (1996). Consolidation Characteristics of Phosphatic Clays, *Journal of Geotechnical Engineering*, 122:4, pp. 295-301.

Beemsterboer, D.; Christophe, J.; Scheepjens, R.; Veldman, M. and van der Wielen, V. (2012). Tiaozini Land Reclamation: Preliminary Port Area Design, *Delft University of Technology*, Delft, Netherlands, pp. 62-68.

Carroll, R. P. (1994). Submerged geotextile flexible forms using non-circular cylindrical shapes, *Geotechnical Fabrics Report*, IFAI, St. Paul, MN, 12:8, pp. 4-15.

Craig, R. F. (2004). *Craig's Soil Mechanics* (7th ed., pp. 227-276). New York, NY: Spon Press.

Dana, J. D.; Hurlbut, C. S.; and Klein, C. (1977). *Manual of Mineralogy* (19th ed.). n.p.: John Wiley & Sons inc. Retrieved June 26, 2014

Dassault Systems, (2013). Abaqus Overview, *Abaqus Unified FEA*. Retrieved July 29, 2013, from http://www.3ds.com/products-services/simulia/portfolio/abaqus/

Gibson, R.E.; England, G.L. and Hussey, M.H.L. (1967). The theory of one-dimensional consolidation of saturated clays, I. Finite nonlinear consolidation of thin homogeneous layers, *Geotechnique*, 17:3, pp. 261-273.

Helwany, S. (2007). *Applied Soil Mechanics with ABAQUS® Applications*, pp. 21-197. Hoboken, NJ: John Wiley & Sons, Inc.

Howard, I.L. and Trainer, E. (2011). Use of Geotextile and Geomembrane Tubes to Construct Temporary Walls in a Flooded Area, *SERRI Report 70015-003*, SERRI, pp. 28-55.

Leshchinsky, D.; Leshchinsky, O.; Ling, H.I. and Gilbert, P.A. (1996). Geosynthetic Tubes for Confining Pressurized Slurry: Some Design Aspects, *Journal of Geotechnical Engineering*, 122, pp. 682-690.

Liu, J.C. and Znidarcic, D. (1991). Modeling One-Dimensional Compression Characterisitcs of Soils. *Journal of Geotechnical Engineering*, ASCE, 117:1, pp. 164-171.

PLAXIS, (2013). Plaxis 2D, *Plaxis 2D Geotechnical Software*, Retrieved July 29, 2013, from http://www.plaxis.nl/plaxis2d/

Somogyi, F. (1979). Analysis and Prediction of Phosphatic Clay Consolidation: Implementation Package. *Tech. Report.* Florida Phosphatic Clay Research Project, Lakeland, Florida.

Tyagi, V.K. (2005). Applications of Geosystems as Retaining Structures in Marine Environments, *Slopes and Retaining Structures under Seismic and Static Conditions*, 1:1, n.p.

Tyagi, V. K. and Mandal, J. N. (2005). Physical and Numerical Modelling of Stacked Geotubes subjected to Dynamic Loads, Proceedings from *Civil Engineering in the Oceans VI*, Baltimore, MD, pp. 356-365.

Wood, D. M. (1990). *Soil Behaviour and Critical State Soil Mechanics*, pp. 112-317. Cambridge, NY: Cambridge University Press.

Yao, D.T.C.; Oliveira-Filho, W.L.; Cai, X.C. and Znidarcic, D. (2002). Numerical solution for consolidation and desiccation of soft soils, *International Journal for Numerical and Analytical Methods in Geomechanics*, 26:2, pp. 139-161.

Yiming, S.; Gang, L. and Yan, X. (2010). Structural Stability and Filling Materials on Geotube Dams. Proceedings from *Earth and Space 2010: Engineering, Science, Construction, and Operations in Challenging Environments*, Honolulu, HI, 720-728, ASCE.